AGSO Record 1999/27

Geophysical Investigation of North Central Australia

Images, Algorithms & Crustal Models

by
C. Z. Tarlowski and D. L. Scott

Report 1999/27

COPYRIGHT

Published by the the Australian Geological Survey Organisation, Department of Industry, Science and Resources, Canberra, Australia. Issued under the authority of the Minister for Industry, Science and Resources.

Copies of this CD may be obtained from:

AGSO Sales Centre,
GPO Box 378,
Canberra, ACT 2601
Phone (02) 6249 9519
Facsimile (02) 6249 9982

It is recommended that this CD be referred to as:

Tarlowski, C.Z., and Scott, D.L., 1999 -
Geophysical Investigation of North Central Australia - Images, Algorithms and Crustal Models.
Australian Geological Survey Organisation. AGSO Record 1998/27

WEB ADDRESS: ***http://www.agso.gov.au/***
http://www.disr.gov.au

Readme.doc

Geophysical Investigation of North Central Australia
Images, Algorithms and Crustal Models

INSTALLATION

The presentation on this CD was created using standard Adobe Acrobat PDF format. You will need version 3.0.1 or later of the Adobe Acrobat Reader, to view the presentation.
The CD contains Adobe Acrobat 3.0.1 Reader installation files for various platforms, and these are located in the ACROBAT directory.
If you are using WIN95 or NT and do not have Acrobat on your computer:
Access the CD through a file manager.
Go to the ACROBAT directory and double click on setup.exe to install the Acrobat Reader.
Other platform readers are available from the ACROBAT directory or via Adobe's Web address: www.adobe.com/acrobat

TO VIEW THE REPORT

Commence by accessing the REPORT directory through a file manager.
Double click on AGSO1999-27.pdf. Then use Acrobat to navigate around the report.

INTERNET ACCESS

Parts of this presentation require internet access through a standard web browser.

DIRECTORIES ON THE CD

ACROBAT directory:
A directory of Adobe Acrobat Reader installation files for various platforms. This directory includes setup.exe, Adobe Acrobat Reader installation file, for WIN95 and NT users.

REPORT directory:
Contains AGSO1999-27.pdf, the report presentation, including text and diagrams.

Geophysical Investigation

of

North Central Australia

Images, Algorithms and Crustal models

by

Chris Z.Tarlowski & Deborah L. Scott

Australian Geological Survey Organisation Record 1999/27

Executive Summary

This synopsis of the geophysical research expands on earlier presentations (e.g., Tarlowski & Scott 1997) as an aid to understanding the physical meaning of the various geophysical transformations and depth to magnetic basement algorithms. We assess the preservation of the integrity of the data and what artifacts are introduced when dealing at both the simple model and large regional scales.

An investigation into geophysical transformations of the observed magnetic and gravity fields at a regional scale have enabled us to refine our understanding of the geological and crustal evolution of north central Australia. This investigation, a contribution to the 'North Australian basins resource evaluation' (NABRE) project, focussed on problems particular to regional-scale geophysical coverages with variable data density and quality.

We present a case study at the scale of the entire **NABRE project area** (~1000 km^2), wherein the data density and quality are highly variable. We also provide a series of the same transformations of the densely covered, high quality data of the Camooweal 1:250 000 map sheet.

We have investigated some frequently used geophysical transformations of magnetic data, namely, an analytic signal, reduction of the magnetic data to the pole, derivatives of the total magnetic intensity and upward continuation. Starting with a simple model consisting of two vertical prisms, the physical meaning of all but the last of these transformations are explained and the magnetic response visualised in three dimensions. The less commonly used "tilt" of the horizontal gradient of the magnetic data is also described and assessed for the model. Psuedo-code for the Tilt transformation is provided.

We have applied these transformations to magnetic data at the regional scale and provide a series of images of the results. These images can be compared to images of the gravity data and an image of the application of a terracing operator to the gravity data. The usefulness of these transformations for the extraction of information on the nature of the crust is discussed.

Special emphasis has been given to investigation of techniques for estimating depths to magnetic sources. Two techniques have been assessed with respect to inherent assumptions and effects produced during preparation. These are the Naudy and Phillips deconvolution methods. The two methods have been compared practically by application to the case study data sets and comparison with other regional data (e.g., gravity). A series of images give the reader a clear view of the effect of both of the algorithms, the difference between their effect on high quality versus variable quality data sets and their correlation to igneous outcrops. In addition, similar treatment is given to variously filtered original magnetic data prior to the application of the depth estimate calculation.

The series of geophysical images provided allows the viewer an efficient and complete view of the regional geophysical response of both case study areas, without the cost and time involved in obtaining, developing and processing the raw data. Our

assessment of the validity of various transformations also provides the viewer with constraints on the limits of interpretation of the images.

A suite of image and traverse interpretations have been undertaken (Leven et al 1997, Scott et al. 1997; this record) to construct a regional geological model. The North Australian Craton (after Shaw et al. 1995; 1996; Meyers et al. 1996) defines the core of North Central Australia. The craton is flanked by the Kimberley block and Halls and Pine Creek belts to the west, the Arunta and associated crustal belts to the south and the Mount Isa belt to the East. This record provides the geophysical images and some of the interpretations are synthesised into a possible geological model of North Central Australia. Alternatives are clearly possible.

The focus of the NABRE project has been on the significantly mineralised Palaeoproterozoic packages from ~1790-1550 Ma exposed in the Palaeoproterozoic outcrop belts along the eastern and northern flanks of North Central Australia (the Mount Isa, South Nicholson, Murphy and McArthur regions). Outcrop belts of similar age also occur in the centre (the Tennant Creek and Davenport regions) and on the western edge (the Victoria River Basin, Halls Creek, Birrindudu and Tanami regions) and southern flank (Arunta region) of the craton (NATIONAL MAP; see **Fig. 25**). The geophysical data sets are the only data that are available to extrapolate the outcrop geology across the large areas within North Central Australia where rocks of this age are under younger cover.

Large scale regional cross sections constrained by surface geology are forward modelled to test their ability to reproduce the observed potential-field data. These traverse models are used to extend the geophysical elements model derived from the image interpretations to the subsurface. The geological models were constructed with an emphasis on speculations about the geometry and distribution of Palaeoproterozoic basins of the ~1790-1550 Ma period and the underlying basement within the central craton. The packages that comprise the traverse models are extrapolated to map view interpretative contour maps to derive a basement model, a pre-1730 Ma crustal model and a ~1750-1575Ma basin distribution model. We are particularly interested in developing and contributing to hypotheses of crustal evolution for the region. The interpretative traverse and planview models are integrated with other regional data sets (e.g., geochemistry and geochronology) for this purpose in Scott et al. (2000).

The material presented in this record is an invaluable instructive tool to both geologists and geophysicists. It also provides a unique opportunity for viewing and analysing a compendium of geophysical expressions from a large portion of the Australian continent. It should prove useful to explorationists who wish to expand their more detailed local studies regionally, to researchers into the nature of the earth in this area and as an educational tool for both geologists and geophysicists.

Introduction

Scope and Objective

We have investigated the value of regional-scale potential-field data to an interpretation of geological and crustal evolution. Our data cover a ~1000 km^2 area in north central Australia — between lats. 11 and 24ºS and longs. 126 and 141ºE — which coincides with the study region of AGSO's 'North Australian basins resource evaluation' (NABRE) project. The objective of this investigation was to assess the usefulness of both geophysical transformations and techniques for estimating depths of magnetic sources from gridded data and to construct a geological model, which is consistent with the observed data.

Methods used

Potential-field data traditionally have been used to produce contour maps. However, it is now more common to derive raster colour image-maps of the magnetic and gravity fields. Whereas contour maps represent structural information according to the orientation, spacing, and relative values of contour lines, raster images represent the same information by changes in the continuity of colour patterns. Consequently, the way that an image derived from potential-field data is enhanced can greatly influence the derived geological interpretation.

We have used the HSI (hue, saturation, intensity; Milligan et al. 1992) model for image enhancement as it sharpens anomaly edges, thus promoting the expression of structural geological information. In this model, the colour maps are constructed by converting image grids from RGB (red, green, blue) to HSI. Pixel hues are chosen from natural colours ranging from blue to magenta. The saturation and intensity components are taken from a gradient or sun-angle routine applied to the original data.

Geophysical transformations of potential-field data are methods intended to facilitate geological interpretation by transforming measured data into some new form. In general, they do not precisely define the distribution of the sources, but provide insights that help to build a better understanding of the nature of the sources. Simplistic interpretation of the transformed potential-field data can lead to erroneous geological interpretation. Interpretations of the data are non-unique, and multiple interpretations can be made that are consistent with the observed data. Thus, other data are required for constraining the most appropriate interpretation. Understanding the nature of the data and the transformations applied to the observed data is an important first step in any interpretation. Using a simple synthetic model composed of two vertical prisms, we have attempted to elucidate some frequently used geophysical transformations of magnetic data and the less common tilt transformation.

One of the most important aspects of an interpretation of potential-field data is estimating the depths to the sources of anomalies. This applies whether the magnetic bodies or the geometry of the overlying non-magnetic material (e.g., in basin analysis, for determining the thickness and geometry of sedimentary packages) are the focus of interest. In general, the techniques for estimating source depths fall into two categories: those based on gridded data and those based on line data.

The techniques based on line data are computationally more efficient, because the methods based on gridded data commonly require a computationally expensive inversion of the data over the region of interest. As we are dealing with large data

sets at the regional scale, the logical choice was to use the techniques based on line data. The drawback of using line-based methods is the assumption that the sources of anomalies are two- dimensional and perpendicular to the strike of the line, which is generally inappropriate over the distances under consideration. When a structure is oblique to a given geophysical profile, the depth estimate is a maximum unless corrections are made for the true strike of the anomaly.

The techniques based on line data can be divided into two classes depending on the type of source body used as a model. Statistical techniques assume sources of random intensity distributed over a two-dimensional surface at depth. Deterministic techniques assume a model composed of two-dimensional sources of polygonal cross-section (e.g., dykes, edges, polygons, etc.).

The Phillips deconvolution technique (Phillips 1975; INTREPID 1998) uses a stochastic model and provides a solution independent of the more commonly used deterministic model. On the other hand, the Naudy method (Naudy 1971; INTREPID 1998) belongs to the class of deterministic techniques for automatic interpretation of magnetic profiles and utilises a dyke model, thin sheet, or edge model. We provide a comparative analysis of the two methods through a series of images for both the Camooweal 1:250 000 Sheet area and the whole NABRE region.

The data

We used two principal data sets in our investigation: aeromagnetic and Bouguer gravity (**Fig. 11** and **14**). The gridded data encompass areas of highly variable density and quality of data, thus integration, processing and transformation of the total dataset becomes critical to validating geological interpretations from them.

The aeromagnetic data are part of AGSO's national grid of magnetic values (Tarlowski et al. 1996a). This national grid has a cell-size resolution of 15 s of arc. Using the data from long aeromagnetic traverses (Tarlowski et al. 1996b), we relevelled the national grid during this investigation. A subset area between lats. 11 and 24ºS and longs. 126 and 141ºE was extracted from the relevelled national grid for use in this study.

The national grid was compiled from data that were recorded along lines mostly at a nominal height of 150 m above ground level and spaced 1500 m apart. Data for the northwest and northeast corners of the study region were acquired during aeromagnetic surveys flown in the 1990s along lines 500 m or less apart at an altitude of 100 m or less. These high-resolution data have been incorporated into the national grid. The interested reader is referred to the source diagram on the second-edition 'Magnetic anomaly map of Australia' sheet (Tarlowski et al. 1996a). The national grid of magnetic values represents the magnetic residual anomaly of the total field — i.e., the line data were reduced by subtracting the geomagnetic reference field for the given epoch and gridded. To the gridded values of the residual field, a constant of 5000 nT was added.

The gravity data are part of AGSO's national grid of gravity anomaly values (Murray et al. 1997). The national gravity grid has a cell-size resolution of 90 s of arc. The quality of the source data for the national magnetic and gravity grids varies over the NABRE region (c.f.,. Tarlowski et al. 1996a; Murray et al. 1997; or contact the custodians of AGSO's national data sets). No raw data are provided herein, but we present images of all the transformations that we discuss.

In addition to these two data sets at the cratonic scale, we used high-resolution aeromagnetic data for the Camooweal 1:250 000 Sheet area (a subset of the area of our investigation; between lats. 19 and 20ºS and longs. 138 and 139.5ºE). These

high-quality data, now on open file, were obtained from the Camooweal Ashton 1985 and Mammoth Mines Ashton 1984 surveys. Geoimage Pty Ltd compiled a grid of residual total magnetic values at a cell size of 50 m for the entire 1:250 000 Camooweal Sheet area. With kind permission from Ashton Mining Pty Ltd, the NABRE project purchased these data before their public release. In our investigation of the Camooweal area, we used the Geoimage grid at a cell size of 100 m for comparison with the lower quality data extracted from the national grid.

The models

We have combined the enhanced understanding of the geophysical data and comparison of the geophysical characteristics of the various transforms and surface geological data to derive a series of geological models, which are consistent with the observed geophysical data.

A geophysical elements interpretation derived from the images divides the region into broad tectonic provinces. The geophysical elements interpretation is extended to the subsurface and refined by developing regional traverse models. The geological packages that comprise the traverse models are extrapolated to interpretative thickness and depth-to-basement contour maps. The distribution and character of the packages form the basis for the development of a basement model, an ~1750 Ma crustal model and a basin distribution model.

Hypotheses relating to the crustal architecture, its influence on geological systems, and implications for crustal evolution are only briefly discussed. The geological models of this investigation are incorporated and extended to regional geodynamical hypotheses by integration with other regional data sets (e.g., geochemical and geochronological) to address some of these issues (Scott et al. 2000).

Geophysical transformations of magnetic data: their uses and pitfalls

Introduction

We chose a model consisting of two vertical prisms of finite extent for illustrating the effect of geophysical transformations on the signal of a magnetic source (**Fig. 1**). The prisms in this model are quite simplistic relative to the probable complexity of real magnetic sources in the geological record. Thus, they lack the geometry typical of geological structures — such as dipping bodies, stacked sheets or layered and wedge-shaped bodies that may contribute to an integrated TMI signal. In addition, the model fails to address such natural phenomena as gradients of physical properties through a single body. Nonetheless, the response of such a simple model helps us to understand the ambiguous nature of geological interpretation of geophysical data.

We chose to represent the two simple prismatic bodies in our model as occurring at different depths, and having overlapping responses, so we could investigate how some of the geophysical transformations of the data may help us discriminate between shallow and deeper sources of anomalies and improve our geological interpretation.

Contours of TMI show a steep gradient at the edges of the shallower body (2 in **Fig. 1**), but do not clearly define the edges of the deeper body (1). Indeed, contours cross three of the edges of body 1 at a high angle. At the contour level of detail shown in Figure 1, only one positive anomaly from the shallower source is contoured. Thus, an interpreter probably would not identify the existence of two separate bodies.

Without further constraining data, an interpretation of one or more faults or an elongate, possibly trapezoidal, possibly dipping body is equally valid.

According to the three-dimensional view of the magnetic anomaly response resulting from the prisms (**Fig. 2**), the difference in the magnitude of amplitude and the 'saddle' between the two peaks suggests two linked or overlapping anomalies; thus, the interpretation of two distinct bodies may be plausible. Even so, alternative interpretations like those mentioned above are still possible, and differentiation of the validity of any of them requires further transformation of the data and/or independent geological information.

We consider below the following transformations of the magnetic response of the two vertical prisms: reduction of total magnetic intensity to the magnetic pole; vertical and horizontal derivatives of the total field; analytic signal; and tilt of the horizontal gradient of the magnetic field.

Total Magnetic Intensity reduced to the magnetic pole

When dealing with two-dimensional magnetic data, an important step in data processing is to simplify the complex information contained in the original data. One such simplification is to derive a map in which the amplitude of the displayed field is directly related to the physical properties of underlying geological bodies. In the case of gravity data, a simple relationship between the density of the rocks and values of the gravity field exists. That is, the peaks of gravity anomalies are placed directly over the source bodies. Thus, in our simple model (**Fig. 1**), the simplest interpretation of our magnetic response would be a single body centred under the high-amplitude anomaly produced by the shallow body (2).

However, peaks of magnetic anomalies, especially in low latitudes, are offset from the source owing to the obliqueness of the inducing field. Therefore, it is desirable to transform the original data in such a way that anomalies are placed more symmetrically over the magnetic bodies. This repositioning of the peaks of magnetic anomalies is accomplished by the reduction-to-the-magnetic-pole (RTP) transformation (RTP; Mesko 1984).

Such a transformation enhances the perception of two bodies by accentuating two distinct peaks separated by a saddle (**Fig. 3**). The contrasting heights and gradients of the peaks are distinct, lending credence to the interpretation of two bodies of different depth and size.

One of the dangers of the RTP transformation lies in the assumption that an inclination of the inducing field is constant over the area of interest. This assumption is quite valid for small areas where the change in the direction of the inducing field is small, but is intrinsically incorrect for large data sets at regional scale. Thus, large areas must be subsetted and transformed and then restitched — a process that may introduce artifacts, particularly at joins.

Another limitation involves later remanent magnetisation. When the region of interest contains remanently magnetised bodies, the RTP transformation is not valid. Later remanent magnetisation will generally not be related to the same magnetic pole as original magnetisation and thus produces an asymmetric anomaly over a source that would produce a symmetric anomaly if no remanent magnetisation were present. Interpretation of reduced to the pole data can lead to non-valid geometric and therefore geological conclusions in the presence of remanent magnetisation.

Derivatives of Total Magnetic Intensity

An interpretation commonly benefits from an enhancement of the signal from a shallow source and a suppression of the responses of deeper magnetic bodies, or vice versa. Enhancing the edges of source bodies is also beneficial. A shallow source response is commonly suppressed by applying frequency filters to the data, because generally higher-frequency signals are associated with shallow sources. Frequency filtering of the response from our simple model is not treated here.

Suppressing the responses of deeper magnetic bodies and enhancing the response of body edges can also be accomplished by applying derivatives to the TMI signal. A TMI anomaly can be mathematically described as a function of three variables in Euclidean space; therefore, we can easily calculate derivatives of TMI the in x, y, and z directions (**Fig. 4, 5,** and **6**).

The z derivative (**Fig. 4**) — or the first vertical derivative, as it is commonly called — sharpens the peaks of anomalies resulting from shallow sources, and suppresses the responses of deeper sources. For simple, separate bodies with vertical sides, the first vertical derivative has a zero value over their edges, is positive over the bodies, and is negative outside. This attribute allows us to position our bodies in space, and make a qualitative assessment of the depths of the bodies by reviewing the extent to which the signal is changed by this transformation. The transformation also more clearly expresses the distinct duality of the sources in the model.

The x and y derivatives (**Figs. 5 and 6**) enhance the effects of edges of source bodies in the direction perpendicular to the direction of differentiation. It is worth pointing out that a differentiation is unstable in the numerical sense, and noise in the data is amplified by this operation. Geophysical transformations based on the derivatives of the signal must consider this effect.

Analytic signal of Total Magnetic Intensity

The analytic signal transformation incorporates both horizontal and vertical derivatives. The mathematical definition of the analytic signal is expressed pictorially in **Figure 7**. The x, y, and z derivatives are represented by three vectors in the x, y, and z directions, respectively. The analytic signal is expressed as a magnitude of the vectorial sum of these three vectors.

The analytic signal response exhibits maxima over magnetisation contrasts, and is independent of the inducing field and the magnetisation direction (**Fig. 8**). It is evident from Figure 8 that the magnitude of the analytic signal response is smaller for deeper sources than for shallower ones. However, the sense of the change of the magnetisation contrast is lost in the absolute value of the analytic signal, from which the susceptibility of a source body relative to that of its surroundings is indeterminate. This loss has significant ramifications for interpreting image data resulting from this transformation — as exemplified in the Camooweal case study (see below).

Tilt of the horizontal gradient of Total Magnetic Intensity

The tilt transformation of the horizontal gradient of total magnetic intensity — or, simply, tilt transformation (Miller & Singh 1994) — is similar to the analytic signal transformation; both are formed through a combination of vertical and horizontal derivatives of the TMI anomaly. The mathematical definition of the tilt transformation is expressed pictorially in **Figure 9**. The tilt transformation simply represents the angle between horizontal and vertical derivatives at the given point.

The tilt transformation deals with the ratio of the vertical and horizontal gradient, and therefore allows good resolution of shallow and deep sources. However, **Figure**

10 demonstrates that it may obscure the relative depths of two bodies by blurring the difference between the magnitude of the two peaks. It has the attractive property of being positive over the source, crosses through zero at or near the edge of a source with vertical sides, and is negative outside the source.

In contrast to the analytic signal transformation, the sign of a magnetic contrast is preserved. Thus, it is possible to determine whether a given source has higher or lower susceptibility than its surroundings — an important factor in geological interpretation, especially in igneous terrains. The contrast between resulting tilt and analytic signal transformation images is striking in the Camooweal case study (see below).

General considerations of transformations of Total Magnetic Intensity

The above review of geophysical transformations is not exhaustive. Our aim was to elucidate the physical meaning of some of the transformations that we have used in our investigations.

Although we used a simple model to analyse the effects of different transformations on the magnetic response, it has illuminated the strengths and limitations of each method. Depending on the geological model conceived, one or more transformations will do a better job than the others of producing a correlative image. Accordingly, it is prudent to perform a variety of geophysical analyses before attempting a geological interpretation. In addition, it is important to assess and compare the diverse effects of each transformation on the magnetic source response, and to test geological models (particularly with regard to boundaries) against their effects, when attempting a geological interpretation of the data. The following series of examples of transformations applied to a large regional dataset further reinforces the need to perform a series of transformations and tests of the data.

Geophysical characteristics of the North Central Australia study region

Introduction

The north central Australian study region (lats. 11–24ºS and longs. 126–141ºE) roughly corresponds to the north Australian mega-element and a small portion of the central Australian mega-element of Shaw et al. (1995, 1996; see also Meyers et al. 1996). Images supporting the following descriptions of geophysical data enhancements and transformations are presented in Simple Conic Projection with a central meridian at 132ºE and the standard parallels of 18 and 36ºS. The 1:250 000 Sheet graticule overlaid on the images helps to locate the anomalies.

Transformations

Total Magnetic Intensity

A TMI image for the region (**Fig. 11**) has a reprojected grid of 3677 rows and 4198 columns, and a grid cell size of 400 m. Using the HSI model with the rainbow colour lookup table, Pelton's hill-shading algorithm (Pelton 1987), and ERMapper software, we enhanced the image with a northwest illumination.

Long, linear N–S belts of long-wavelength positive and negative anomalies are prominent along the eastern margin of the image. The southern third is likewise characterised by ESE belts of anomalies that trend and splay and diffuse toward the ENE. Both zones, and another in the NW corner, appear to have an overall higher-frequency content than the central and northern interior zones.

Upward continuation of the Total Magnetic Intensity

A pseudocolour image (**Fig. 12**) represents the total magnetic intensity after upward continuation to the level of 500 m above ground level (INTREPID 1998). It has 1839 rows and 2099 columns, and a grid cell size of 800 m. This transformation is commonly used to subdue shallow sources and provide a better understanding of the deeper nature of the magnetic field. However, the transformation has not greatly changed the character of the geophysical response. The long linear belts of anomalies in the east and south are still prominent. Their extreme amplitudes suggest that they are caused by sharp, deep boundaries between bodies of greatly contrasting physical properties or deeply penetrating deformation of originally sheet like magnetic sources, in line with the geological understanding of these belts as intensely folded and thrusted terranes. The large positive anomaly at ~16ºS, 129ºE corresponds to basal Phanerozoic Antrim Plateau Volcanics, which can be mapped in outcrop as largely subhorizontal mafic igneous sheets. The small (at this scale) ellipsoidal anomaly just northeast of 18ºS, 138ºE has been modelled as a thrust sheet containing outcropping basic Palaeoproterozoic Seigal Volcanics (Leven et al. 1997).

Tilt of the Total Magnetic Intensity

The orientation of a feature in space is a function of its strike and dip. These are fundamental parameters of any geological model or map. By definition, the strike is the direction of the line of intersection between the Earth's horizontal surface and the plane containing the bed or body. The dip is the angle between the inclined bed plane and the horizontal, measured in a vertical plane perpendicular to the strike. The tilt of the gradient of the total magnetic intensity is a geophysical expansion of this common geological description to the magnetic data. As outlined above the tilt angle is defined as the ratio of the first vertical derivative of the potential-field to the horizontal gradient of the total field (Miller & Singh 1994).

This concept has been implemented by calculating the x, y and z derivatives of the TMI for the north central Australian region (INTREPID 1998), and then applying the formula described in the previous section. A pseudocode for implementing this transformation is presented in **Appendix I**.

A pseudocolour image showing the results of the tilt transformation applied to the aeromagnetic data for the whole north central Australian region (**Fig. 13**) comprises 3674 rows and 4197 columns and has a grid cell size of 400 m. It represents a different perception of the structural content of the anomalies. The internal structure within the magnetically consistent linear belts along the eastern and southern flanks is apparent. From this image, we can define more precisely the edges of the structures within monotonous zones in the TMI image.

Concomitantly, high-frequency-content noise added to the data is a major drawback of this transformation. Another problem, reflecting the joining of two data sets of contrasting quality, is apparent from the clearly different responses across a N–S transect at ~133.5ºE in the north central part of the image area, where the quality of the data is higher to the east. This effect is subdued in the TMI image.

The tilt enables the interpreter to determine the approximate horizontal location and lateral extent of the sources, both shallow and deep, by locating more clearly than the horizontal derivatives the edges of the source bodies. The geophysicist and geologist must collaborate closely to be able to identify these areas. As the tilt transformation is expressed as the ratio of two derivatives of the field, the noisy data or the difference in resolution of data between neighbouring regions can diminish the usefulness of the transformation. None of these problems appear to adversely affect consistently high-quality data over a 1:250 000 Sheet area — as seen in the Camooweal case study — so the tilt transformation appears to be a useful tool to add to the compendium of large-scale regional analyses of magnetic data.

Bouguer gravity

We have extracted the Bouguer gravity anomaly data for north central Australia (at the national grid resolution of 90 s of arc grid cell size), and reprojected it to Simple Conic Projection with a central meridian of 132ºE and standard parallels of 18 and 36ºS. The reprojected grid contains 587 rows and 670 columns, and has a cell size of 2500 m. A gradient enhanced Bouguer gravity anomaly image (**Fig. 14**), based on the HSI model with rainbow-colour lookup table, reflects the Pelton hill-shading routine with northwest illumination enhancing short-wavelength features.

Comparison of this image with the TMI and Upward Continuation of TMI images (**Figs.11** and **12**) demonstrates the different patterns seen in each type of data. There is apparently very little correspondence between anomalies of the gravity and magnetic data using these traditional treatments. In part, this is due to the depth of material contributing to the gravity response versus a much shallower limit of material contributing to the TMI.

Terraced Bouguer gravity

Terracing is a simple procedure for transforming a smoothly varying, continuous gravity (or magnetic) field into a stepped 'terraced' function composed of both steeply dipping and flat zones (Cordell & McCafferty 1989; see also Phillips 1992). The terracing operator uses the direction of the field's local curvature to produce a transformed field composed of uniform domains separated by abrupt domain boundaries; small variations within domains are neglected. The results of the terracing operation on the gravity field resemble conventional density mapping. However, the terraced function is a true step function and cannot be depicted by means of contour lines. This method is a suitable tool for creating a gravity domain map, without the bias or knowledge of an interpreter, in a form suitable for presentation and interrogation in a GIS.

The pseudocolour image (**Fig. 15**) represents Bouguer gravity anomaly after application of the terracing operator. The image contains 587 rows by 670 columns, and has a grid cell size of 2500 m.

Depth estimates of the magnetic sources at a regional scale

Introduction

Our main geophysical research objective has been to assess methods for estimating depths to magnetic sources for the north central Australia region. This is standard practice both in industry and for research, but rarely is the size of the dataset so large or complex in terms of both quality and content.

Techniques that have been developed for gridded data sets are still not capable of dealing with such a large variable grid efficiently and effectively. The Euler deconvolution method (Thompson 1982) is generally suitable for gridded data and can be used on large data sets. However, successful geophysical interpretation of the data often depends on experience with model studies to make appropriate starting assumptions, assign appropriate algorithm parameters and the availability of non-geophysical constraints. The methods based on 3D inversion (Chenot & Debeglia 1990; Oldenburg et al. 1997) are difficult to implement, and usually require an inversion of large matrices that is computationally expensive. Thus, we have used methods, which focus on line data.

The techniques for interpreting magnetic profiles can be divided into two classes depending on the type of source used as a model. Statistical techniques assume sources of random intensity distributed over a two-dimensional surface at depth. Deterministic techniques assume a model with two-dimensional sources of polygonal cross-section. We have applied two different techniques on a variety of filtered data for depth estimation in order to compare their results. A synopsis of this work in a series of images (**Figs. 16–21**) facilitates comparisons between them and with other data types and transformations.

The methods

The Phillips method (Phillips 1975) is a statistical technique, which assumes that the magnetic sources define a two-dimensional basement surface, and that a magnetic profile is measured in the horizontal plane above the surface. The direction of the profile is assumed to be perpendicular to the strike of the anomalies. The magnetic basement is represented as an aggregate of thin dyke-like bodies extending infinitely with depth and in the direction perpendicular to the profile. The observed magnetic anomaly along the profile is assumed to be a superposition of all anomalies produced by each of the dykes.

In order to estimate the depth to the source, an operator window of data is chosen. The rule of thumb is to choose a length of the window equal to the maximum depth to the sources along a profile, which must be assumed. Within the window, the anomaly is assumed to originate from a source at a single constant depth. According to these restrictions, the magnetic anomaly in the window can be represented as the convolution of the magnetisation function and an impulse response equivalent to the anomaly caused by a single dyke. Consequently, the autocorrelation function of the magnetic profile can be expressed as the convolution of the autocorrelation function of the magnetisation and the autocorrelation function of the impulse response of the single dyke within each window. The depth estimates for the whole profile are obtained by solving the convolution equation under the assumption that magnetisation is not correlated to a white noise sequence with a zero mean. Because the method is looking for a sheet-like boundary, it is conceptually more akin to the problem of solving the geological problem of identifying the magnetic basement of a sedimentary basin.

In Naudy's (1971) method, the orientation of the profile is perpendicular to the strike of geological structures in two dimensions. As the function can be separated into even and odd parts, the method is able to focus on just the even (or symmetrical) parts of magnetic anomalies within the profile. It uses a matched filter based on the anomaly over a tabular body (in most practical cases over a vertical or dipping dyke). This filter is then correlated with the symmetrical parts of the anomaly from the observed magnetic profile and the anomaly from the profile obtained by reducing the data to the magnetic pole. At each point along the profile where a high correlation is observed, the depth to the source, and often parameters such as dip and susceptibility, may be calculated.

As noted above for depth estimates of gridded data, the Naudy method requires an initial assumption of the geological model. Choices of models include: 1) dykes (used here); 2) thin sheets (vertical) or 3) thin plates (horizontal). Each starting assumption results in different absolute depths for a given anomaly.

In both methods, the assumption that the profile is perpendicular to the strike of geological features results in maximum depth estimates for a given anomaly. Corrections for true strike and dip will result in shallower estimates. Our choice of performing estimates on segments of the regional traverses has minimised this effect, however, the depth estimates obtained must still be considered only relative and not absolute.

Estimation of depths for north central Australia

We have used both the Phillips deconvolution and Naudy methods to estimate depths to magnetic sources for the whole region. The quality and the resolution of aeromagnetic data in the region vary. Some parts of the composite grid were obtained by digitising old contour maps from 1960; other parts were generated from modern surveys flown at a line spacing of 400 m and at an altitude of 80 m above the ground. The quality variability can have an undesirable effect of introducing artifacts, mainly along the edges of the surveys with different specifications. The altitude at which data have been collected has an effect on depth estimates because the response from shallow sources is suppressed more in high-flown surveys. Our objective of determining the general shape of sedimentary basins meant that we sought to suppress the influence of shallower sources. Thus, we filtered the gridded data by using a systematically varying low-pass filter. The original grid was smoothed, and the profiles for the analysis were extracted from the smoothed grid. We applied no filters (**Figs. 16** and **17**), a series of averaging filters (3x3, 5x5, 7x7, 9x9, and 13x13; ERMapper 1998) (**Figs. 18–21**)., and estimated the depths by both methods. Time restrictions and the sheer volume of data precluded us from analysing the aeromagnetic data directly from the flight lines. Instead of using line data, we have extracted profiles from the relevelled national aeromagnetic grid.

The magnetic profiles have been extracted from 1:1 000 000 subsections of the relevelled grid at a resolution of 15 s of arc. The extracted profiles are oriented N–S or E–W, depending on the prevailing strike direction of the geological structures in the 1:1 000 000 area. The space between the extracted profiles was equal to 120 s of arc or ~3200 m. For each subsection, profiles were reprojected from geodetic co-ordinates to Australian Metric Grid (AMG) co-ordinates. The two methods were applied to all profiles, and depth estimates to magnetic sources were obtained. The estimates were gridded using minimum curvature techniques, and reprojected from AMG co-ordinates to geodetic co-ordinates. The grid of depth estimates for the whole region was obtained by joining together individual 1:1 000 000 grids. The composite grid of estimates has been reprojected from geodetic co-ordinates to a Simple Conic Projection (central meridian of 132°E and standard parallels of 18 and 36ºS) for ease of comparison with other data sets and interrogation in conjunction with the available GIS geology coverage.

Figures 16 and **17** show the depth estimate images for the region according to the Phillips deconvolution and Naudy methods, respectively. Any comparison of these two images should take into account the conceptually different approaches of the two methods in estimating the depth to magnetic sources. The Phillips method estimates depth to magnetic basement (i.e., the depth to the boundary between sediments and basement rocks), whereas the Naudy method picks the top of vertical dyke-like bodies. The former method is conceptually more akin to our geological understanding of the region. However, in practice, the geological conceptual difference may be greater than the geophysical difference in the methods.

The results obtained by both techniques depend on the size of data window used for analysis, and the quality of the data. In our regional-scale analysis of depth to magnetic sources, we were primarily interested in the problem of finding outlines (boundaries) of sedimentary basins in the region; thus, accurate relative depths — not the absolute accuracy of the depth estimates — was the important information we wanted to obtain.

General considerations of the use of transformations

The use of transforms and various methods of estimating the depth to magnetic sources on large, variable quality regional data sets have been explored in this section. The tilt algorithm, sharpens the edges of magnetic sources, but introduces considerable noise. However, the introduced noise is relatively negligible when a high quality data set is available (see Camooweal section below).

Comparison of the depth images with a GIS coverage of igneous polygons, constraining the depth of the magnetic source to zero, suggests that the Phillips deconvolution technique shows a higher correlation to the shallow sources and is better for identifying smaller bodies and their subsurface extensions (**Figs. 22** and **23**). We find that the for the large variable quality study area, the Phillips method enhances the correlation of the magnetic data with the gravity data. This correlation between gravity and magnetic data is most useful when the objective is understanding the distribution of sedimentary basins.

Geophysical contributions to crustal studies

Introduction

The objective of our geophysical research is to enhance the ability of an interpreter to obtain geologically meaningful information. Of particular interest in the NABRE project is the distribution and geometry of sedimentary basins. We are most interested in the geodynamic evolution of these basin systems, and in aspects of their structure, geometry and development that may help constrain the location of mineral deposits.

The focus of the NABRE project has been the elucidation of the timing of the Palaeoproterozoic basin systems identified in the extensively mineralised Mount Isa, Murphy and McArthur regions (**Fig. 25**). The stratigraphic package of rocks spanning ~1730–1585 Ma is assigned to the Isa Superbasin, and the preceding package — thought to have been deposited between ~1800 and 1730 Ma — is referred to as the Leichhardt Superbasin (Scott et al. 1998a). Both packages contain primarily stratiform mafic igneous rocks intercalated with large accumulations of sediment. Regional episodes of felsic igneous activity during the evolution of both basin systems comprise some stratiform acid packages, but more commonly consist of separated but coeval felsic intrusive bodies of variable dimensions.

Although the main emphasis of chronostratigraphic investigations has focused on the Isa Superbasin, the NABRE project has also investigated the underlying Leichhardt Superbasin. An understanding of the architecture of the Leichhardt Superbasin is important, as it forms the regional basement to the Isa Superbasin. On the southern flank of the Murphy Inlier, seismic data and some outcrop of the two Superbasin packages help constrain the interpretation of geophysical data there (Scott et al. 1998b). Project work has also focused on refining correlations of units in the Superbasin packages between the Mount Isa and McArthur regions, and resolving the significance of the Murphy Inlier and its structural trends (Jackson et al. in press). Our attempt to interpret the geophysical images and to construct regional traverse and plan-view models is primarily concerned with speculating about the extent and nature of the Isa and Leichhardt Superbasins.

Geophysical elements

Variously transformed gravity and magnetic images of the NABRE area were interpreted with respect to domain, fabric, and lineament distribution. An example (**Fig. 26**) shows the interpreted fabric texture overlain on a greyscale Bouguer gravity image, and highlights areas of different frequency and style of anomaly. The resulting interpretations were used to construct a combined regional geophysical elements map (**Fig. 27**). This map reflects the main crustal features determined by Shaw et al. (1996), whose analysis focused on categorising the geophysical characteristics of crustal elements evident in the national geophysical data sets. The complex array of geophysical elements presented by Shaw et al. (1996) accentuates the variability of crustal and geological terranes. However, detailed correlation of geophysical signature to particular geological systems of specific regions was not the main aim of their study.

To help us understand the geophysical characteristics, we overlaid geopotential and geological coverages in a GIS (e.g., Martin et al. 1997; cf. **Figs. 22** and **23**). The overlay facilitates correlation of the magnetic and gravity signatures with surface lithological and structural features and their extrapolation into the subsurface. This exercise was particularly useful for identifying outcropping magnetic units in folded

packages, and for distinguishing subsurface geometries.

The geophysical data subsetted from the national magnetic and gravity grids **(Figs. 11** and **14**) correspond roughly to the north Australian mega-element of Shaw et al. (1996) and the north Australian craton of Meyers et al. (1996). The southwest corner of the data coverages impinge on the central Australian mega-element of Shaw et al. (1996) and the central Australian terranes of Meyers et al. (1996). As an alternative to the geophysical elements map of Shaw et al (1996), we have developed an elements map of north central Australia derived from the enhanced image data from the NABRE region (**Fig. 27**) according to a conceptual geological model which emphasises regional lithostratigraphic package distribution. The model extends the interpretation of stacked superbasins as derived from the sequence stratigraphic work of the NABRE project (Krassay et al. 1999; Southgate et al. 1999) and detailed study of the northern Lawn Hill Platform (Scott et al. 1998a; Bradshaw & Scott 1999).

We have divided the north central Australian region into the north Australian craton, and three flanking linear anomaly belts: the Halls Creek/Pine Creek belt (HC-PC), which separates the craton from the Kimberley Block (KB) in the northwest; the Arunta belt (AB), in the south; and the Mount Isa belt (MI), in the east (**Fig. 27**). The north Australian craton (NAC) comprises southern, central, and northern elements (E_S, E_C, and E_N).

Each of the linear flanking belts contains Palaeoproterozoic outcrop and is a focus of active exploration and research (e.g., Rutland & Drummond 1997; Shaw et al. 1996; Meyers et al. 1996; and bibliographies therein). Within the NAC, the Tennant Creek and Davenport regions (**Fig. 25**) also contain outcropping rocks of a similar age. Our research aims to promote an understanding of the geometry of the Palaeoproterozoic basin successions between these areas of outcrop. In particular, we develop a basement model and a crustal model to propose a tectonic architecture at the time of the initiation of the Isa Superbasin (~1730 Ma). We also derive a possible Isa Superbasin distribution model. Geodynamic and resource distribution implications of this model are only briefly discussed, but are more fully developed in an integration of this work with other regional data sets (e.g., geochronology and geochemistry) from the outcrop belts (Scott et al. in press).

The three major geophysical elements of the north Australian craton are elongate along a NW–SE axis, and separated by boundaries of similar orientation. They are truncated in the east by the north-trending MI element and in the west by the northeast-trending HC-PC element. They are subparallel to the AB element, to the south, from which a prominent salient juts into the central E_S.

The northern element (E_N) is characterised by high, very short-wavelength, randomly distributed 'pitted' gravity anomalies (**Fig. 26**), and a variable magnetic signature (**Figs. 11**-**13**) of both long- and short-wavelength high-amplitude curvilinear, linear, and areally equant anomalies. The boundary between E_N and central (E_C) elements, best determined from the gravity data corresponds with a steep gradient from an area of gravity high to the north-northeast and gravity lows to the south-southwest (**Fig. 14**). The steep gravity gradient trends northwesterly and steps northeasterly en echelon towards the east.

The central element (E_C) is characterised by generally low gravity anomalies compartmentalised by slightly higher diffuse elongate gravity anomalies that trend northeast to east-northeast and are interpreted to be three major transverse structures or zones (WXFR, CXFR, and EXFR; **Fig. 27**). These transverse structures compartmentalise each element into western (1), central (2) and eastern (3) domains. The magnetic signature of the central element is also variable, and is characterised

by long-wavelength anomalies. Lineaments trending northeasterly dominate those of several other orientations. Northeast-trending diffuse magnetic highs in E_C appear to correspond to the jogs in both the northern and southern boundaries of the central element.

The boundary between the central (E_C) and southern element (E_S) also trends northwesterly and steps northeasterly en echelon towards the east. The boundary between E_C and E_S is less distinct in the pseudocolour gravity image. However, it marks a change from a 'smooth' long-wavelength anomaly character in the central element to a 'pitted' short-wavelength and curvilinear anomaly character in the southern element, evident in both the regional greyscale Bouguer gravity and magnetic images. An overall increase in average magnetisation across this boundary into E_S is evident in the psuedocolour TMI image (**Fig. 11**).

The southern element (E_S) is characterised by moderately high Bouguer gravity values, higher than E_C, but lower than E_N (**Fig. 14**). Widespread high magnetisation in the east of the element contrasts with prominent low magnetisation in the west. A prominent NW–SE fabric is apparent in the magnetic data in the west, whereas an east–west grain appears to characterise the eastern portion (**Fig. 13**).

Conceptually, the gravitationally low central element, E_C, corresponds broadly to a structurally interconnected basin system wherein thick Isa Superbasin equivalents may have accumulated. Depositional sub-basins may or may not have been connected. Our modelling attempts to identify areas where thick accumulations of the Isa Superbasin equivalent packages may overlie well developed Leichhardt Superbasin equivalent packages. The relationship between the two superbasins in the model is analogous to that interpreted for the northern Lawn Hill Platform (Scott et al. 1998a; Bradshaw & Scott 1999) and mineralised areas (e.g., Mount Isa and McArthur River deposits) to the north and south. That is, the two superbasin successions are conformable in places and juxtaposed in a high-angle unconformity elsewhere. The scale of our geophysical modelling is not overly sensitive to the variation in angle between the superbasin packages. The cross-sectional models are forward calculated and compared to the observed magnetic anomaly pattern. Extrapolation of the geometry of the packages in the traverses to thickness and distribution maps also provides possible insights into the development of these two superbasin packages.

Traverse Models

The data and method

We extracted eight traverses from the regional gravity, magnetic, and depth-to-magnetic-source images (**Fig. 27**). The arc-grid cell-size resolutions we used are 90 s for the regional Bouguer gravity grid, 15 s for the regional residual TMI grid, and 60 s for the regional depth-estimates-to-magnetic-basement grid (**Fig. 19**). The extracted traverses of gravity, TMI and depth estimates were reprojected from geodetic co-ordinates to Simple Conic Projection with two standard parallels of 18 and 36°S. The values of gravity, TMI, and depth estimates along traverses were interpolated to 2500 m step size, to maintain consistency in the locations of features for each dataset along the traverses.

Four of the traverses are oriented SW–NE, to provide dip sections across the primarily NW–SE geophysical fabric of the north Australian craton elements (**Figs. 28–31**). The other four are oriented NW–SE, three of them as strike lines through each of the elements (E_N, E_C, and E_S) and the fourth to tie the grid to the Arunta belt

where some pertinent information is available (**Figs. 32–35**). We constrained the traverse models by extrapolating geological mapping data at 1:2 500 000 scale (BMR 1976a, b, c) into the subsurface, and by incorporating information about the thickness of the packages for each outcrop belt from the literature.

The traverse models comprise 'basement' blocks overlain by five broadly stratiform lithological packages, each with similar internal bulk properties (discussed in detail below), and emphasise structural features extending to the basement–cover interface. Using the commercially available Potent© software, we forward-modelled the constructed traverse models by calculating their expected magnetic responses for comparison with the observed data. We modified the geometry of the traverse models interactively until we accomplished a 'best fit' to the observed geophysical data, and iterated the geometric changes to maintain consistency at traverse intersections and with geological information.

One of the limitations of Potent© is the maximum number of points along the traverse that can be used for inverse modelling. As the length of the traverses ranges from 1000 to 1800 km, we divided each traverse into four sections to take into account likely variations in the magnitude, inclination, and declination of the inducing field over distances of 250–450 km. We assigned values of these parameters appropriate to the mid-point of each traverse section.

The constructed traverse models were too large and complex for Potent© to derive consistent results in forward-calculations of their gravity responses. Accordingly, we constructed simplified traverse models to test the general compatibility of the models against the observed gravity. The observed gravity data profiles are plotted on all the geological models (**Figs. 28–35**) for direct comparison. The gravity response calculated for the simplified models is illustrated only for traverse 1 (**Fig. 36**, cf**. Fig. 28**). Simple models of all the traverses produced similar results (not shown).

The estimated depth curves derived from the application of the Phillips method to the extracted profile data are also shown. The depth estimates along the extracted grid data profiles are not everywhere consistent with the geology in the traverse models. Failure to accurately define a single source may be a function of the TMI signal reflecting an integration of responses due to different magnetic properties and sources. In addition, the data are not truly 'line' data as acquired, and represent an integration of data of different quality and acquisition parameters. The scale of the models may also be a factor, for we have used 'bulk properties' rather than individual unit magnetisation values. Finally, not all boundaries or structures in the traverse models are perpendicular to the strike of the profile, but this has not been accounted for in the depth estimates, which were calculated prior to the construction of the traverse models. However, comparison of **Figures 11, 14 and 19** demonstrates the usefulness of calculating depth estimates on large regional, gridded data sets for integration with gravity data and delineating sedimentary basins.

The construction of realistic geological models for evaluating observed geophysical data requires the incorporation of all available constraints, but even in the best scenario there are always multiple models that may fit the observed data. The important variables the interpreter must constrain include the physical properties and geometry of bodies, the scale of the model, and the detail of the geophysical signal. The traverses (**Figs. 28–35**) range from 1000–1800+ km long. They are presented at a severe vertical exaggeration (~18:1) for complete viewing on a standard screen. Thus, features need to be stretched considerably in the mind's eye to obtain realistic geometries of boundaries between packages.

The interplay between the physical properties and geometry of the geological

bodies means that the dip of model boundaries is commonly not unique. As noted by Leaman (1994), the calculated curve is extremely sensitive to the subtended angle within a wedge-shaped or trapezoidal magnetic body. Likewise, the best-fit dip of a boundary between two bodies with different physical properties depends on the magnitude and sign of the contrast between those properties. Assigning physical properties to unsampled bodies is always an assumption. Another problem is that any physical property of a geological body is more likely to vary across a gradient than be consistent throughout (e.g., from alteration halos). The ability to assign gradients of physical properties to single bodies was not available in this study. Finally, the scale of the traverses precludes the construction of geological models at any great detail.

Stratigraphic constraints for the traverse models

The five broadly stratiform lithological packages represented in our models loosely correspond to pre-Isa Superbasin (packages 1 and 2); Isa Superbasin ± generally thinner Meso- and Neoporoterozoic units (package 3); and post-Isa Superbasin (packages 4 and 5).

Packages 4 and 5 consist of basal Phanerozoic mafic igneous packages (e.g., the Antrim Plateau Volcanics; package 4) and undifferentiated Phanerozoic sedimentary units (package 5). They are incorporated in the models because the units they represent are components of the surface geology, but are otherwise not considered in this study. Correlating package 4 with shallow long-wavelength anomalies in the west (see previous section on **geophysical characteristics**) has influenced — indeed, constrained — our use of stratiform bodies to underlie them.

The following table provides some examples of the age and types of geological groups included in the packages:

Package	**Examples**
Basement (Yellow & Pink)	Non-strataform material older than ~1800 Ma with low susceptibilities (e.g., Granites of the Tanami region; Kalkadoon Granite; Nicholson Granite Complex)
Package 1 (Blues)	Archaean (e.g., Rum Jungle and Billabong complex through Leichhardt Superbasin and equivalents (e.g., Haslingden Group; Tawallah Group); deeply emplaced mafic intrusions or 'underplating'
Package 2 (Orange)	Strataform felsic material ~1900-1800 Ma (e.g., CliffdaleVolcanics, Scrutton Volcanics, Bottletree Formation)
Package 3 (Green)	Isa and Roper Superbasin and equivalents (e.g., Mount Isa Group; McNamaraGroup; Roper Group; South Nicholson Group; Victoria River Group)
Package 4 (Purple)	Early Phanerozoic mafic units (e.g., Antrim Plateau Volcanics; Pica Pika Volcanics; Helen Springs Volcanics)
Package 5 (Yellow)	Undifferentiated Phanerozoic strata

All the lithological packages, except those in the basement, are assumed to have been generally stratiform before the deformation shown in the models (e.g., southeast end of traverse 6, **Fig. 33**). This assumption is consistent with the surface observation of the long-wavelength anomaly produced by the subhorizontal sheet-like Antrim Plateau Volcanics, and with the outcrop of thick successions of intercalated strata and igneous rocks which represent the Proterozoic rocks of interest. Within the north Australian craton, intrusives coeval with basin development of any age can be represented simply as a shallowing of the basement package, because their physical characteristics are probably similar to those of the basement, as discussed below.

Although minor variations in the susceptibilities within a package are permissible according to surface geological observations, the susceptibility assigned to a package is held relatively constant throughout the model to limit the geometric options. The bulk properties take into account published global ranges and averages of individual rock types (e.g., Telford et al. 1994), and the measured rock properties of some of the outcropping rocks in the region.

Remanent magnetism and its effects in constraining models

The basement package in the models comprises four subgroups which are all assigned low susceptibilities. The main variable in the basement model is the assigned remanent magnetisation. Natural remanent magnetism (NRM) originates from a variety of sources — including thermal, chemical, detrital, and viscous magnetisation (Butler 1992). It commonly contributes to the total magnetisation, in both amplitude and direction. Its effect, however, is complicated by the magnetic history of the rocks. The need to incorporate the effect or contribution of remanent magnetisation to the total magnetisation in interpretation has long been recognised (e.g., Hood 1963). Though the use and distribution of remanence is not commonly acknowledged in published models, several case studies have documented the occurrence and importance of remanence in Precambrian terranes globally (e.g., Lidiak 1974; Coles & Currie 1977).

There is ample evidence, outlined below, that significant and widespread remanent magnetisation occurs in north central Australia. A regional analysis of magnetic data from the McArthur, Murphy and Mt Isa regions included the use of remanent magnetisation, but details of its distribution, magnitude and contribution to the total magnetisation are lacking (Leaman 1998).

For the southwestern Arunta belt and Cloncurry basement areas, Mutton & Shaw (1979) concluded that remanent magnetisation is ‘frequently a significant factor in total magnetisation‘. They identified no ‘non-magnetic granites’ [sic] in their study, and attributed the magnetic contrast between crustal blocks in the Arunta belt largely to differences in the remanent magnetisation of the various rock types (e.g., granulites and granites versus gneisses). A more recent analysis of a much larger sample set confirms the widespread contribution of remanence, and particularly anomalous remanence, in gabbros in the southeastern Arunta belt (Whiting 1988).

Whiting’s (1988) evaluation of over 2400 measurements on rocks from the southeastern Arunta belt addressed the geological processes contributing to the magnetic properties of major rock groups. From his database, Whiting concluded that SiO_2 content is the primary factor in magnetic differences between rock bodies. A further, prominent contribution to the nature and distribution of magnetic properties is due to late-stage alteration, metamorphism, and changes in oxygen fugacity. Owing to the widespread distribution of metamorphism and alteration in outcropping

Proterozoic belts in north central Australia, we believe that a considered use of remanent magnetisation is appropriate in the interpretation of regional magnetic data.

Kelso et al (1993) analysed ~200 samples from the Arunta belt for their rock magnetic properties. According to their results, granulites are highly remanently magnetised (median value of 4.1 A/m and Koenigsberger ratio of 7.2) and contribute greatly to the long-wavelength anomalies. This study of remanent magnetisation has guided our assignment of values for this parameter.

Rocks with strong remanent magnetisation, including sedimentary rocks, are cited in measurements taken from the Pine Creek region (**Fig. 25**; tables 2 and 3 in Tucker et al. 1979). Directions of remanent magnetisation in this region are considered close to present-day geomagnetic directions, whereas directions in the Arunta region to the south are highly variable and largely reversed (Mutton & Shaw 1979; Whiting 1988). Tucker et al (1979) noted that the mean net magnetisation for the Pine Creek area is fairly low and uniform, but that basic igneous rocks (e.g., Zamu Dolerite), normally considered to be highly magnetic, are less magnetic than the surrounding sediments. This study also yielded information about the magnetic properties of known Archaean rocks.

Especially relevant to our investigation is a database compiled by Hone et al. (1987), whose report documents measured physical properties of rock samples from the Mount Isa Inlier. The database includes 193 samples representing most of the sedimentary and volcanic units occupying the Isa and Leichhardt Superbasins and the underlying successions (op.cit. table 4). It also includes (op. cit., table 5 and 6) 14 analyses of mafic intrusives and 87 analyses of granites of diverse ages. Remanent magnetisation is ubiquitous in the samples analysed by Hone et al., whose data highlight the variability of physical properties — even within a single unit: variations amount to two orders of magnitude across as little as 10-m intervals in both sedimentary and volcanic packages. Hone et al. (1987) also noted a contrast in magnetic properties of granites within the older Kalkadoon Granite and all other granites in the region.

We have used the measured property values from the cited sources as guides to assigning bulk values in the models presented here. The physical properties are within the range and consistent with the measured values. Notwithstanding that, we emphasise that the geological models derived from the geophysical data are not unique, primarily because the assumptions that we made in assigning physical properties to such large-scale systems. The following descriptions are general, and intended only as a guide and starting point for more detailed investigations. Some alternatives that we tested proved to be adequate, and, where they pertain to the geological interpretation, they are discussed in the following text. In addition, the scale of the models limits the precision to which individual faults are located.

Basement model

The interpreted basement model in north central Australia (**Fig. 37**) can be broken into two main categories: high- (types 1–4; 2.0-4.0 A/m) and low- (types 5–10; 0–1.5 A/m) intensity remanence. The high-remanence area encompasses the western and southern margins and the southwestern third of the region. This configuration is consistent with observations of high remanence in the Arunta belt (Whiting 1988) and Granites–Tanami region (Mutton & Shaw 1979). The basement model suggests increasing remanence intensities to the southwest (types 1 and 2).

Our ultimate aim is to assess the nature of the crust at the initiation of the Isa Superbasin at ~1730 Ma. Meyers et al. (1996) recognise this period as the

culmination of a major, two-phase orogeny (Strangways). Thus, we have assigned remanence with a dip and azimuth thought to be consistent with an age of a ~1730 Ma remagnetisation throughout most of the model on the assumption of a pronounced geomagnetic polarity bias in that period (M.Idnurm, AGSO, personal communication, 1998). We have assigned a different ('older') remanence azimuth and dip directions to the Kimberley Block (type 4) in accordance with observed differences in the directions noted in previous studies (e.g., Tucker et al. 1979; Mutton & Shaw 1979).

The area of low remanence intensity extends over most of the North Australian Craton, underlying all of E_C and E_N and the eastern portion of E_S. Small bodies of this type of low remanence intensity basement are included in the model as perched (**Fig. 28** at ~400 km and **Fig. 35** at ~400 km) or possibly late-stage intrusions (**Fig. 29** at 0-400 km). The interpretation of additional magnetised bodies beneath these smaller granitic bodies and the association of high remanence bodies with negative magnetic anomalies are consistent with the findings of Mutton & Shaw (1979). The depth to the top of the basement package contour map (**Fig. 38**) is highly generalised and is only indicative of the depths to which strataform packages are likely to be present.

The deepening of the contours in belts coincident with the HC-PC and MI belts reflects the highly deformed nature of these areas. Although variations in the MI belt as modelled (e.g., SE end of Traverse 6, **Fig. 33**) appear extreme, when the vertical exaggeration is removed the geometric framework is reasonable for crustal scale folding and faulting. There is only a general correspondence of this contouring with the interpreted elements within the North Australian Craton. However, a case can be made for a corresponding deepening of basement in the western compartment of E_C, a relative high corresponding to the central compartment of E_S and a relative high corresponding to the eastern transverse boundary (EXFR) along its northern end. A central N-trending alignment of contours (arrows in **Fig. 38**) corresponds to a geophysical division recognised by Shaw et al (1996) and a tectonic division recognised by Meyers et al (1996) in their 1830-1700 Ma reconstruction. The basement model can be subdivided into more specific pre-Isa Superbasin crustal types (**Fig. 37**) on the basis of its combination with the overlying Packages 1 and 2 discussed below.

Crustal Model at ~1730 Ma

Package 1 is the most conceptually diverse package. It is a wide-ranging set of possible underlying lithologies to the Isa Superbasin and equivalents. In the south, it corresponds to outcropping Archaean or Palaeoproterozoic successions which are intercalated with younger Proterozoic successions in a complex thrust and fold belt (e.g., SW ends of Traverses 1 and 2, **Figs. 28** and **29**). At about 300 kms on Traverse 3 (**Fig. 30**), it is undifferentiated highly deformed and sheared Archaean to Palaeoproterozoic rocks. In the northern portions, the form and position suggests this package may be underlying Archaean or early Palaeoproterozoic basins (e.g., central portions of Traverses 2, 4 and 6, **Figs. 29**, **31** and **33**, respectively). In the north and particularly the northwest, the thickness and extent of the bodies of Package 1 may suggest some occurrence of modified 'underplating' as envisaged by Etheridge et al (1987). This package has the highest susceptibilities of all the strataform packages. It is only about half of "average" mafic igneous material (Telford et al. 1994) reflecting our concept that it contains a significant proportion of sediments with low or negligible susceptibilities. It has been assigned slightly lower susceptibility and remanence intensity in the south to reflect the largely sedimentary composition of the package in

that region.

Package 1 has been assigned moderate to low remanence intensity depending on the magnitude of susceptibility. The assigned remanence has the same azimuth and dip parameters as the basement to reflect its conceptual and stratigraphically older age than the ~1730 Ma remanence. Thickness contours of all of Package 1 are provided in **Figure 39**. A large zone where Package 1 does not occur cuts the area in a N-S direction from the Gulf of Carpentaria to EXFR within E_C. The zone then bends west through E_S, cutting the western half of area and encompassing the entire Kimberley block. The N-S zone corresponds roughly to the Batten Trough (see Traverse 5, **Fig. 32**). An excursion of non-occurrence into the western compartment of E_C corresponds to a "deep" in the depth to basement contours (**Fig. 38**).

Package 2 is restricted to the NW quadrant (**Fig. 40**). It is generally strataform (e.g., Traverses 1, 5 and 6, **Figs. 28**, **32** and **33**, respectively) but on Traverse 7 (**Fig. 34**) it has a "rooted" geometry which may represent a source area for this package. Alternatively, this geometry may represent deep deformation. This package overlies Package 1 bodies where they are characterised by relatively high susceptibility, moderate remanence intensity and are very thick (i.e., those conceived to contain 'underplating') as seen in **Figures 28**, **32** and **33**. However, on Traverses 1 and 6 Package 2 also underlies Package 1 bodies where they are thinner. This geometry reflects the dual character of Package 1 rocks, which may span a substantial period of time. It is also consistent with our conceptual view that Package 2 may represent felsic volcanics older than the Leichhardt Superbasin and its equivalents, but would still overly Archaean crust or underplated material.

Package 2 has unusual physical properties in that it has quite low susceptibility and high remanence intensity. The presented traverse models have been chosen on the basis of the simplest geological model that produces a good fit and is consistent with outcrop geology. However, small bodies of Package 2 in some instances can replace elevated basement with as good a fit to the observed data. For instance, at around 900 km on Traverse 4 (**Fig. 31**), the profile extends across the extension of the outcropping Murphy Inlier. A small body of Package 2 can replace the shallow basement shown, producing as good a fit (see geophysical profile models in Scott et al. 1998a). On the basis of this trial, we infer this package to comprise felsic igneous rocks which were significantly modified during the ~1730 Ma remagnitisation, perhaps of similar characteristics to the Cliffdale Volcanics and Nicholson Granite Complex of the Murphy Inlier region (Grimes & Sweet 1979).

Combining Package 2 and moderate remanence intensity, thick Package 1 results in the thickness contour interpretation presented in **Figure 41**. This map provides a picture of the substrate to Package 3 and thin Package 1 that is not basement. The distribution of the combined substrate shows a strong correlation to the low remanence basement. The N-trending corridor where 'older' Packages 1 and 2 do not occur is a striking feature of this interpretation (**Fig. 39**). Outside of this corridor, a zone of slight thinning of the combined package occurs over E_C and E_N, along a NW trend. The zone is very subtle and not precisely coincident with the central element. The interpretative contours suggest a thinning over the western transverse structure (WXFR). The "rooted" style of Package 2 noted earlier produces a significant local thickening which appears to coincide with the intersection of the boundary between E_C and E_S and the central transverse structure (CXFR).

Combining Packages 1 and 2 with the basement package allows for a subdivision of crustal types within the low remanence intensity area of the North Australian Craton (**Fig. 37**, Types 5-10). This crustal model is consistent with the observed data

and suggests a highly heterogeneous crust that influenced the evolution of the Isa Superbasin.

Discussion

The purpose of the modelling is to predict the distribution, character and underlying crustal architecture of the Isa Superbasin and, to a lesser extent, the Leichhardt Superbasin. An understanding of the pre-existing crustal architecture is paramount to understanding basin-forming mechanisms and subsequent basin evolution.

The subdivisions of the crust shown in **Figure 37** suggest that the crust in E_N is composed of a different set of bodies from that of the central (E_C) and southern (E_S) elements. The thick Package 1 (crustal types 7 and 8) that possibly includes an 'underplating' or deeply emplaced mafic unit(s) occurs primarily in this northern element. The distribution of crustal elements in the model is largely dependent on the distribution of Packages 1 and 2 and differences in the remanence intensity of the basement.

The interpreted distribution of Packages 1 and 2 appears to correspond to the area of high-frequency, high magnitude Bouguer gravity anomalies (c.f., **Figs. 14** and **26**) and thus could be validly interpreted to be elevated Archaean crust. The Archaean crust interpretation is supported by limited Archaean outcrop (e.g., the Rum Jungle complex in the NW). The traverse models and thickness contours of Package 1 show that the high density area has thicker Package 1 than elsewhere. The thickened Package 1 can be interpreted in several ways. It may represent well-developed (thick), fairly shallow magnetic igneous units and/or highly magnetic sedimentary successions. Alternatively, it may comprise thinner, deeper mafic intrusions with very high susceptibility (e.g., 'underplating' or Archaean crust) overlain by relatively non-magnetic packages. As much of the Palaeoproterozoic and limited Archaean outcrops have relatively low magnetic susceptibilities, the model of 'underplating' has some appeal. Likewise, this interpretation lends itself to compatibility with the high density model required by the gravity data.

The development of northerly and easterly structural trends has been postulated for a mid- to early 1800 Ma event (Etheridge et al. 1987). These structural trends are also documented during the development of the mafic units in the Leichhardt Superbasin (~1790-1750 Ma) (Bain et al., 1992). The following features of Packages 1 and 2 derived from the modelling are consistent with these geological constraints.

The N-trending zone where Packages 1 and 2 do not occur is restricted to the central compartments of E_N and E_C. This corridor corresponds roughly to the Batten Trough. This model contrasts with models proposed by Leaman (1998). Leaman's (1998) model through the McArthur Region contains a thickened volcanic succession older than or belonging to the Leichhardt Superbasin equivalents throughout and suggests an even thicker volcanic package within the trough. The apparent rapid thinning of the mafic units in the Leichhardt Superbasin towards the NW in the outcrop belt across the Murphy Inlier (Jackson et al. in press) and the lack of any outcrop evidence in the McArthur region of a thickened magnetic unit of any age suggests that the relatively good fit of Leaman's (1998) models may be due to a) different treatment of the geophysical data (e.g., no removal of regional trends, profiles taken from an earlier version of the national dataset) or b) very different physical properties of bodies.

The regional geophysical trends in the Mount Isa belt (MI) are also N-trending. However, the extensive anomaly belts are comprised of en echelon NW- and NE-trending segments, suggesting the regional northerly trend pre-dates the en echelon

offsets.

Subtle thinning of the combined Packages 1 and 2 in the interpretation in **Figure 41** occurs through parts of the central element, but its correlation to the compartmentalisation caused by the NNE transverse structures is stronger than a correlation to the elements. Trends of the contours are dominantly N-NNE in the north. Strong NW-trends in the south are associated with the AB and EC boundary. The N trend appears to terminate against the NW trend. The interpretation of ~N and ~E trends involving Packages 1 and 2, suggests that this fabric was largely imposed on the pre-Isa Superbasin crust.

The portions of Package 1 that are thinner and represent Leichhardt Superbasin equivalents occur simultaneously with the thick Package 1 in crustal type 8 in the western compartment of E_N. Here a thick Package 2 is also included in the pre-Isa Superbasin bodies. The thinner Package 1 and Package 2, combined with low remanence basement occurs only in the west (i.e., crustal types 8 and 9). low remanence basement with solely Package 2 (i.e., crustal type 10) occurs only at the intersection of the western transverse structure (WXFR) and the boundary between E_C and E_S. West of a broadly NE-SW zone characterised by no intervening packages between low remanence basement and Package 2 (i.e., crustal type 5) both E_C and E_S are characterised by only the thinner Package 1 and low remanence basement (i.e., crustal type 6). Thus, the model suggests substantial heterogeneity within the crust to explain the focussing of possible major basin bounding and transverse structures. The heterogeneity of the model predicts a highly variable thermal and mechanical lithosphere prior to the development of the Isa Superbasin.

Isa Superbasin Model

Package 3 is conceptually the Isa Superbasin and equivalents (+/- overlying Neoproterozoic) throughout the North Australian Craton. It has been assigned quite low susceptibilities, with minor variations to reflect information regarding outcrops of virtually non-magnetic Neoproterozoic and Mesoproterozoic packages (e.g., ~700 km on Traverse 6, **Fig. 33**), outcrops with minor to moderate volcanic intercalations (e.g., ~800-1100 km on Traverse 1, **Fig. 28**) and outcrops with a higher volcanic or highly magnetic sedimentary content (e.g., ~700-1300 km on Traverse 5, **Fig. 32**). As Package 3 is conceptually co-eval or younger than the inferred ~1730 Ma age of regional remagnetisation, no remanence is assigned to it.

As we have used bulk properties to define the large, diverse packages (i.e., Packages 1-3, there is every possibility that Package 3 bodies in the models also incorporate upper Leichhardt Superbasin non-magnetic sedimentary units. Conversely, where Package 1 is relatively thin and of similar geometries to Package 2, (e.g., Traverse 4, 300-1000 km, **Fig. 31** and Traverse 7, **Fig. 34**), Package 1 may represent a basal magnetic unit to the Isa Superbasin or broadly conformable Leichhardt Superbasin magnetic units. Thus, the geometrical configuration of fault blocks and boundaries between Packages 1 and 3 and the angular relationship between the packages cannot be precisely defined on this scale of the traverse models.

Figure 42 represents the distribution and generalised thickness characteristics of Package 3 within the North Australian Craton. Package 3 rocks of the flanking belts are not considered in this interpretation as they are highly deformed and original thickness cannot be ascertained. “Deeps” or thicker preserved accumulations appear to correspond to the central and western compartments of E_C. Thinner zones show reasonable correlation to E_N and E_S and the transverse structures. However,

relatively localised, presumably fault related thickness (e.g., see variations between 400-600 km on Traverse 6, **Fig. 33**) also occur in the eastern compartment of E_S.

Assuming the above discussion of crustal types and their correlation to the structural inferences from interpreted elements of the North Australian Craton are valid, an interpretative thickness/structural map of the Isa Superbasin system can be produced (**Fig. 43**). In this interpretation, the thicker 'underplating' Package 1 bodies are not included.

Faults are drawn near element boundaries where suggested by interpolation of Package 3 thicknesses. That is, we assume element boundaries may be likely zones for focusing of later structural reactivation. Their coincidence with closely spaced or sharp orientation changes of thickness contours supports this view. We make no claim for the precision of the location of major bounding faults. However, we put forward the hypothesis that depocenters or sub-basins where thicker Isa Superbasin successions may occur are within and at the boundaries of the central element and near or along the transverse structures (EXFR, CXFR and WXRF). Isopachs of Package 3 predict thickened Isa Superbasin successions particularly in the western compartment of E_C (**Fig. 43**).

The type of intracratonic sub-basin or depocenter that developed is dependent upon the orientation of the pre-existing heterogeneity to the regional Isa Superbasin stress regime (e.g., there may be a likelihood of strike-slip sub-basins along the transverse structures, whereas growth into normal faults may be localised at element boundaries for N directed intra-plate stress). The transverse structures may also have been the locus for the intermittent igneous intrusive episodes. Both of these hypotheses have implications for fluid flow and mineralisation models by making predictions where both lateral and fault controlled fluid flow is most likely and where anomalous thermal conditions may reach the basin sediments.

Some of the isolated, localised, fault-bounded thickness anomalies that occur along the boundary of E_S and AB appear to relate primarily to Package 1 (e.g., Traverse 2 at about 500 km, **Fig. 29**). The interpreted faults have a distinctly different orientation from those bounding the compartments of the NAC. These thickness anomalies may therefore relate more to a pre-Isa Superbasin system.

The elongated N-S thickness anomaly in the MI belt in the east probably has more to do with tectonic thickening by later deformation of Packages 1-3 by folding and thrusting than with depositional thickness variations. It is therefore difficult to isolate the development of either superbasin with geophysical data.

The Murphy Inlier is associated with the intersection of EXFR and the central and northern elements boundary and as noted above can be successfully modelled using the two Superbasin concept (Scott et al, 1998a). Detailed work in this area, constrained by seismic reflection data, has refined the variable geometric relationship between the two superbasins and demonstrated the rapid changes in thickness of each of the superbasins in these intersecting zones (Bradshaw & Scott 1999; Jackson et al. in press). The area is associated with the world class Century Pb-Zn deposit. The models developed here predict the location of thick Superbasin successions elsewhere in the NAC. This prediction, combined with their inferred association with crustal scale structures and areas of anomalous thermal conditions, suggests there is potential for mineralisation similar to that in the Mount Isa and McArthur regions elsewhere in the craton.

The coincidence of the timing proposed for the superbasins and the Strangways Orogeny by Collin & Shaw (1995) suggests there is a geodynamical link between the events. Basin-forming mechanisms associated with orogenic belts range from flexure

of the lithosphere (e.g., Quinlan & Beaumont 1984; Molnar & Lyon-Caen 1988; Cobbold et al. 1993) to extensional systems behind the evolving orogenic belt (e.g., Dewey 1988; England & Houseman 1989). It is not within the scope of this report to develop geodynamical models. However, this study is integrated with other available data at the regional scale in Scott et al. (in press) for this purpose.

Camooweal High Resolution TMI Data set: a case study

Introduction

The Camooweal study area extends from 138 to 139.5°E and from -19 to -20°S. The main objectives of this geophysical study were to test the tilt algorithm against more traditional transformation methods on a high-resolution large-scale dataset and to better understand the effect of data quality on the depth estimates methods. Thanks to industrial interest in this objective and release of confidential (at the time) data from Ashton Mining Ltd., we had at our disposal two data sets for Camooweal. The first data set was obtained from the aeromagnetic survey flown by Bureau of Mineral Resources, Geology and Geophysics in 1964. These data were acquired at an altitude of 230 m in an E-W direction and a line spacing of 2300 m. This is the currently available coverage for this map sheet within the national data set. The original line data containing the residual field were gridded at a resolution of 15 sec of arc (approximately 400 m grid cell size).

As outlined in the introduction, the second data set was obtained from two modern aeromagnetic surveys of the region, namely Camooweal Ashton 1985 and Mammoth Mines Ashton 1984 acquired for Ashton Mining Pty. Ltd. by Geoterrex. The surveys were flown at an altitude of 80 m in a N-S direction and a 300 m line spacing for most of the area (small parts of the survey were flown at a 250 m line spacing). The merged residual total magnetic intensity grid for the Camooweal 1: 250 000 map sheet area at a resolution of 50 m grid cell size was purchased by the NABRE project from Geoimage Pty. Ltd. at the inception of the project. For the purpose of our study, we have found that a grid at lower resolution (100 m grid cell size) is fully satisfactory. The grid is georeferenced in AMG Zone 54.

Organisational changes and limited time and resources have precluded a more detailed analysis of the geological meaning using modelling techniques. However, this data set is now available to be included in the national data set. The better data should allow refinement of and improve upon earlier geological interpretations of the data (Duffett 1998; Leaman 1998). We present the images for comparison of the effect of transformations on a modern, consistently high quality large-scale data set versus the more difficult problem of the variable NABRE regional data set.

Transformations

Total Magnetic Intensity (TMI) for Cammoweal

The image in **Figure 44** represents the residual magnetic intensity grid for the Camooweal 1: 250 000 map sheet. The grid contains 1087 rows and 1590 columns and a grid cell size of 100 m. This grid has been imaged using Pelton's hill shading routine with north west illumination, an elevation of 45° and a vertical scale of 20 (Pelton 1987). The HSI model has been used and the rainbow colour lookup table has been applied.

First vertical derivative of the TMI for Camooweal

The grey scale image of the first vertical derivative of the TMI for are is shown in **Figure 45**. It was generated from the TMI grid described above. The enhancement of the short wavelength features and the suppression of the long wavelength can be noticed in this treatment (c.f. with **Fig. 44**).

Analytic signal of the TMI for Camooweal

The pseudo-coloured image of the analytic signal of TMI is shown in **Figure 46**. It was also generated from the TMI grid. The locations of the maxima of the analytic signal result are usually used to define the outlines of magnetic sources. **Figure 46** would suggest two large deep structures in the western part of Camooweal area with a weak analytic signal amplitude. However, the sign (i.e., + or -) change of anomalies in the northwest corner could be very misleading if these data are interpreted in isolation. In addition, the edges of the structures are not very well resolved.

The shallow structures in the eastern part of the region exhibit a stronger analytic signal response. This treatment of the data should be interpreted with care, as the amplitude of analytic signal varies with the effective magnetisation (e.g., in the south east corner). The analytic signal of magnetisation contrasts that are closely spaced or dipping is more complicated than in the case of a simple model consisting of two vertical prismatic bodies discussed above. Finally, the analytic signal over the structures that intersect at an acute angle is more complicated than a simple bell-shaped function as in the case of the simple model used above, because of the non-linear combination of individual signals.

Tilt of the TMI for Camooweal

The tilt transformation of the TMI (or as it is alternatively called: the tilt of the horizontal gradient of the TMI) is presented in **Figure 47**. The tilt transformation appears better at resolving the edges of the structures than the analytic signal and thus helps to detect geological boundaries more easily. As the tilt transformation deals with the ratio of the vertical and the horizontal gradient of the TMI, it also allows good resolution of deep and shallow anomaly sources. Since it is based on the spatial derivatives of the field, the tilt magnifies not only the high-frequency content of data but has the unfortunate effect of magnifying the noise in data. This is visible in the north west corner of the area, but note the conservation of the original sign of the anomalies in this same corner.

Depth estimates to magnetic sources for Camooweal

We have estimated depths to magnetic sources for the Camooweal 1: 250 000 area using both Naudy and Phillips methods. As was mentioned above, two different data sets of different quality have been used.

Figure 48 shows the depth estimates obtained from the low quality aeromagnetic data by the Phillips method. The image grid contains 280 rows by 401 columns, and a grid cell size of 400 m. Lines were extracted from the original grid of residual TMI at a 400 m spacing and in an E-W orientation. The Phillips method (INTREPID 1998) was applied to each individual line using a window width of 16 km. The calculated depth estimates for lines have been gridded using a minimum curvature technique (INTREPID 1998). The image suggests that shallow magnetic sources are located in the eastern part of Camooweal while the deeper sources occur in the western part of the region. However, the poor quality of the original data has a degrading effect on the analysis and interpretation of the depth estimates is ambiguous.

Phillips method depth estimates using a high quality, modern data set are shown in **Figure 49**. In this case, E-W lines 100 m apart have been extracted from the high resolution grid of TMI with a 100 m grid cell size. A 16 km window was used when applying the Phillips method to each individual line. Estimates derived from the line data were gridded in a similar way as in the previous case. The image grid contains 282 rows and 405 columns.

The strike of geological structures in Camooweal area is predominately N-S. Thus, lines were extracted in an E-W direction from the grids of TMI. The numerical tests carried out on the lines extracted in an N-S direction failed to provide meaningful results, emphasising the assumption in the methods that the magnetic profile used for analysis is perpendicular to geological structures. This facet of all the methods precludes their general use in large, highly complex geological terranes with features of variable strike.

Even in the case of high quality data, the interpreter should treat ranges of the absolute values of the calculated depths to the magnetic sources with caution. The depths estimates vary depending on the width of window that is used for calculations. As demonstrated in **Figures 48** and **49**, the quality of initial data can have a big effect on the values of estimates. The spatial distribution of the deep and shallow sources and their relative depths seems to agree in the both cases, giving us some confidence that conclusions about the buried geological structures are at least partially valid.

We also have computed depth estimates (**Fig. 50**) for the Camooweal area using an automated Naudy's method (INTREPID 1998). When using Naudy's method an assumption is made that source bodies are represented by infinitely deep and infinite along strike dikes whose strike is perpendicular to the magnetic profiles. Sheet-like bodies are difficult to characterise in the framework of this assumption. The Naudy's method depth estimates image was derived in an identical manner as that described above for the Phillips method using the high quality data set.

Acknowledgements

This study was conducted under the auspices of the NABRE project, a National Geoscience Mapping Accord effort. The custodians of the AGSO national magnetic and gravity data sets and the National GIS data sets (Regions, Crustal Elements and Northern Territory & Mount Isa GIS Geology coverages) are thanked for their assistance in accessing the original raw data for North Central Australia. Ashton Mining Ltd and particularly Keith Jones are thanked for early release of confidential data and permission to use the full grid in the production of the Camooweal images presented herein. Mart Idnurm and Peter Southgate are gratefully acknowledged for early reviews and discussion leading to improvements. The former is particularly acknowledged for sharing his expertise in geomagnetism, which greatly facilitated the constructions of the geological models. Constructive reviews of parts of the manuscript by Russell Shaw, Alan Whitaker and Brian Minty also improved the manuscript. Geoff Bladon is thanked for his editorial review. This product would not have been possible without the considerable technical expertise in image processing and production provided by John Creasey and Andrew Retter. Kathy Ambrose was responsible for the production of the final CD-Rom. Angie Jaensch and Neale Jeffery drafted many of the figures in this record.

References

Bain, J.H.C., Heinrich, C.A. and Henderson, G.A.M., 1992. Stratigraphy, structure, and metasomatism of the Haslingden Group, East Moondarra area, Mount Isa: a deformed and mineralised Proterozoic multistage rift-sag sequence. In: Stewart, A.J. and Blake, D.A. (Editors), Detailed Studies of the Mount Isa Inlier, *AGSO Bulletin* **243**, 125-136.

BMR, 1976a, Geology of Australia, *1:2 500 000 Map*, Parts 1 and 2.

BMR, 1976b, Geology of the Kimberley to Mount Isa Region, Northern Australia, *1:2 500 000 Map*.

BMR, 1976c, Geological Map of the Northern Territory, *1:2 500 000 Map*.

Bradshaw, B.E. & Scott, D.L., 1999. Integrated Basin Analysis of the Isa Superbasin using seismic, well-log and geopotential data: An evaluation of the economic potential of the Northern Lawn Hill Platform, *AGSO Record* **1999/19**.

Butler, R.F., 1992. Paleomagnetism: magnetic domains to geologic terranes. Boston, MA, USA. *Blackwell Scientific Publications*, 319pp.

Chenot, D. & Debeglia, N., 1990. Three -dimensional gravity or magnetic constrained depth inversion with lateral and vertical variation of contrast. *Geophysics*, **55**, 327-335.

Cobbold, P.R., Davy, P., Gapais, D., Rossello, E.A., Sadybakasov, E., Thomas, J.C., Tondji Biyo, J.J. & M. de Urreiztieta, 1993, Sedimentary basins and crustal thickening. *Sedimentary Geology*, **86**, 77-89.

Coles, R.L. & Currie, R.G., 1977. Magnetic anomalies and rock magnetizations in the southern Coast Mountains, British Columbia: possible relation to subduction. *Canadian Journal of Earth Sciences*, **14**, 1753-1770.

Collins, W.J. & Shaw, R.D., 1995. Geochronological constraints on orogenic events in the Arunta Inlier: a review. *Precambrian Research*, **71**, 315-346.

Cordell, L., & McCafferty, A.E., 1989. A terracing operator for physical property mapping with potential-field data. *Geophysics*, **54**, 621-634.

Dewey, J.F., 1988, Extensional collapse of orogens. *Tectonics*, **7**, 1123-1139.

Duffett, M.L., 1998. Gravity, magnetic and radiometric evidence for the geological setting of the Lady Loretta Pb-Zn-Ag deposit; a qualitative appraisal. In: Metallogeny of the McArthur River-Mount Isa-Cloncurry minerals province. *Economic Geology and the Bulletin of the Society of Economic Geologists*, **93**, 1295-1306.

England, P. & G. Houseman, 1989. Extension during continental convergence, with application to the Tibetan Plateau. *Journal of Geophysical Research*, **94**, 17561-17579.

ERMapper, 1998. Image processing software, Version 5.5a, Earth Resource Mapping Inc., Perth, WA, Australia.

Etheridge, M.A., Rutland, R.W.R. and Wyborn, L.A.I., 1987. Orogenesis and tectonic process in the early to middle Proterozoic of northern Australia. In: Kroner, A. (Editor) *Proterozoic Lithosphere Evolution, American Geophysical Union Geodynamic Series* **17**: 131-147.

Grimes, K.G. and Sweet, I.P., 1979. Westmoreland, Queensland, 1:250,000 Geological Series. *Bureau of Mineral Resources, Explanatory Notes* **SE/54-5**.

Hone, I.G., Carberry, V.P. & Reith, H.G., 1987. Physical Property Measurements on Rock Samples from the Mount Isa Inlier, Northwest Queensland. *Bureau of Mineral Resources, Geology and Geophysics*, Australian Government Publishing Service, *Report* **265**, 30 pp.

Hood, P., 1963. Remanent magnetisation--a neglected factor in aeromagnetic interpretation. *Canadian Mining Journal*, **84**, 76-79.

INTREPID, 1998. Geophysical Processing, Interpretation & Archiving Software, Version 3.3. Desmond Fitzgerald and Associates, Brighton, VIC 3186, Australia.

Jackson, M.J., Scott, D.L., & Rawlings, D.R, (in press). Stratigraphic Framework for the Leichhardt and Calvert Superbasins: review and correlations of the pre-1730 Ma successions between Mt Isa and McArthur River *Australian Journal of Earth Sciences*.

Krassay A. A., Bradshaw B. E., Domagala J., McConachie B. A., Lindsay J. F., Jackson M. J., Southgate P. N., Barnett K. W. & Zeilinger I. 1999. Measured sections

and sequence stratigraphic interpretations: upper McNamara and Fickling Groups - Preliminary data release. *AGSO Record* **1999/15**.

Kelso, P.R., Banerjee, S.K. & Teyssier, C., 1993. Rock Magnetic Properties of the Arunta Block, Central Australia, and their implication for the interpretation of long-wavelength magnetic anomalies. *Journal of Geophysical Research*, **98**, 15987-15999.

Leaman, D.E., 1994. Criteria for evaluation of potential-field interpretations. *First Break*, **12**, 181-191.

Leaman, D.E., 1998. Structure, contents and setting of Pb-Zn mineralisation in the McArthur Basin, northern Australia. *Australian Journal of Earth Sciences*, **45**, 3-20.

Leven, J., Tarlowski, C. and Scott, D., 1997. Potential-field modelling around the Murphy Inlier (Abs). NABRE Workshop, March 4-5, *AGSO Record* **1997/12**.

Lidiak, E.G., 1974. Magnetic characteristics of some Precambrian basement rocks. *Geophysics*, **40**, 549-564.

Martin, S., Retter, A. & Scott, 1997. Regional geological applications of GIS (Abs). NABRE Workshop, March 4-5, *AGSO Record* **1997/12**.

Mesko, A., 1984. Digital Filtering: Applications in Geophysical Exploration for Oil. *Pitman Advanced Publishing Program*.

Meyers, J. S., Shaw, R.D. & I.M. Tyler, 1996, Tectonic evolution of Proterozoic Australia. *Tectonics*, **15**, 1431-1446.

Miller, H.G., & Singh, V., 1994. Potential-field tilt - a new concept for location of potential-field sources, *Journal of Applied Geophysics*, **32**, 213-217.

Milligan, P.R., Morse, M.P., Rajagopalan, S., 1992, Pixel map preparation using HSV colour model. *Exploration Geophysics*, **23**, 219-224.

Molnar, P.& Lyon-Caen, H., 1988. Some simple physical aspects of the support, structure and evolution of mountain belts in Clark, S.P., Burchfiel, B.C. & Suppe, J., 1988. Process in Continental Lithospheric Deformation. *Geological Society of America Special Paper*, **218**, 179-207.

Murray, A.S., Morse, M.P., Milligan, P.R., & Mackey, T.E., 1997, Gravity Anomaly Map of Australian Region (Second Ed.), *1 : 5 000 000 Map*, Australian Geological Survey Organisation, Canberra.

Mutton, A.J. & Shaw, R.D, 1979, Physical Property Measurements as an Aid to Magnetic Interpretation in Basement Terrains. *Bulletin Australian Society of Exploration Geophysicists*, **10**, 79-91.

NATIONAL MAP, 1998, New GIS coverage defines geological regions, 'National digital geoscience data sets'. *Australian Geological Survey Organisation Research*

Newsletter, **49**, 4-5.

Naudy, H., 1971. Automatic determination of depth on aeromagnetic profiles, *Geophysics*, **36**, 717-722.

Oldenburg, D. W., Li, Y., & Farquharson, C.G., 1997, Geophysical Inversion: Fundamentals and Applications in Mineral Exploration Problems, Proceedings of Exploration 97; *Fourth Decennial International Conference on Mineral Exploration*, edited by A.G. Gubins, 545-548.

Pelton, C., 1987, A computer program for hill-shading digital topographic data sets. *Computers & Geosciences*, **13**, 545-548.

Phillips, J.D., 1975. Statistical analysis of magnetic profiles and geomagnetic reversal sequences, *Ph D. Thesis*, Stanford University.

Phillips, J.D., 1992, TERRACE: A terracing procedure for gridded data, with Fortran programs, and VAX Command Procedure, Unix C-Shell, and DOS batch file implementations. U.S. Geological Survey, *Open File Report* 92-5.

Potent version 3.08, 1997, Interactive gravity and magnetic modelling software, PC Potentials, P.O.Box 167, ACT 2615, Australia.

Quinlan, G.M. & Beaumont, C., 1984. Appalachian thrusting, lithospheric flexure, and the Paleozoic stratigraphy of the Eastern Interior of North America. *Canadian Journal of Earth Sciences*, **21**, 973-996.

Rutland, R.W.R. & B.J. Drummond (Editors), 1997, Palaeoproterozoic Tectonics and Metallogenesis: Comparative analysis of parts of the Australian & Fennoscandian Shields. *AGSO Record* **1997/44**, 134pp.

Scott, D.L., Tarlowski, C.Z., Leven, J. and Martin, S., 1997. Basement Studies: Current status and dataset integration (Abs). NABRE Workshop, March 4-5*, AGSO Record* **1997/12**.

Scott, D.L., Bradshaw, B.E. & C.T. Tarlowski, 1998a. The tectonostratigraphic history of the northern Lawn Hill Platform, Australia: an integrated intracontinental basin analysis. *Tectonophysics*, **300**, 329-358.

Scott, D., Tarlowski, C., Page, R., Idnurm, M., Rawlings, D., Jackson, M.J. & D. Mackenzie, 1998b. Basement studies in basin analysis: new insights into the evolution of the Lawn Hill Platform*. Australian Geological Survey Organisation Research Newsletter*, **28**, 29-32.

Scott, D.L., Rawlings, D.E., Page, R.W. Tarlowski, C.Z., Jackson, M.J. & Idnurm, M., (in press), Basement Framework for the Isa Superbasin: an integrated review of geophysical, geochronological, geochemical and structural data. *Australian Journal of Earth Sciences*.

Shaw, R.D., Wellman, P., Gunn, P., Whitaker, A.J., Tarlowski, C., & Morse M., 1995,

'Australian crustal elements'map: A geophysical model for the tectonic framework of the continent. *Australian Geological Survey Organisation Research Newsletter*, **23**, 1-3.

Shaw, R.D., Wellman, P., Gunn, P., Whitaker, A.J., Tarlowski, C., & Morse M., 1996, Guide to using the Australian Crustal Elements Map. *AGSO Record* **1996/30**, 44pp.

Southgate, P.N., Sami, T.T., Jackson, M.J., Domagala, J., Krassay, A.A., Lindsay, J.F., McConachie, B.A., Page, R.W., Pidgeon, B., Barnett, K.W., Rokvic, U. Zeilinger, I., 1999a. Measured Sections and Sequence Stratigraphic Interpretations:lower McNamara, Mt Isa and Fickling Groups - Preliminary Edition Data Release. *AGSO Record* **1999/10.**

Tarlowski, C., Milligan, P.R. & Mackey, T.E., 1996a, Magnetic Anomaly Map of Australia (Second Ed.), *1 : 5 000 000 Map* , Australian Geological Survey Organisation, Canberra.

Tarlowski, C., McEwin, A.J., Reeves, C.V., & Barton, C.E., 1996b. Dewarping the composite aeromagnetic anomaly map of Australia using control traverses and base stations. *Geophysics*, **61**, 696-705.

Tarlowski, C.Z. and Scott, D.L., 1997. Regional Potential-field Data: image manipulation techniques and pitfalls (Abs). NABRE Workshop, March 4-5, *AGSO Record* **1997/12**.

Telford, W.M., Geldart, L.P. & Sheriff, 1994, *Applied Geophysics, Cambridge University Press*, 2nd Edition, p.16 and p.76.

Thompson, D.T., 1982, EULDPH: A new technique for making computer-assisted depth estimates from magnetic data. *Geophysics*, **47**, 31-37.

Tucker, D.H., Hone, I.G., Sampath, N., & Ewers, G.R., 1979, Geological and physical characteristics of some magnetic sources in Lower Proterozoic Metasediments Pine Creek Geosyncline N.T., *Bulletin Australian Society of Exploration Geophysicists*, **10**, 54-66.

Whiting, T.H., 1988, Magnetic mineral petrogenesis, Rock Magnetism and aeromagnetic response in the eastern Arunta Inlier, Northern Territory. *ASEG/SEG Conference, Adelaide*, 377-383.

List of Figures

Figure 1: Two simple prisms with the given magnetic properties produce the indicated contoured Total Magnetic Intensity field.

Figure 2: Three-dimensional portrayal of the TMI anomaly produced by the model in Figure 1.

Figure 3: Three-dimensional portrayal of reduction to the pole of the TMI anomaly depicted in Figure 2.

Figure 4: Z-direction derivative of the TMI anomaly depicted in Figure 2.

Figure 5: X-direction derivative of the TMI anomaly depicted in Figure 2.

Figure 6: Y-direction derivative of the TMI anomaly depicted in Figure 2.

Figure 7: The geometrical and mathematical expression of the derivatives used in the Analytic Signal transformation.

Figure 8: Three-dimensional portrayal of the Analytic Signal transformation of the TMI anomaly depicted in Figure 2.

Figure 9: The geometrical and mathematical expression of the derivatives used in the Tilt transformation.

Figure 10: Three-dimensional portrayal of the Tilt transformation of the TMI anomaly depicted in Figure 2.

Figure 11: Psuedo-colour, gradient enhanced Total Magnetic Intensity (TMI) image for North Central Australia.

Figure 12: Psuedo-coloured image of the TMI field for North Central Australia upward continued to the 500 m level.

Figure 13: Psuedo-coloured image of the Tilt transformation of the TMI field for the North Central Australia.

Figure 14: Psuedo-colour, gradient enhanced Bouguer Gravity Anomaly image for North Central Australia.

Figure 15: Terraced Bouguer Gravity Anomaly image for North Central Australia.

Figure 16: Depth estimates for North Central Australia using Phillips' Deconvolution method. No filters were applied. See text for further discussion.

Figure 17: Depth estimates for North Central Australia using Naudy's method. No filters were applied. See text for further discussion.

Figure 18: Phillips' depth estimates from magnetic data after a 5x5 smoothing filter

was applied. See text for further discussion.

Figure 19: Phillips' depth estimates from magnetic data after a 7x7 smoothing filter was applied. See text for further discussion.

Figure 20: Phillips' depth estimates from magnetic data after a 13x13 smoothing filter was applied. See text for further discussion.

Figure 21: Naudy's depth estimates from magnetic data after a 7x7 smoothing filter was applied. See text for further discussion.

Figure 22: Comparison of the GIS coverage of outcropping igneous and volcanic units likely to be contributors to the observed magnetic data with the Phillips' method depth estimates image.

Figure 23: Comparison of the GIS coverage of outcropping igneous and volcanic units likely to be contributors to the observed magnetic data with the Naudy's method depth estimates image.

Figure 24:
This figure, and any reference to it, have been removed from AGSO Record 1999/27.

Figure 25: Regions after the national GIS geological regions coverage showing Proterozoic outcrop distribution.

Figure 26: Interpretation of the fabric expressing the anomaly character of the Bouguer Gravity anomaly image.

Figure 27: Location map of traverses across North Central Australian. Also shown are the geophysical elements and domains interpreted from analysis of the image data. KB=Kimberley Block, HC-PC=Halls to Pine Creek belt, AB=Arunta Belt, MI=Mt Isa Belt, E_S=Southern Element, E_C=Central Element, E_N=Northern Element of the North Australian Craton (NAC), each divided into western (1), central (2) and eastern (3) domains, by the western (WXFR), central (CXFR) and eastern (EXFR) transverse structures or zones.

Figure 28: Traverse 1. Location labels as in Figure 27.

Figure 29: Traverse 2. Location labels as in Figure 27.

Figure 30: Traverse 3. Location labels as in Figure 27.

Figure 31: Traverse 4. Location labels as in Figure 27.

Figure 32: Traverse 5. Location labels as in Figure 27.

Figure 33: Traverse 6. Location labels as in Figure 27.

Figure 34: Traverse 7. Location labels as in Figure 27.

Figure 35: Traverse 8. Location labels as in Figure 27.

Figure 36: Gravity model of Traverse 1. Compare this simple model with the geological model used to calculate the magnetic anomaly match in Fig. 28.

Figure 37: Crustal Elements of North Central Australia.

Figure 38: Depth to “Basement” or non-strataform bodies.

Figure 39: Thickness Contours of Package 1.

Figure 40: Thickness Contours of Package 2.

Figure 41: Thickness Contours of combined Packages 1 and 2 outside of the Arunta Belt.

Figure 42: Thickness Contours of Package 3.

Figure 43: Interpretative thickness and structural style of the Palaeoproterozic basin system proposed to have initiated at ~1750-1730 Ma.

Figure 44: Gradient enhanced image of the Total Magnetic Intensity (TMI) for the Camooweal 1:250 000 map sheet.

Figure 45: Greyscale image of the first vertical derivative (or z-derivative) of the TMI for the Camooweal 1:250 000 map sheet.

Figure 46: Psuedo-colour image of the analytic signal of the TMI for the Camooweal 1:250 000 map sheet.

Figure 47: Psuedo-colour image of the Tilt of the TMI for the Camooweal 1:250 000 map sheet.

Figure 48: Psuedo-colour image of the Phillips’ Deconvolution method of depth estimates of the TMI for the Camooweal 1:250 000 map sheet extracted from the 2nd Edition AGSO national grid.

Figure 49: Psuedo-colour image of the Phillips’ Deconvolution method of depth estimates of the high resolution TMI for the Camooweal 1:250 000 map sheet.

Figure 50: Psuedo-colour image of the Naudy method of depth estimates of the high resolution TMI for the Camooweal 1:250 000 map sheet.

Appendix I

Pseudo-code for the Tilt transformation of total magnetic intensity (TMI).

For every non-nul grid point of total magnetic intensity:

Step 1. Calculate x-derivative (x_derv) of TMI.

Step 2. Calculate y-derivative (y_derv) of TMI.

Step 3. Calculate z-derivative (z_derv) of TMI.

Step 4. Calculate horizontal gradient (hor_grd) of TMI ie.
hor_grd = sqrt (x_derv*x_derv + y_derv*y_derv).

Step 5. Calculate tilt = atan2 (z_derv, hor_grd).

end of algorithm.

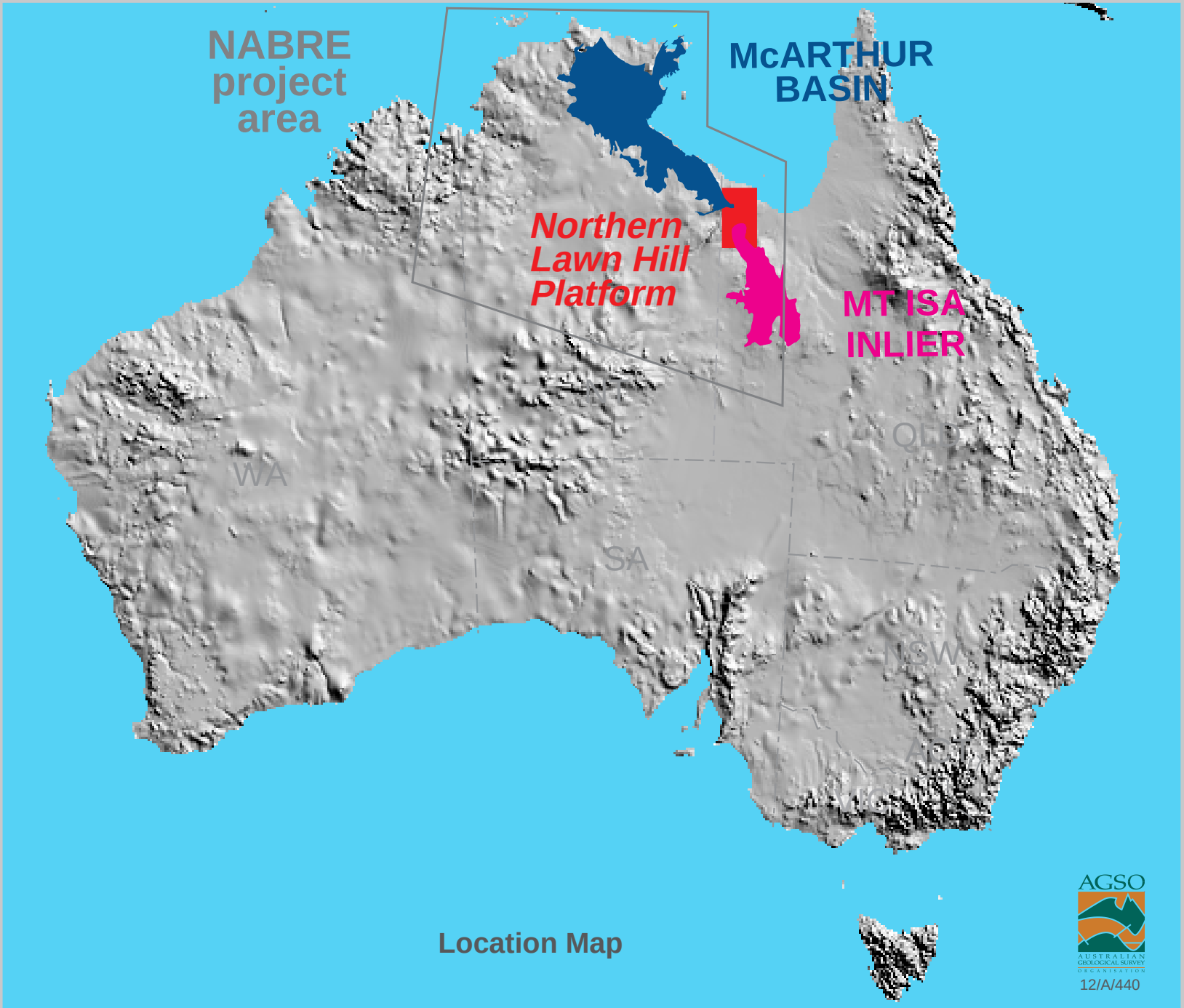

Location Map

AGSO
AUSTRALIAN GEOLOGICAL SURVEY ORGANISATION

12/A/440

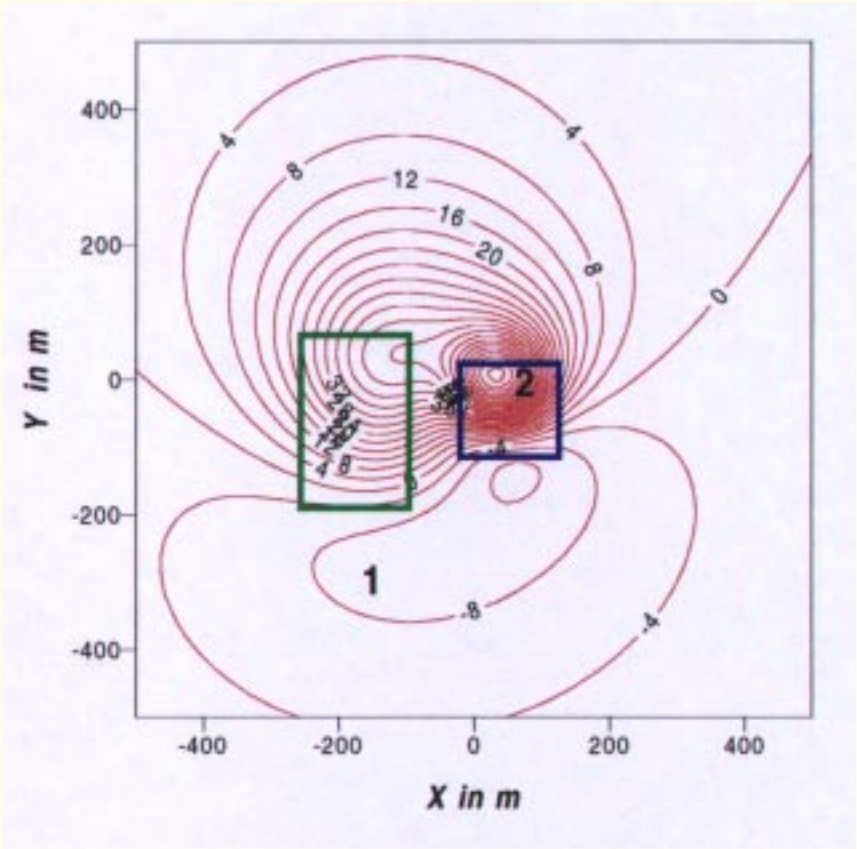

	1	2
DEPTH	150m	50m
WIDTH	100m	100m
LENGTH	200m	100m
HEIGHT	400m	300m
SUSCEPTIBILITY	0.02	0.01
INDUCING FIELD	55000nT	
INCLINATION	-60 deg	
DECLINATION	0 deg	

Fig 1 Contour plan view of TMI anomaly for two vertical prisms

AGSO
AUSTRALIAN GEOLOGICAL SURVEY ORGANISATION

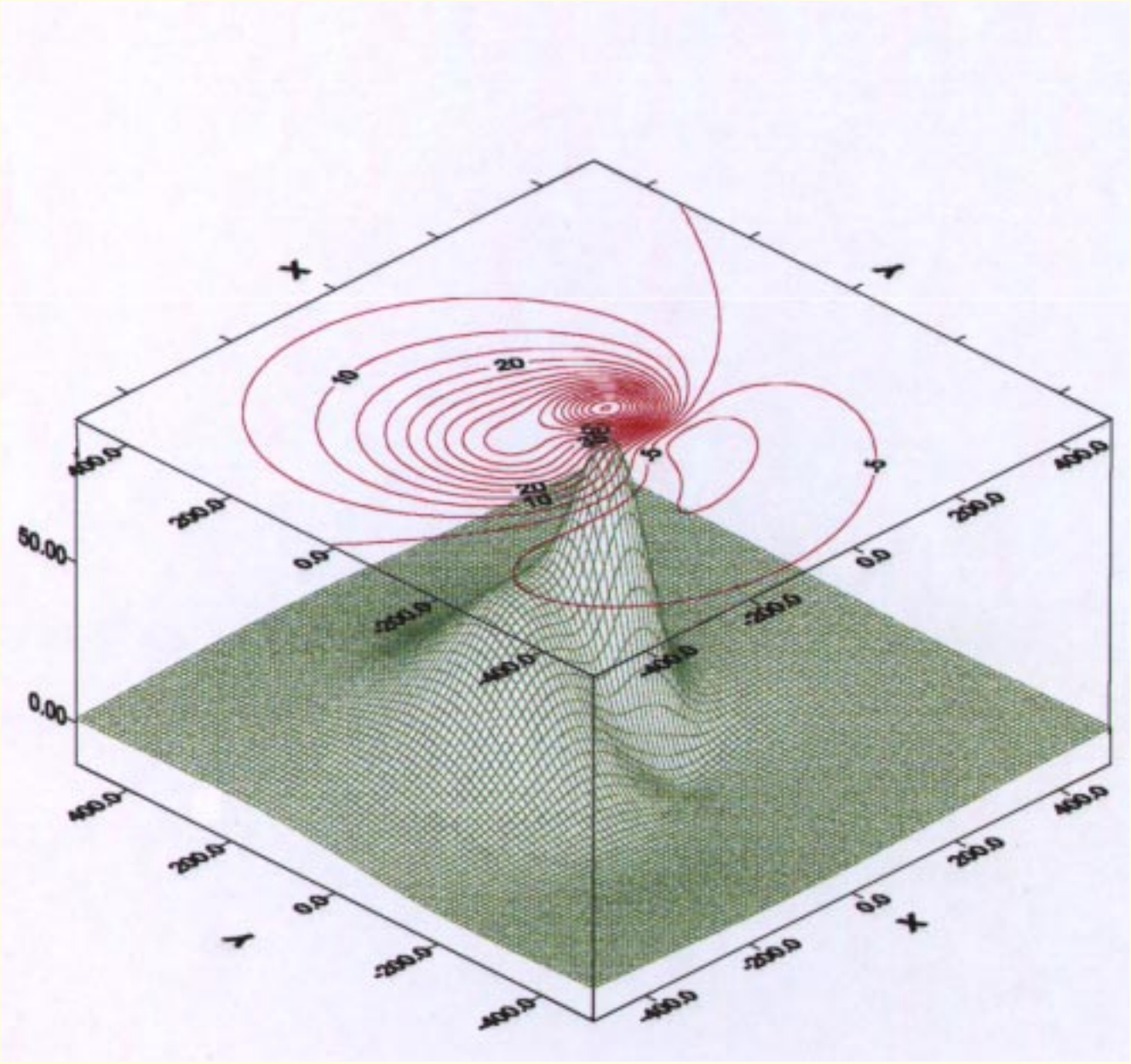

Fig 2 Three dimensional view of TMI anomaly for two vertical prisms

AGSO
AUSTRALIAN GEOLOGICAL SURVEY ORGANISATION

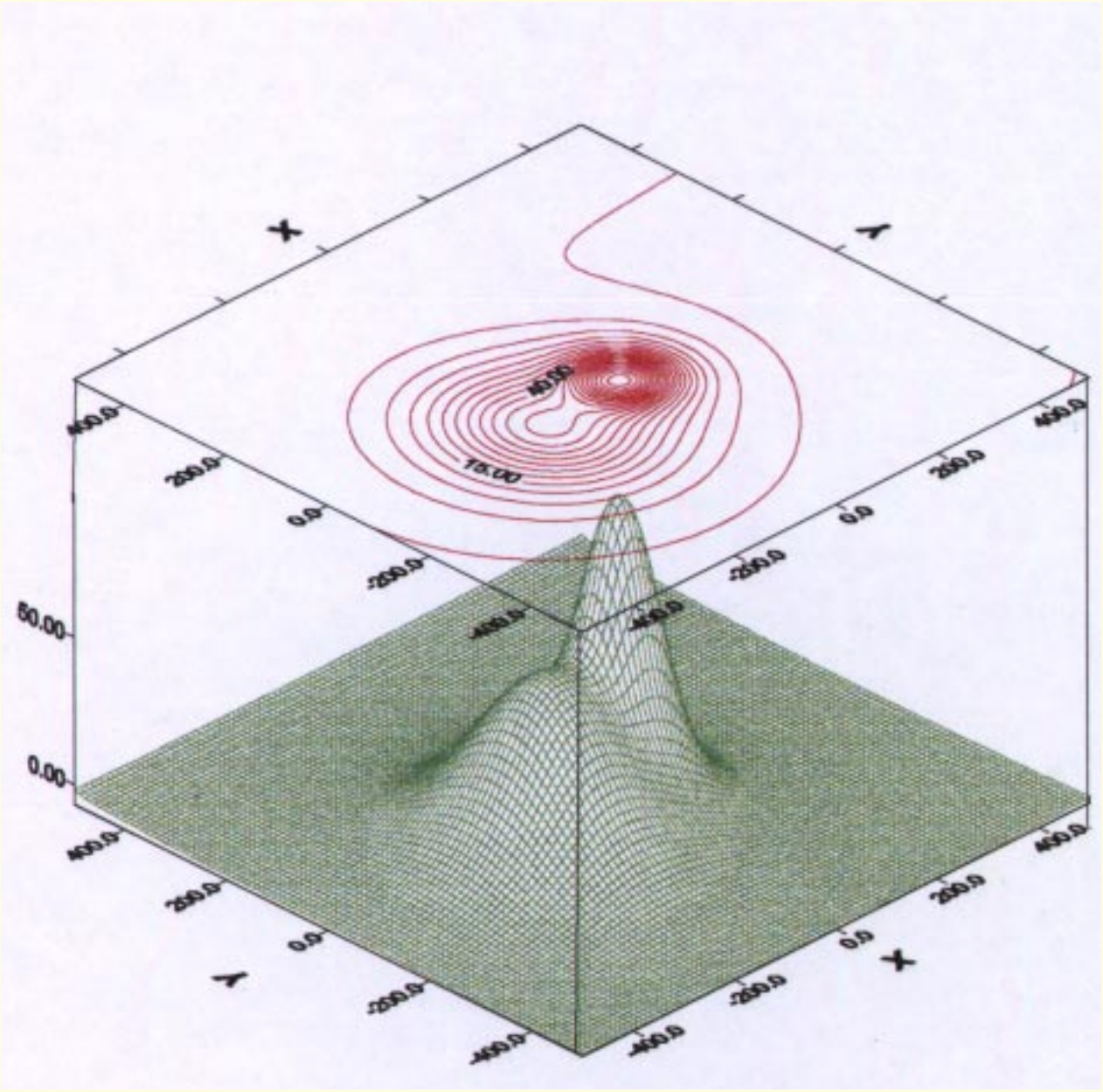

Fig 3 TMI anomaly for two vertical prisms reduced to magnetic pole

AGSO
AUSTRALIAN GEOLOGICAL SURVEY ORGANISATION

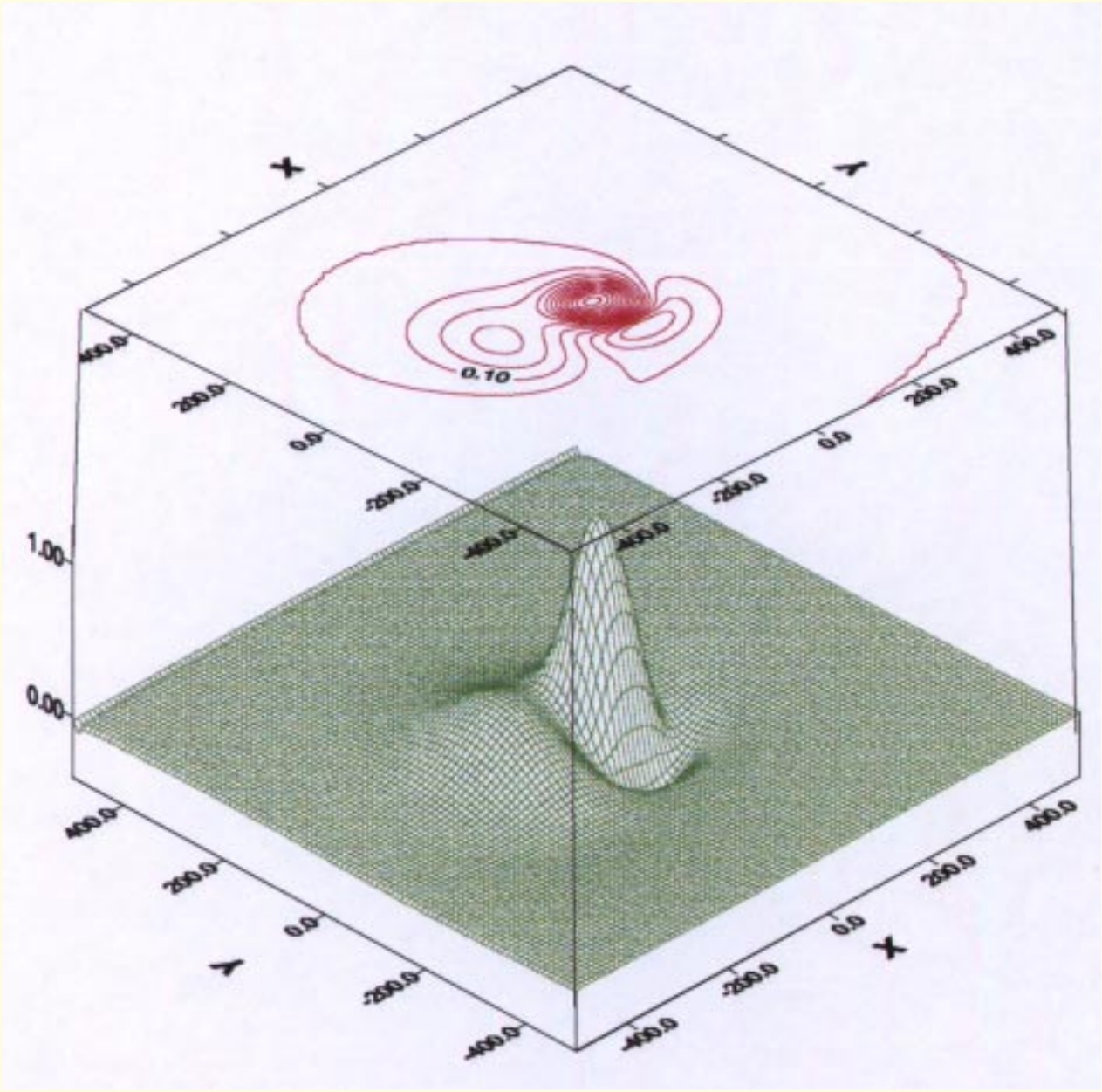

Fig 4 Derivative of TMI anomaly in z-direction

AGSO
AUSTRALIAN GEOLOGICAL SURVEY ORGANISATION

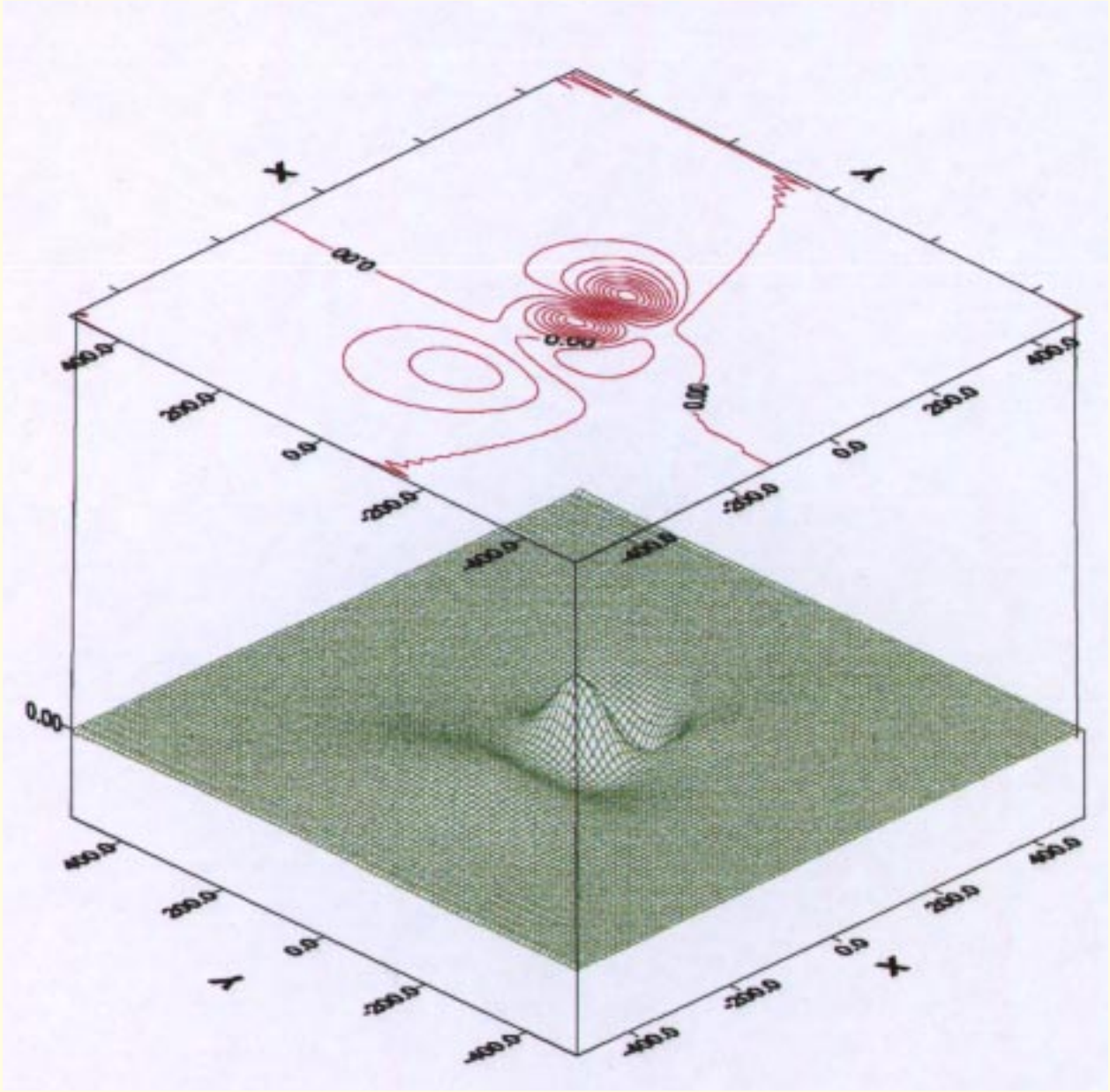

Fig 5 Derivative of TMI anomaly in x-direction

AGSO
AUSTRALIAN GEOLOGICAL SURVEY ORGANISATION

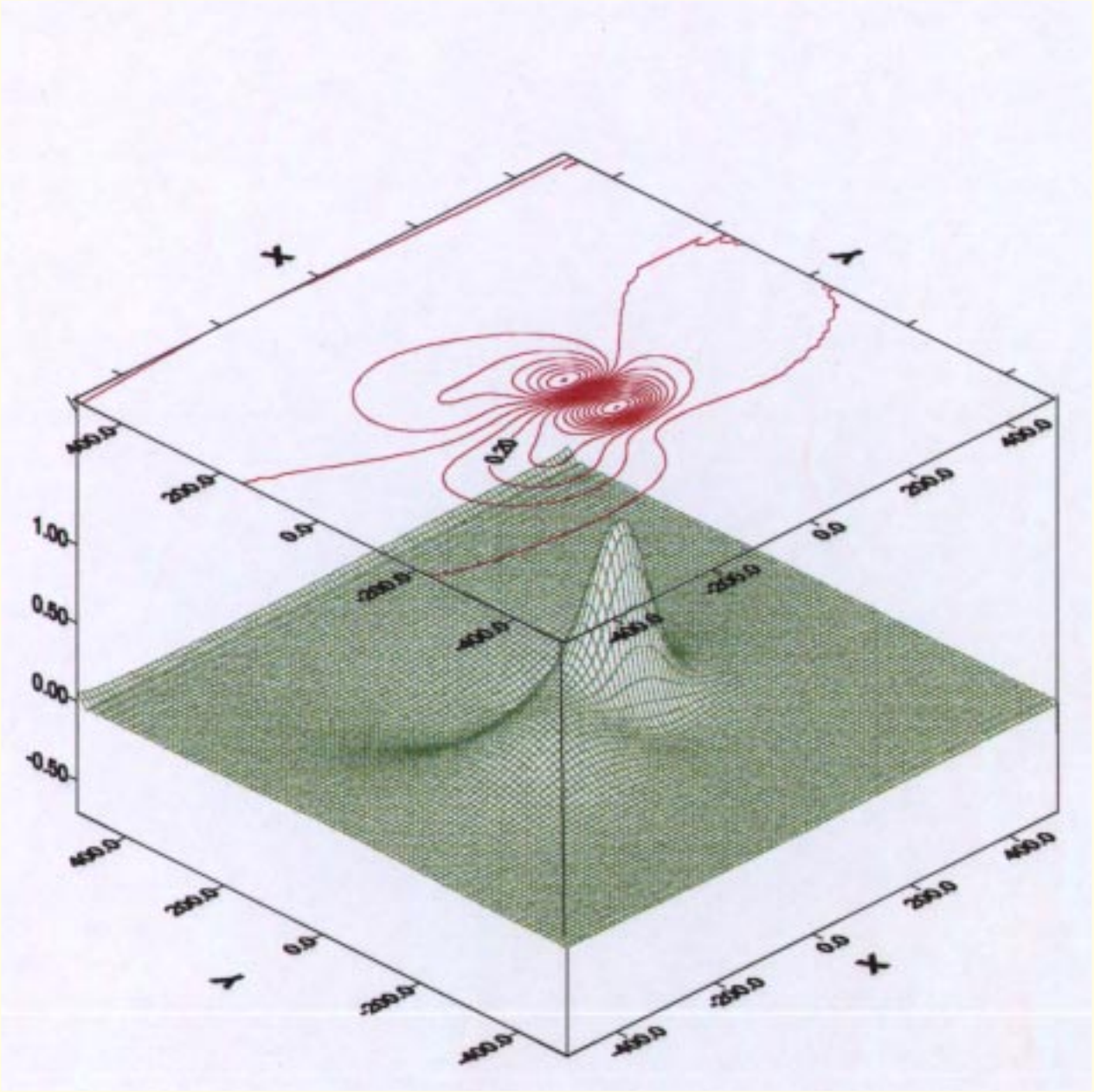

Fig 6 Derivative of TMI anomaly in y-direction

AGSO
AUSTRALIAN GEOLOGICAL SURVEY ORGANISATION

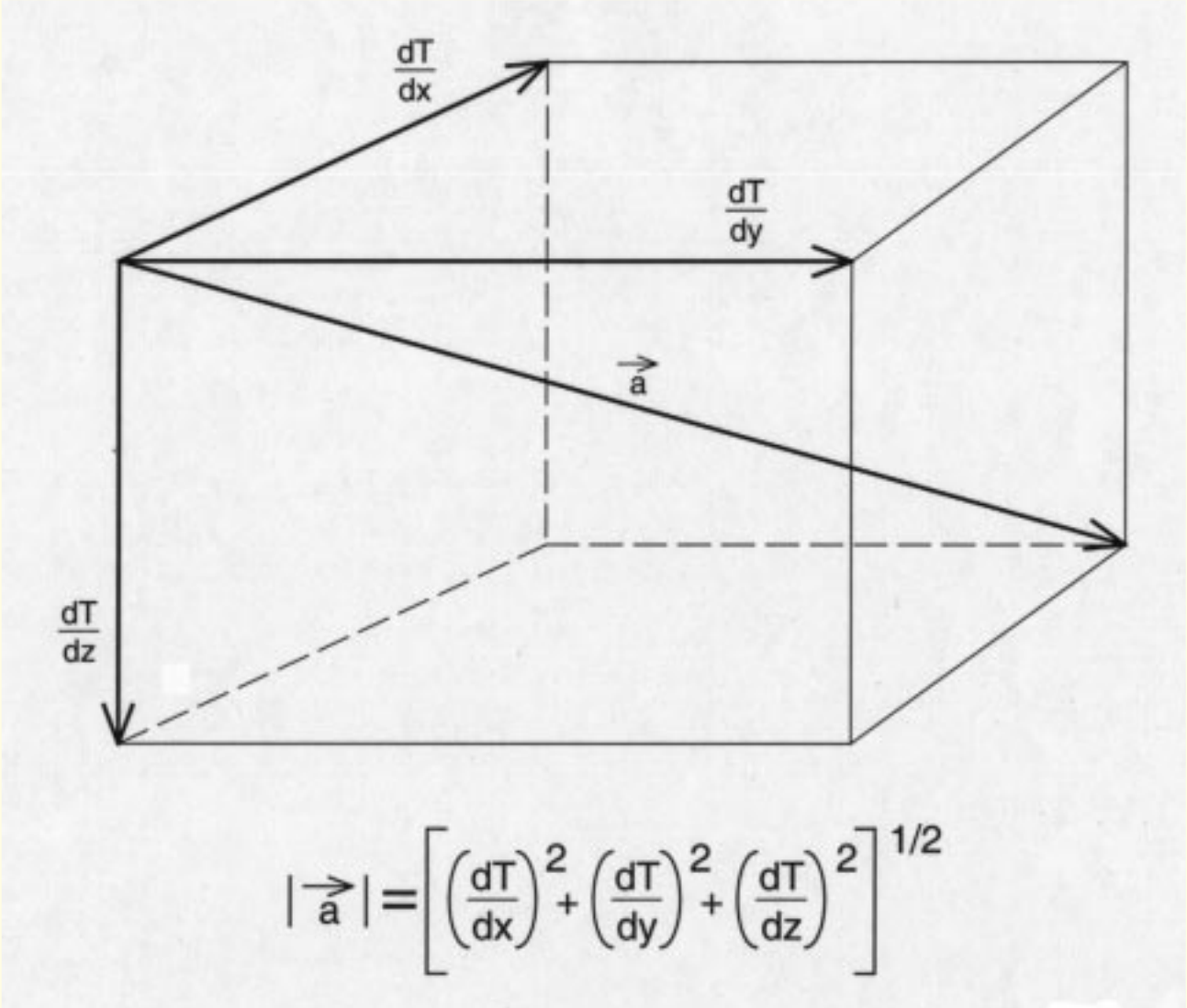

Fig 7 Pictorial expression of the analytic signal transformation

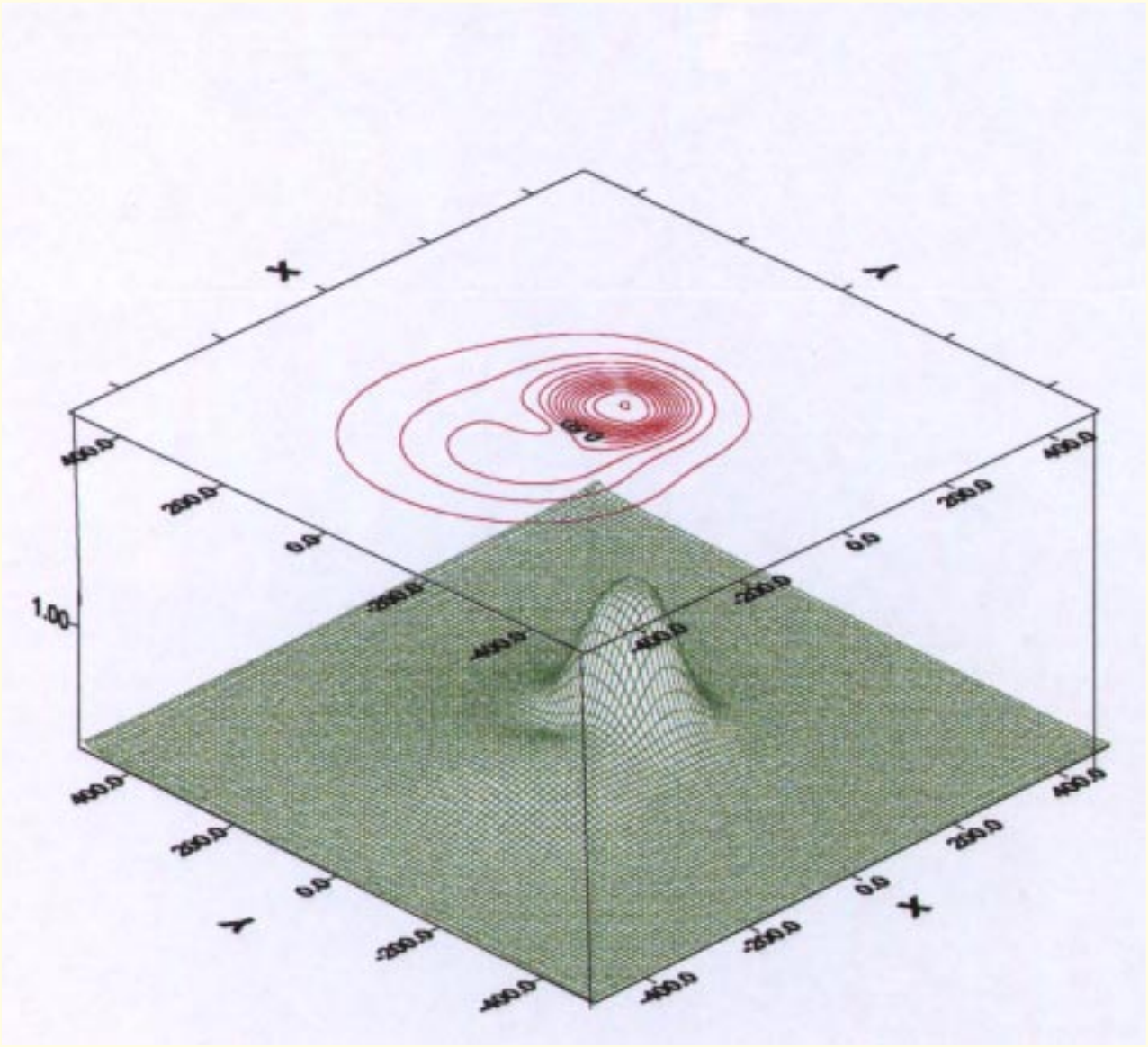

Fig 8 Analytic signal of TMI anomaly for two vertical prisms

AGSO
AUSTRALIAN GEOLOGICAL SURVEY ORGANISATION

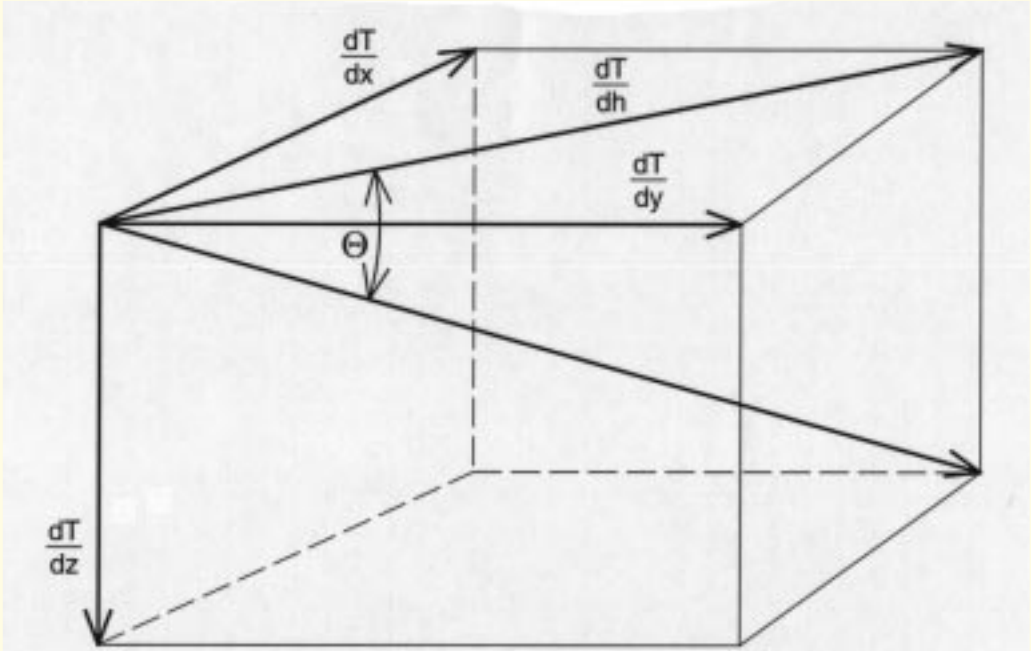

$$\Theta = \tan^{-1} \frac{\frac{dT}{dz}}{\frac{dT}{dh}}$$

where

$$\frac{dT}{dh} = \left[\left(\frac{dT}{dx} \right)^2 + \left(\frac{dT}{dy} \right)^2 \right]^{1/2}$$

Fig 9 Tilt transformation

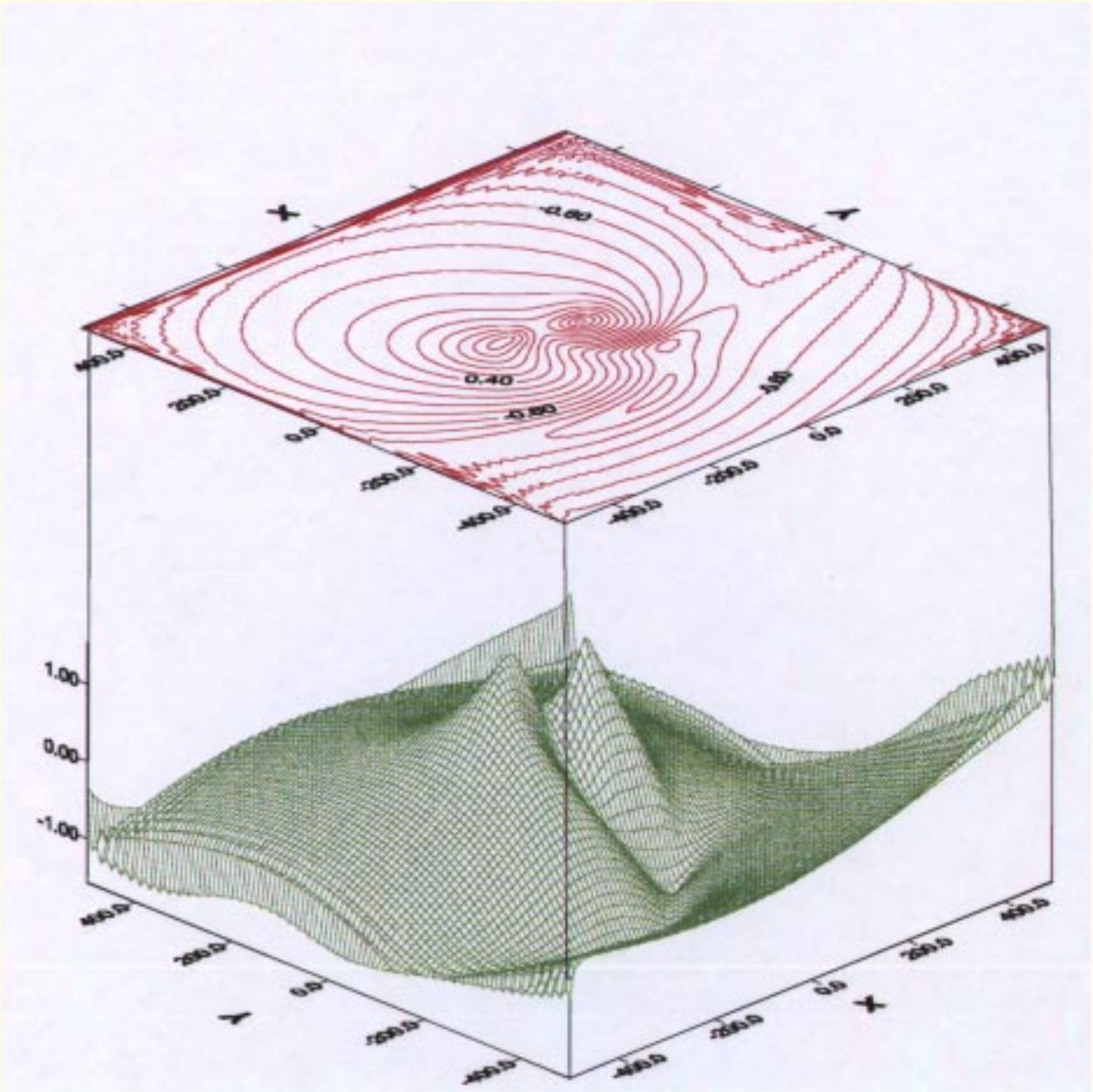

Fig 10 Tilt of TMI anomaly for two vertical prisms

AGSO
AUSTRALIAN GEOLOGICAL SURVEY ORGANISATION

Fig 11 Total Magnetic Intensity (TMI) image

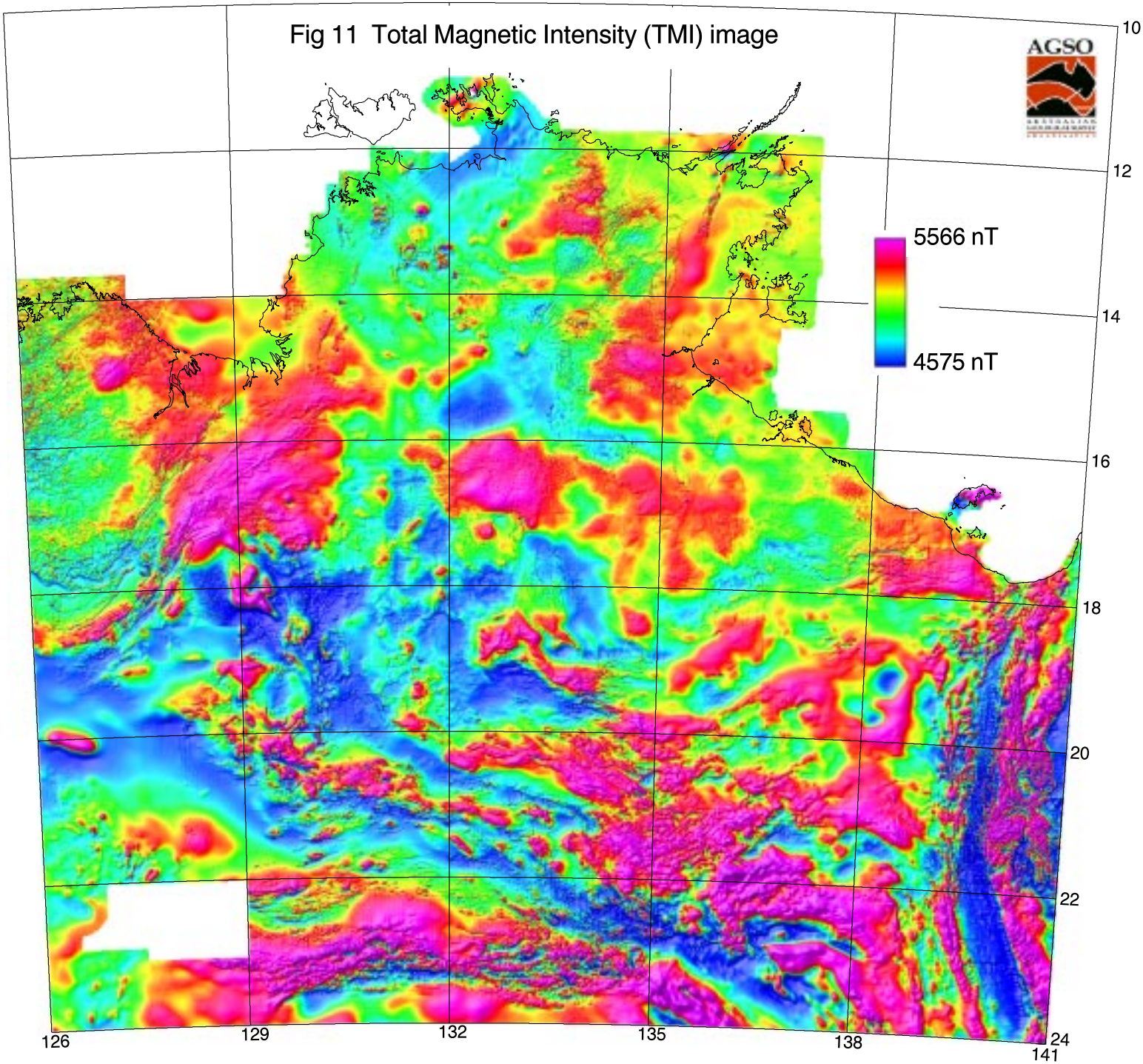

Fig 12 TMI field upward continued to the 500m level

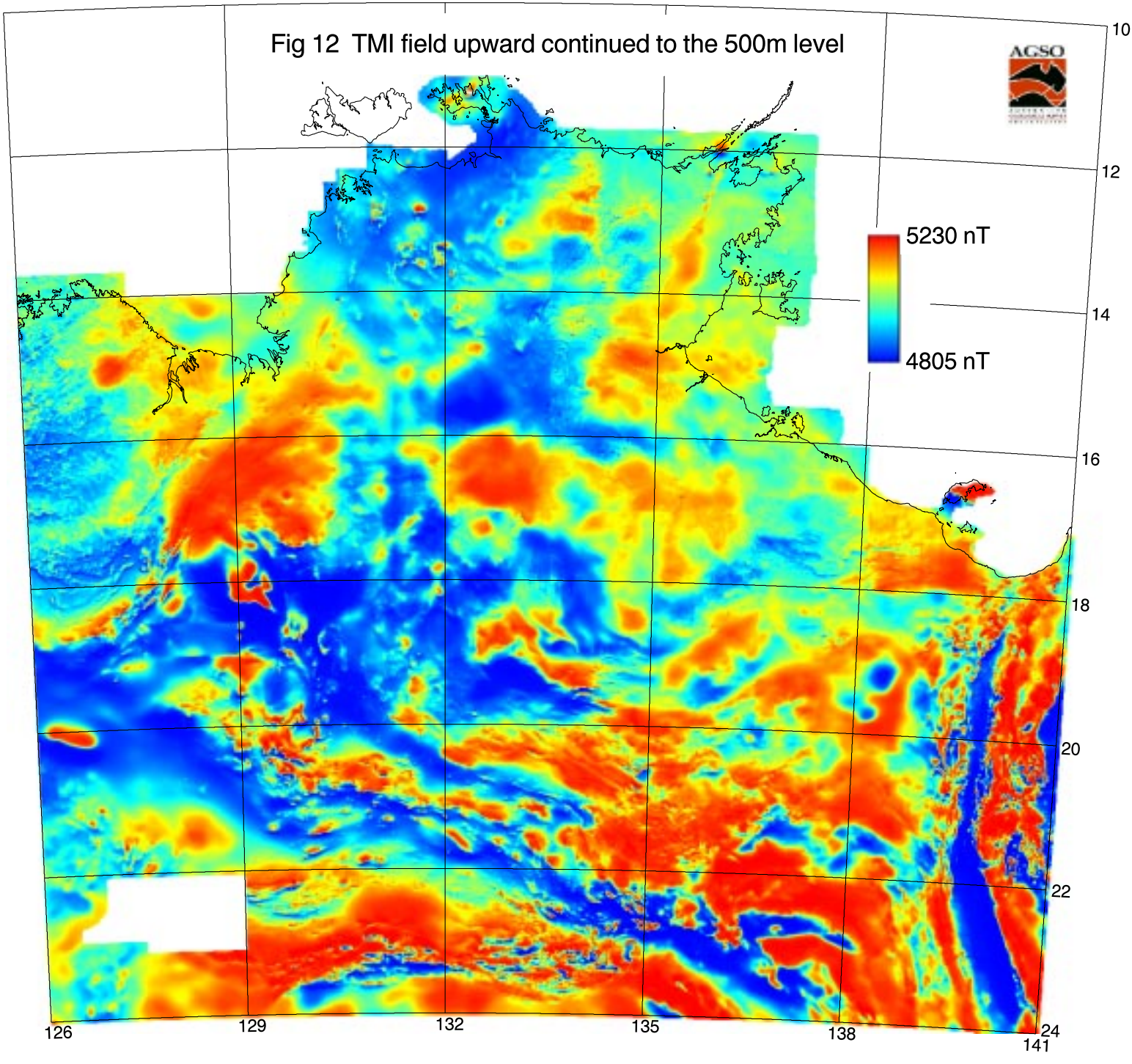

Fig 13 Tilt transformation of the TMI field

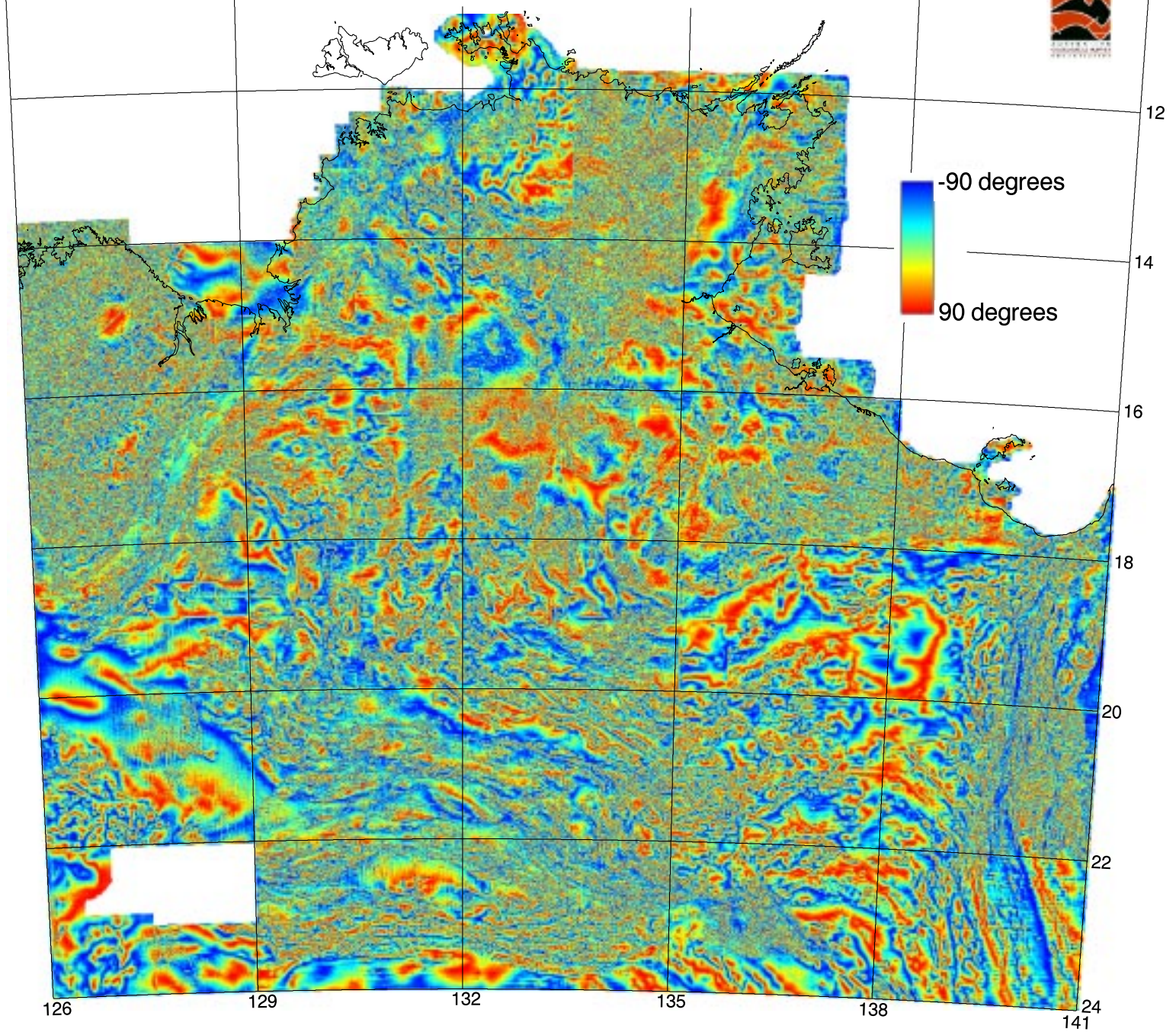

Fig 14 Bouguer Gravity Anomaly image

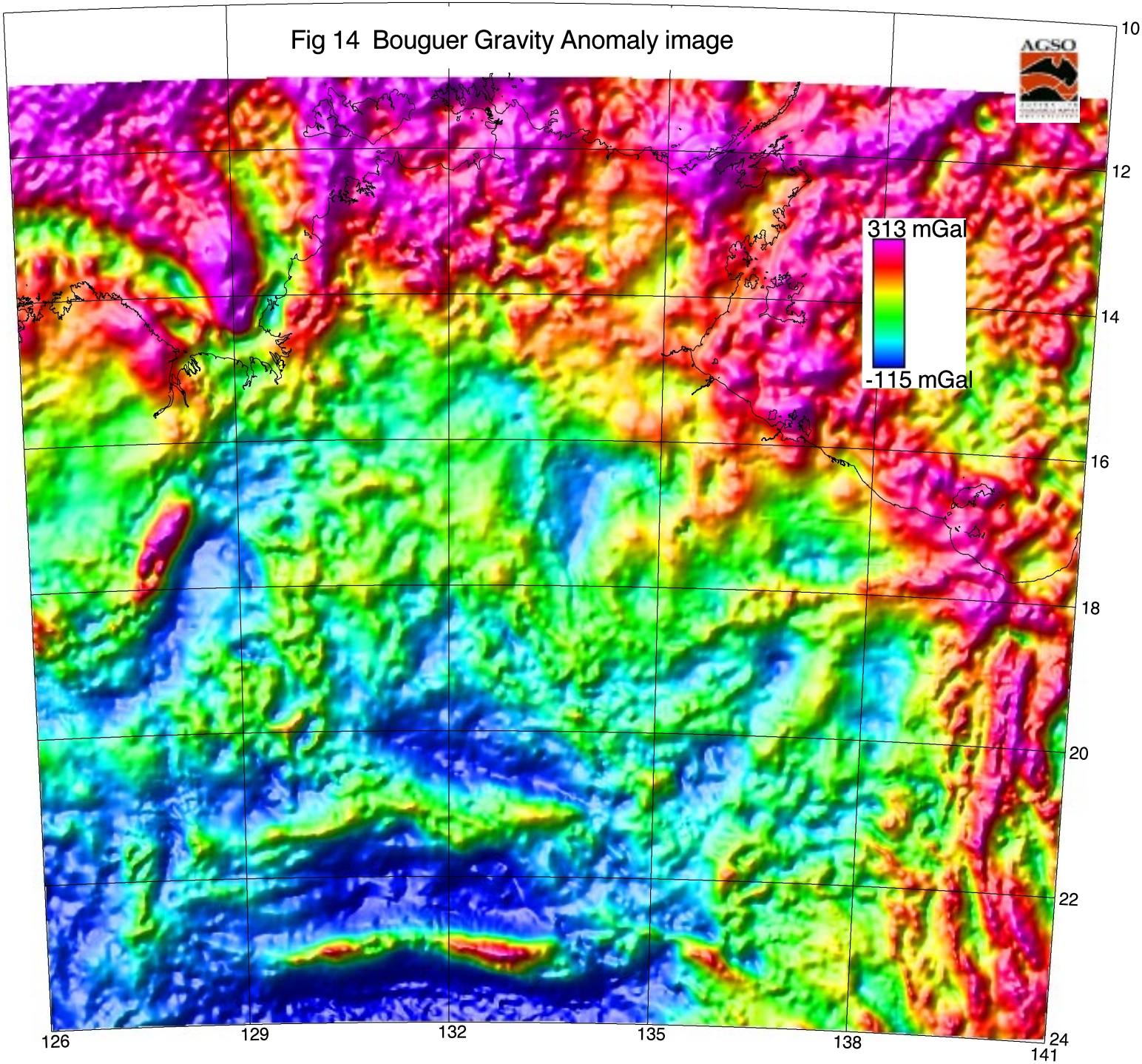

Fig 15 Terraced Bouguer Gravity Anomaly image

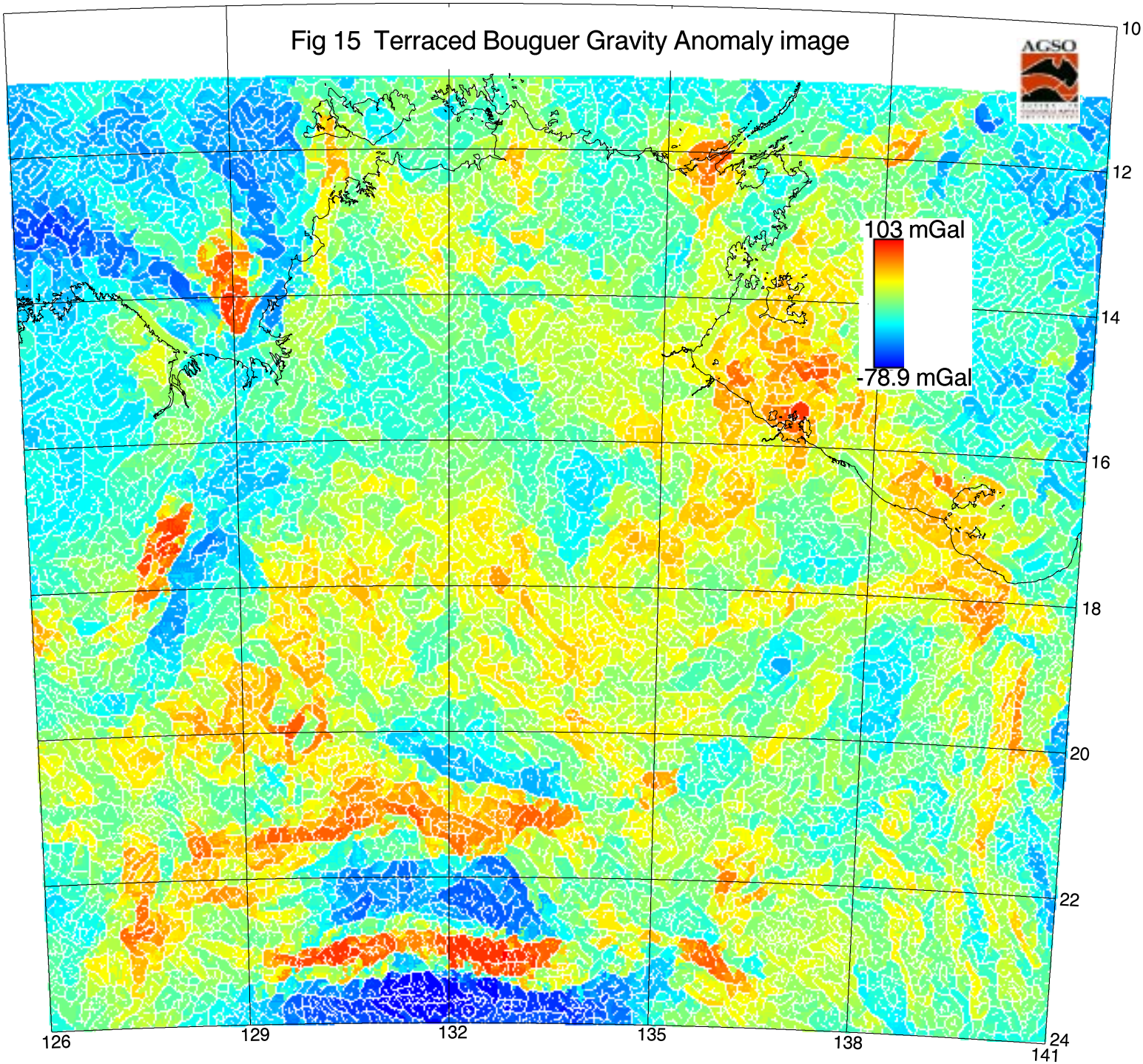

Fig 16 Phillips' method depth estimates image.
(no filter)

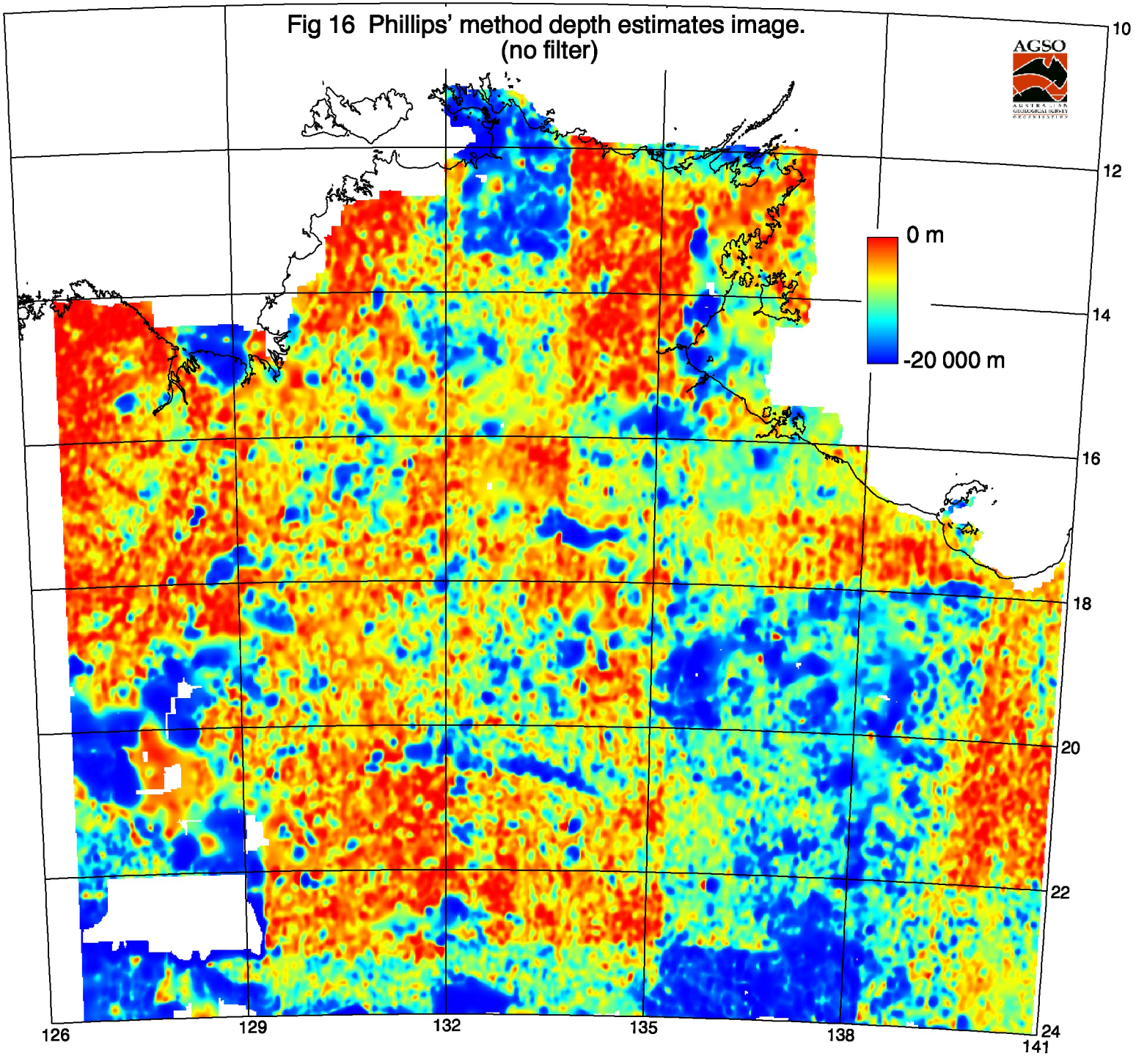

Fig 17 Naudy's method depth estimates image.
(no filter)

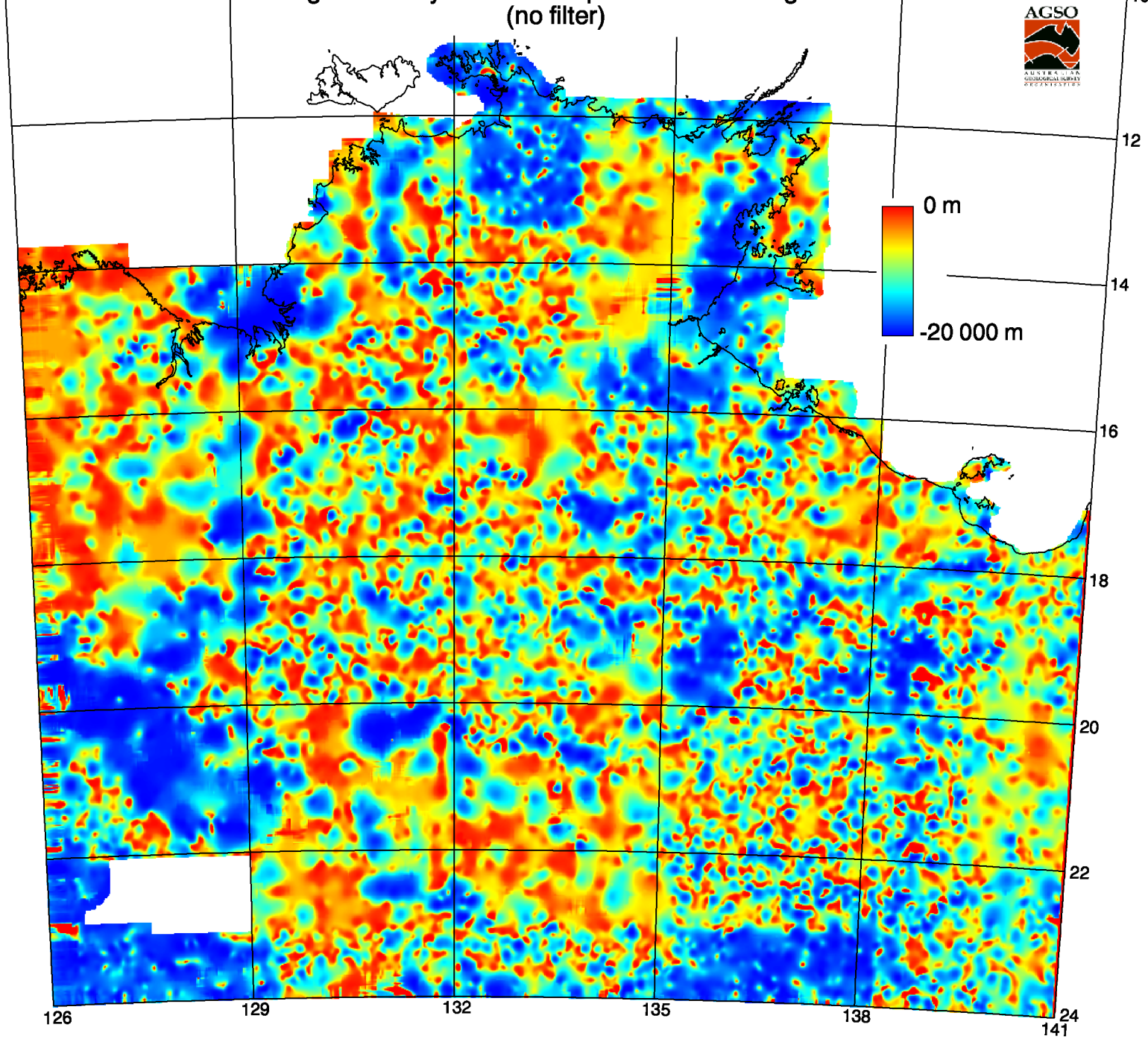

Fig 18 Phillips' method depth estimates image.
(5x5 filter)

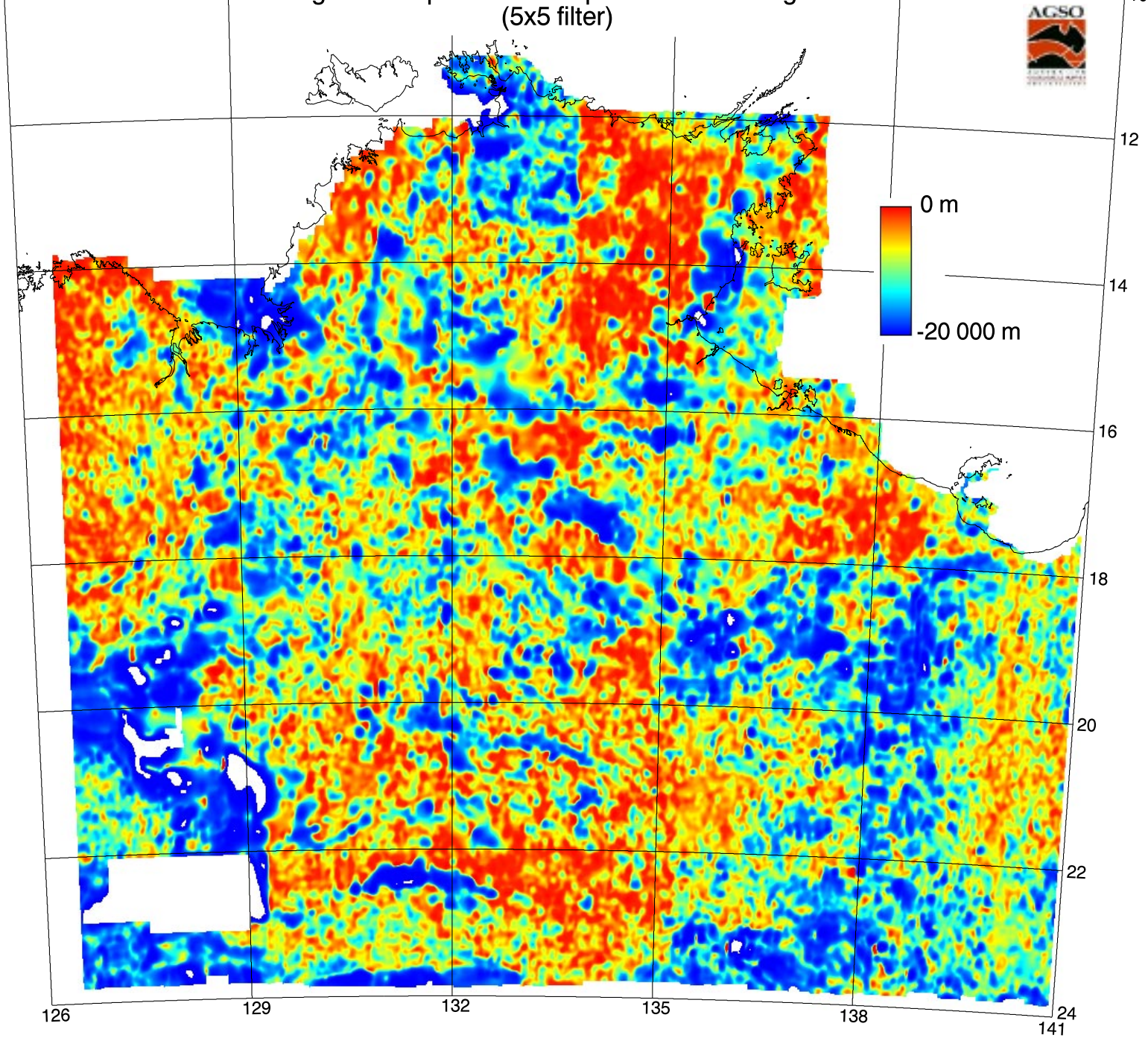

Fig 19 Phillips' method depth estimates image.
(7x7 filter)

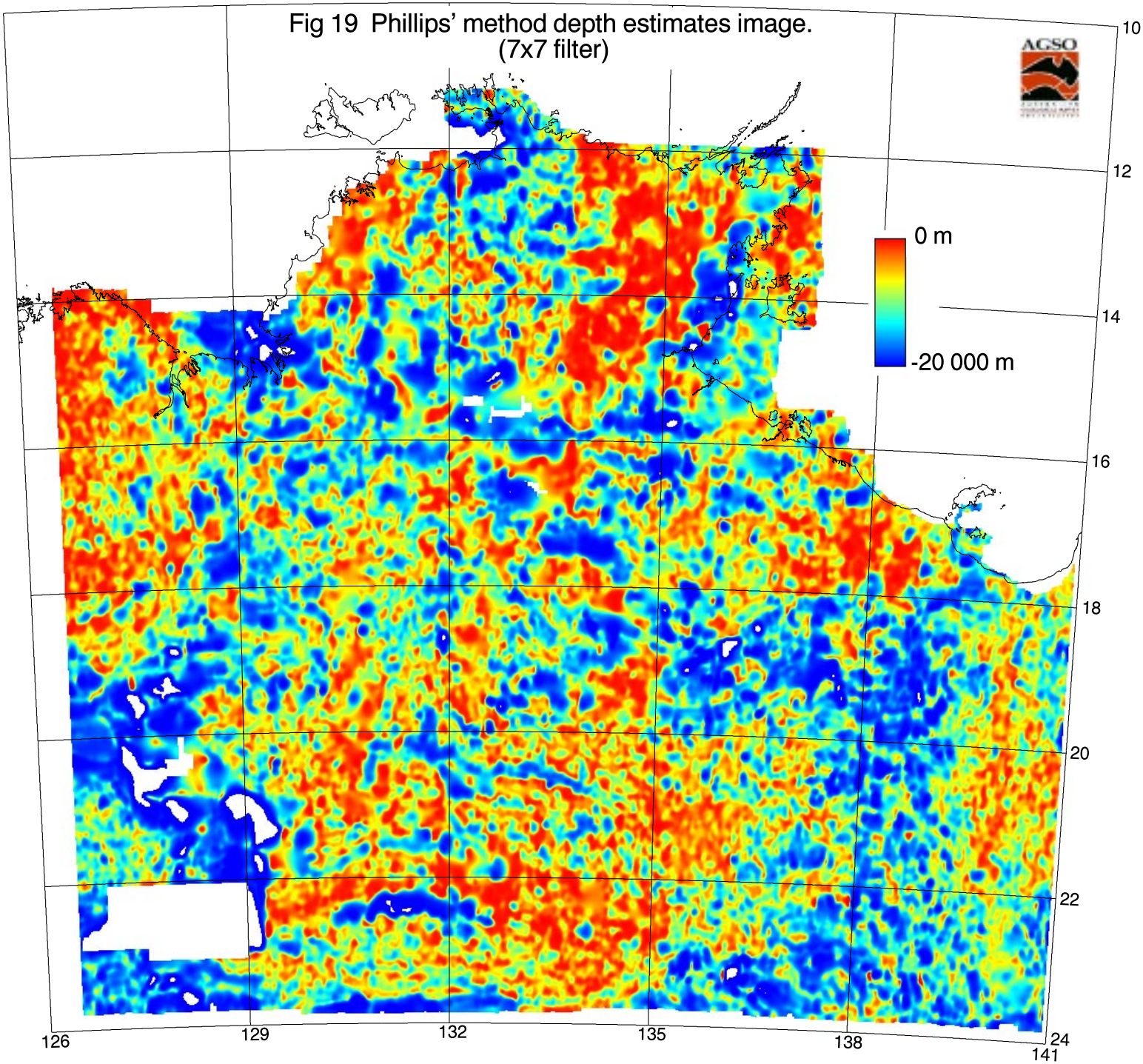

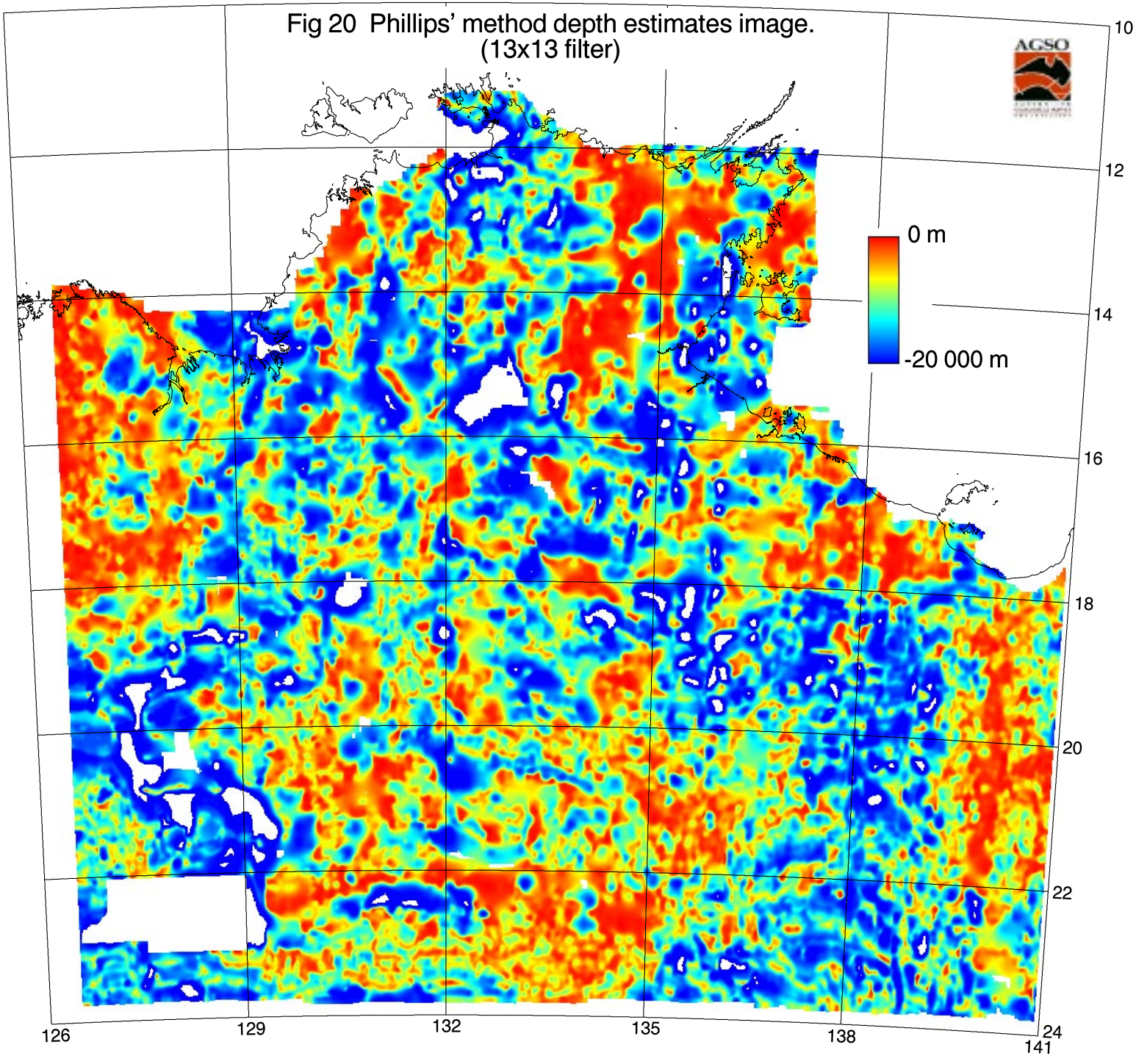
Fig 20 Phillips' method depth estimates image.
(13x13 filter)
AGSO
0 m
-20 000 m
10
12
14
16
18
20
22
24
126
129
132
135
138
141

Fig 21 Naudy's method depth estimates image.
(7x7 filter)

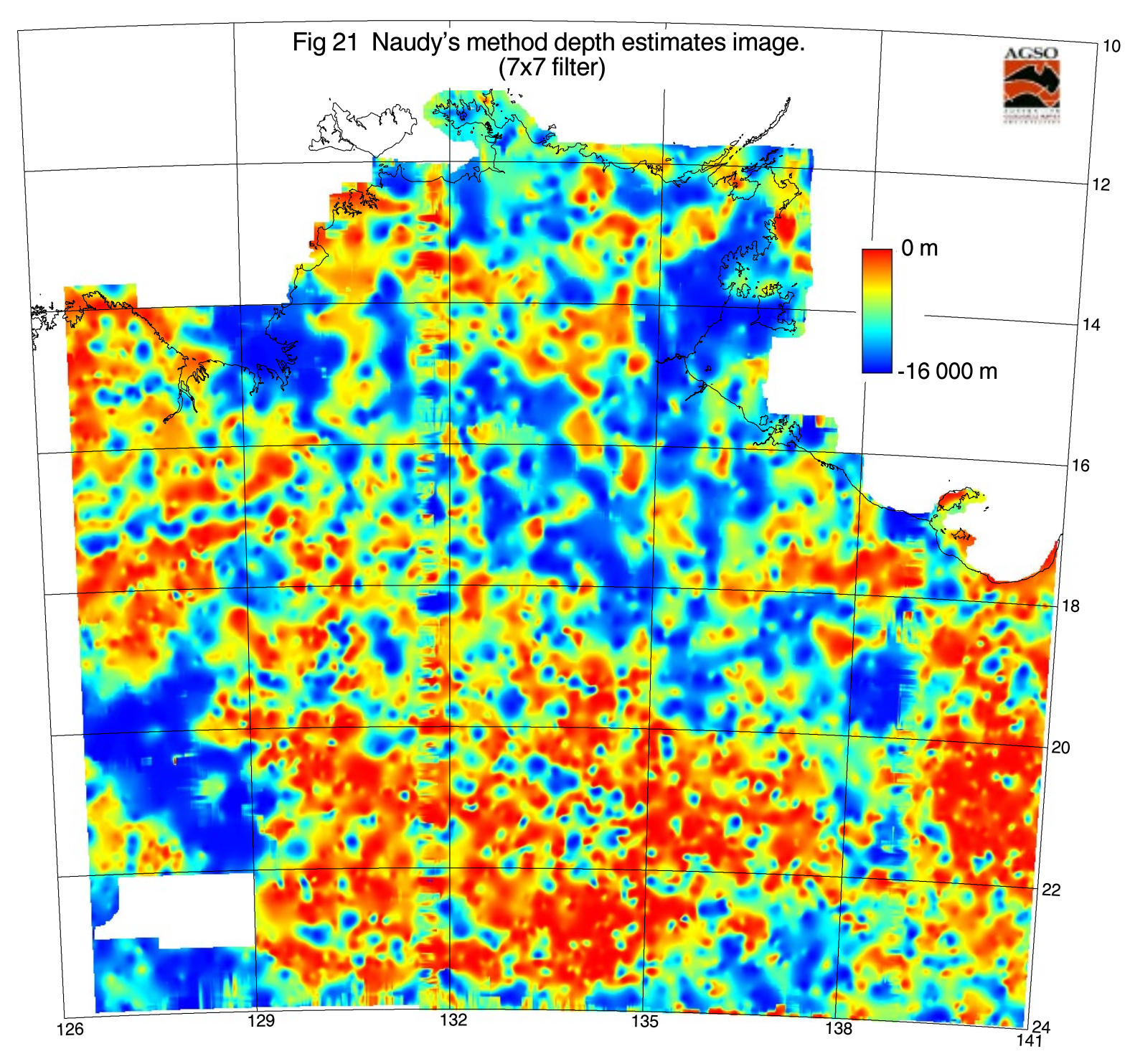

Fig 22 Igneous and volcanic units on Phillips' depth estimates.
(7x7 filter)

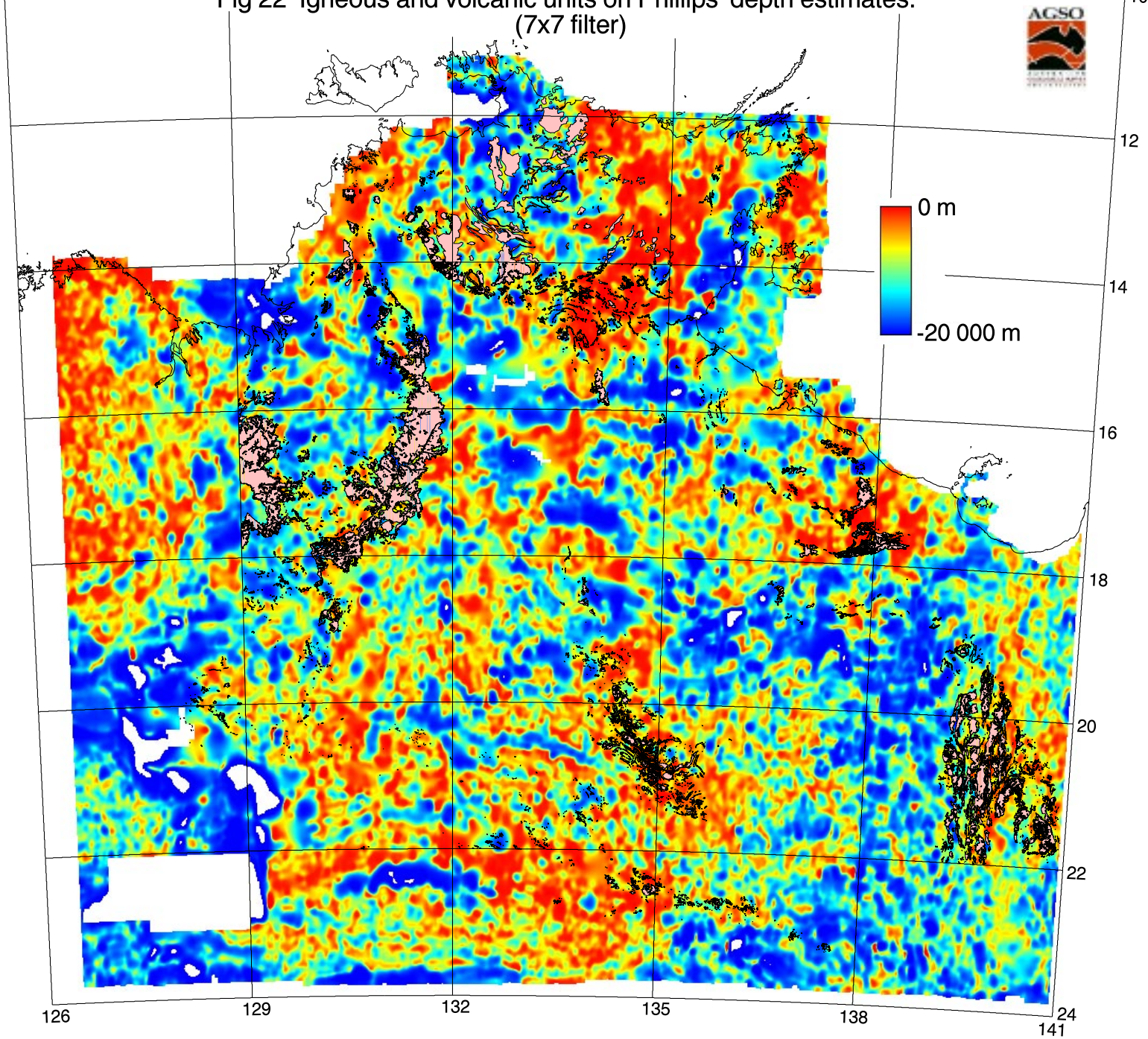

Fig 23 Igneous and volcanic units on Naudy's depth estimates.
(7x7 filter)

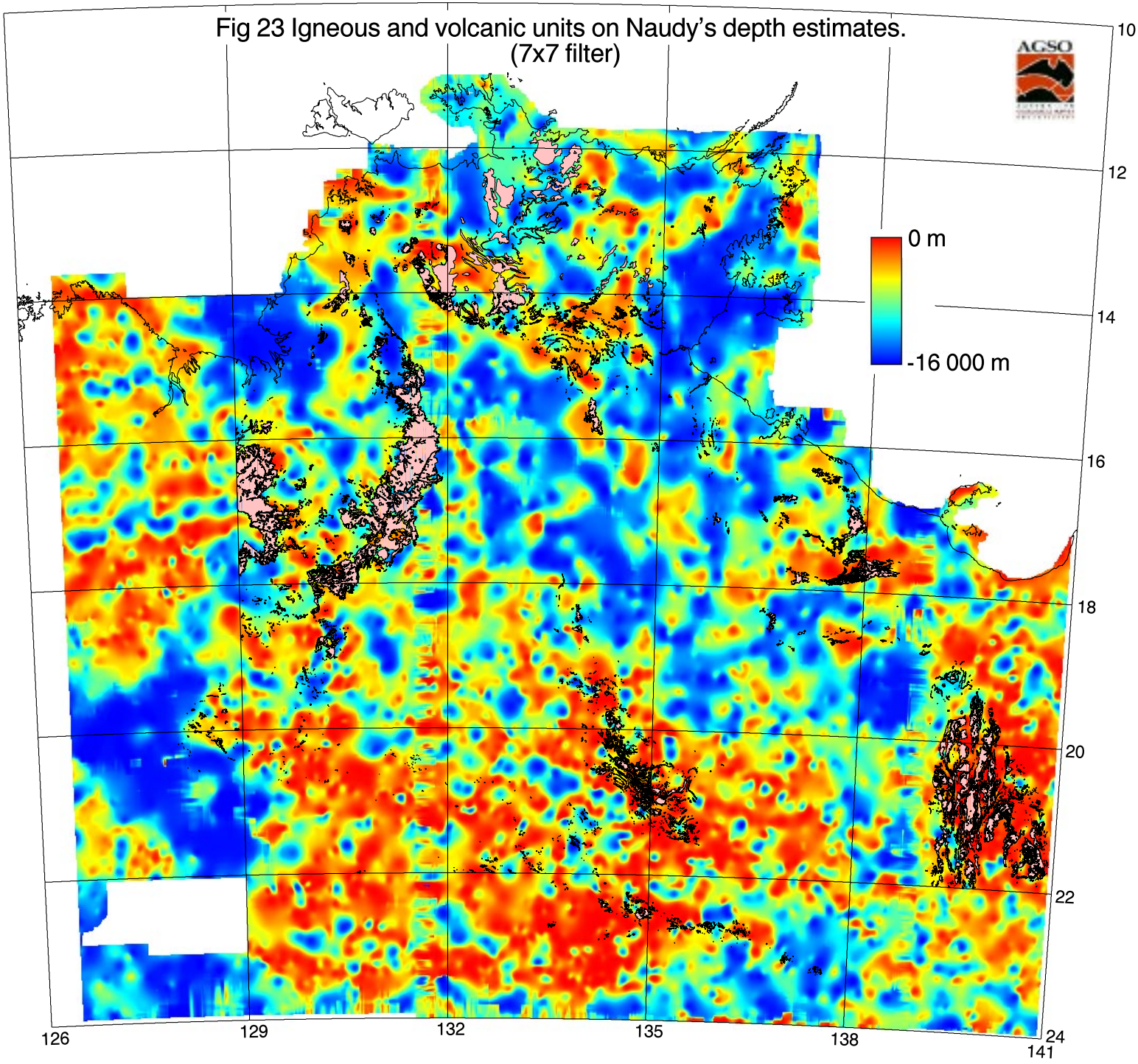

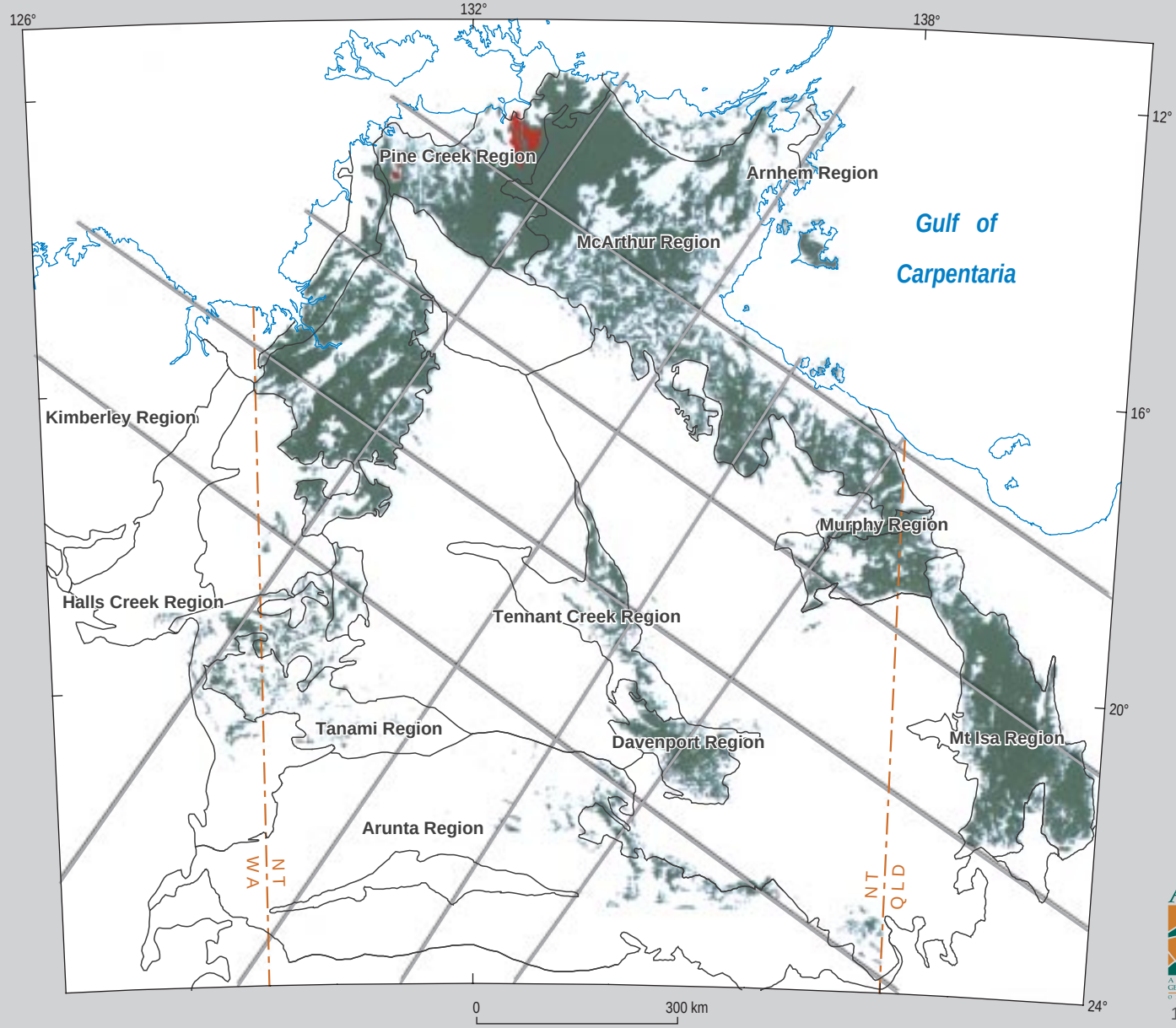

AGSO
AUSTRALIAN GEOLOGICAL SURVEY ORGANISATION

12/A/537

Figure 25 Regions after the national GIS geological regions coverage and Proterozoic outcrop distribution

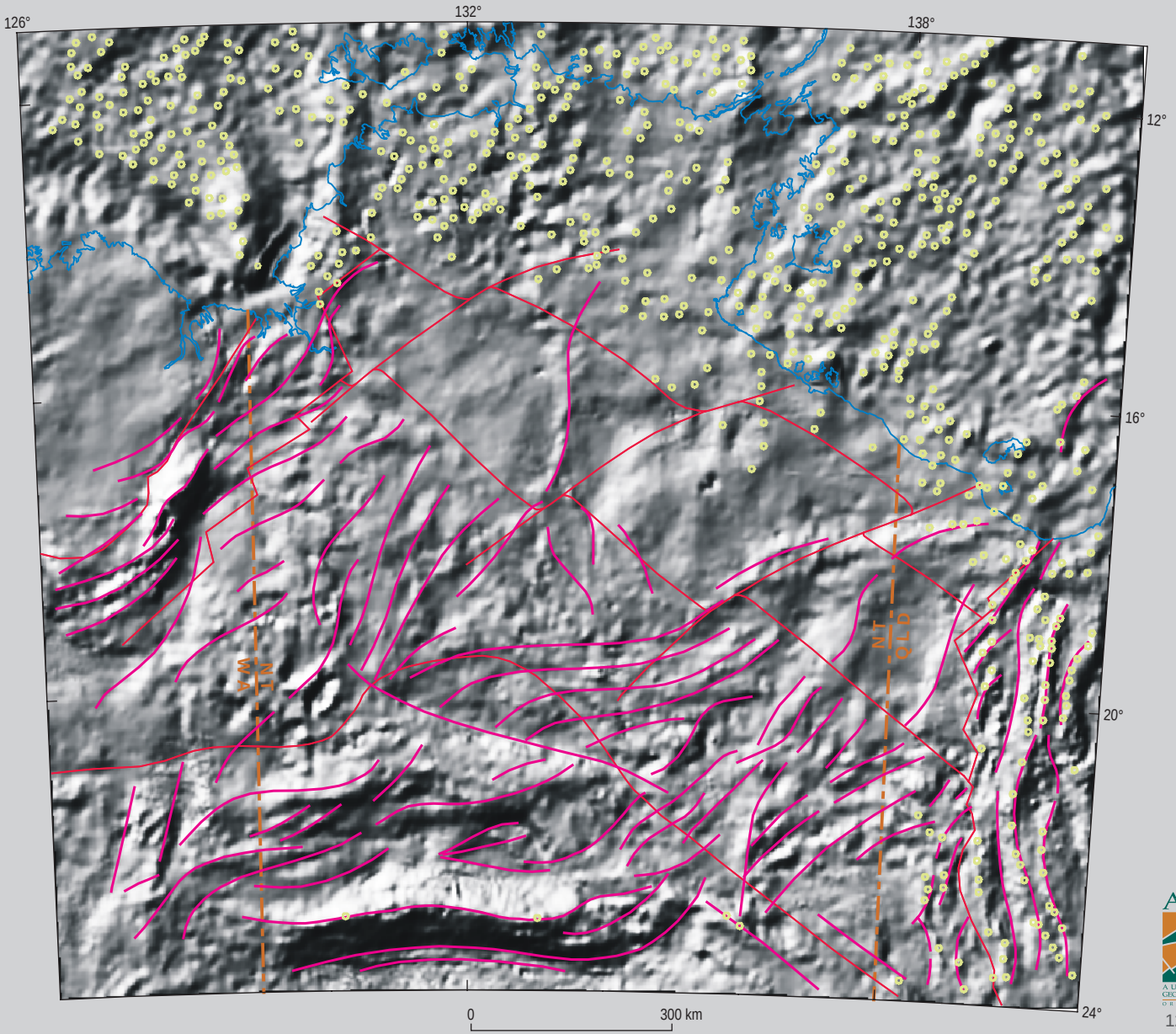

Figure 26 Interpretation of the fabric expressing the anomaly character of the Bouguer Gravity anomaly image

AGSO
AUSTRALIAN GEOLOGICAL SURVEY ORGANISATION

12/A/527

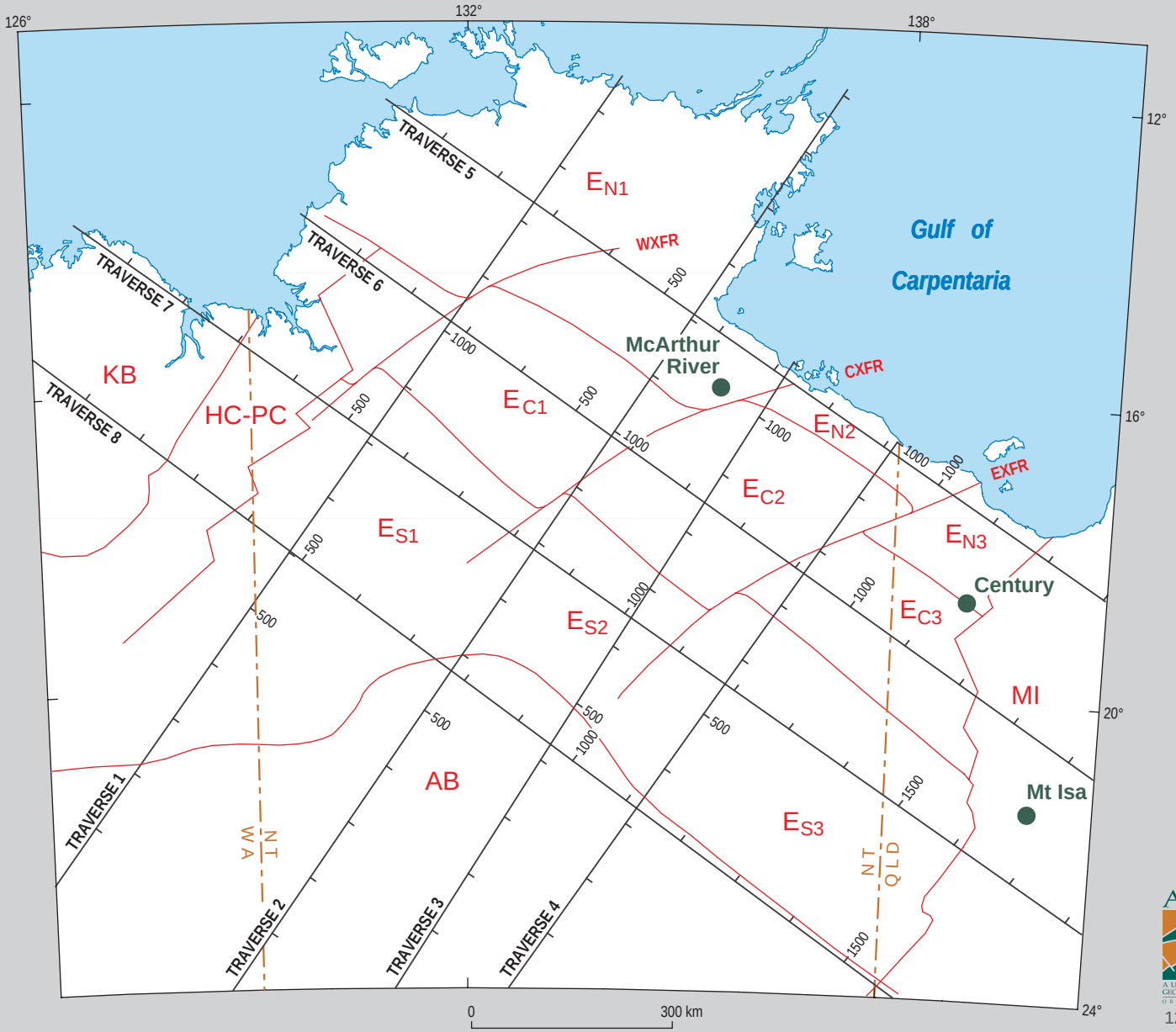

AGSO
AUSTRALIAN GEOLOGICAL SURVEY ORGANISATION
12/A/526

Figure 27 Location map of traverses across North Central Australia. Also shown are the geophysical elements and domains interpreted from analysis of the image data

KB = Kimberley Block, HC-PC = Halls to Pine Creek belt, AB = Arunta Belt, MI = Mt Isa Belt, E_S = Southern Element, E_C = Central Element, E_N = Northern Element of the North Australian Craton (NAC), each divided into western (1), central (2) and eastern (3) domains, by western (WXFR), central (CXFR) and eastern (EXFR) transverse structure or zones.

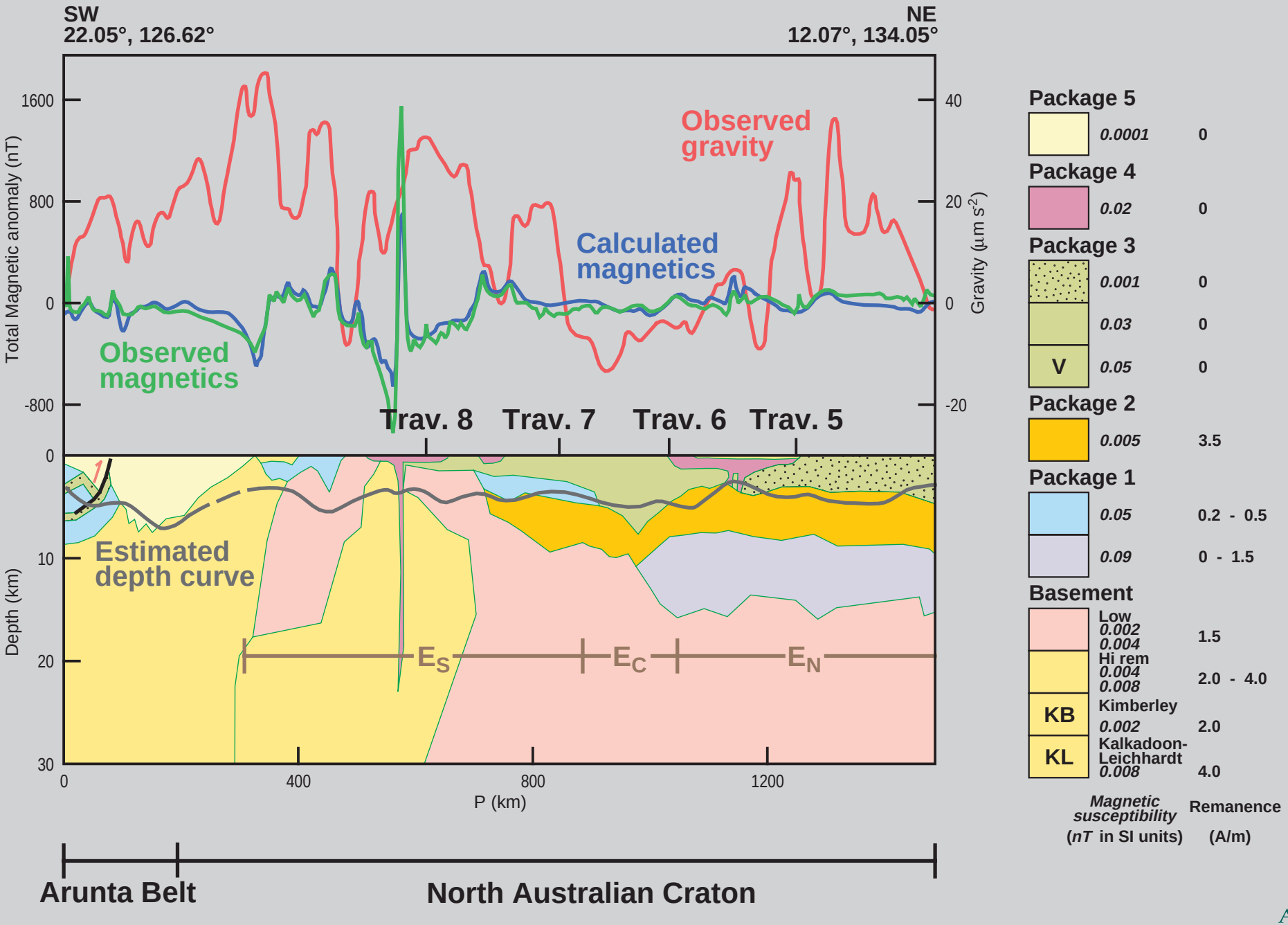

Figure 28 Traverse 1

KB = Kimberley Block, HC-PC = Halls to Pine Creek belt, AB = Arunta Belt, MI = Mt Isa Belt, E_S = Southern Element, E_C = Central Element, E_N = Northern Element of the North Australian Craton (NAC), each divided into western (1), central (2) and eastern (3) domains, by western (WXFR), central (CXFR) and eastern (EXFR) transverse structures or zones.

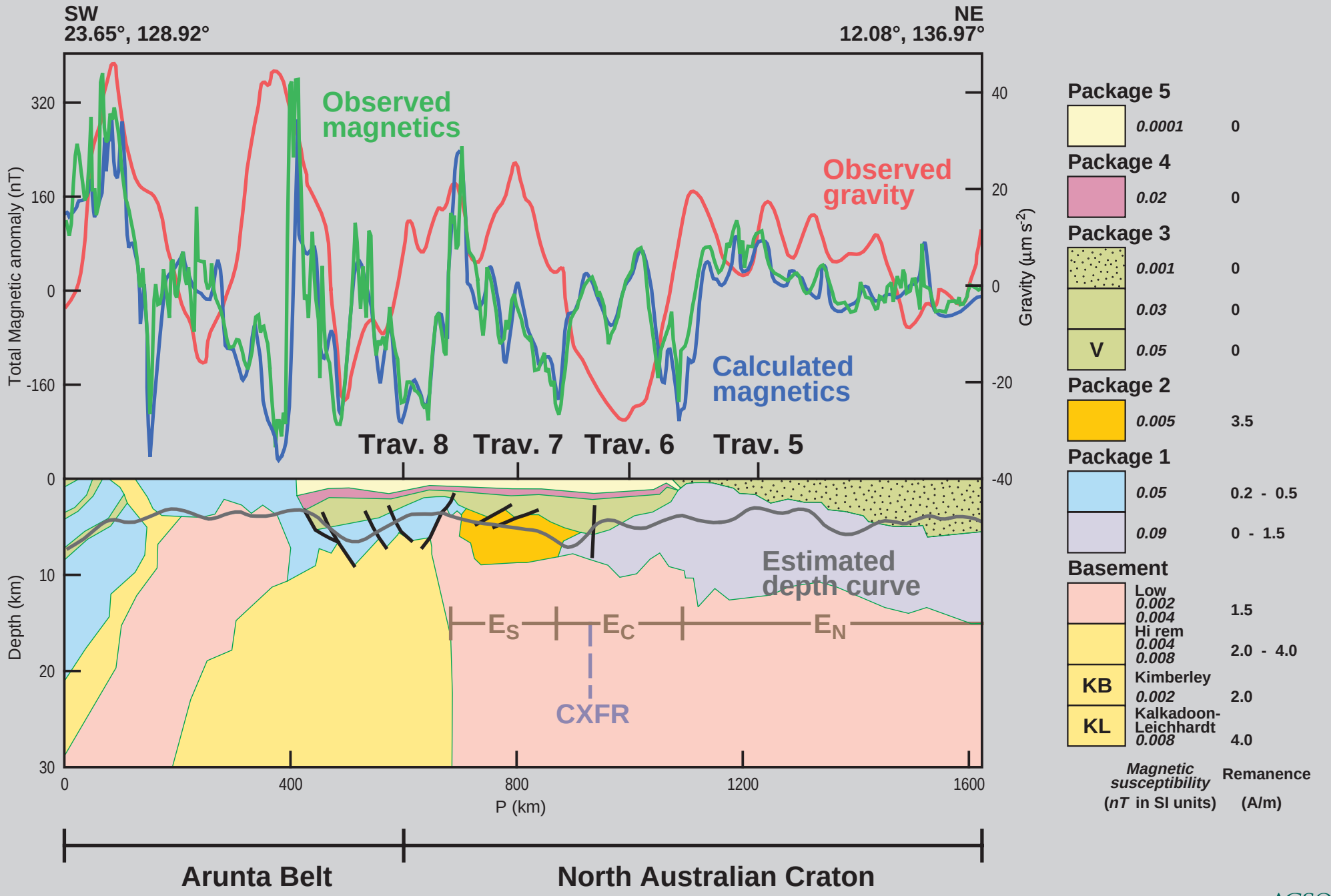

Figure 29 Traverse 2

KB = Kimberley Block, HC-PC = Halls to Pine Creek belt, AB = Arunta Belt, MI = Mt Isa Belt, E_S = Southern Element, E_C = Central Element, E_N = Northern Element of the North Australian Craton (NAC), each divided into western (1), central (2) and eastern (3) domains, by western (WXFR), central (CXFR) and eastern (EXFR) transverse structures or zones.

AGSO
AUSTRALIAN GEOLOGICAL SURVEY ORGANISATION
12/A/529

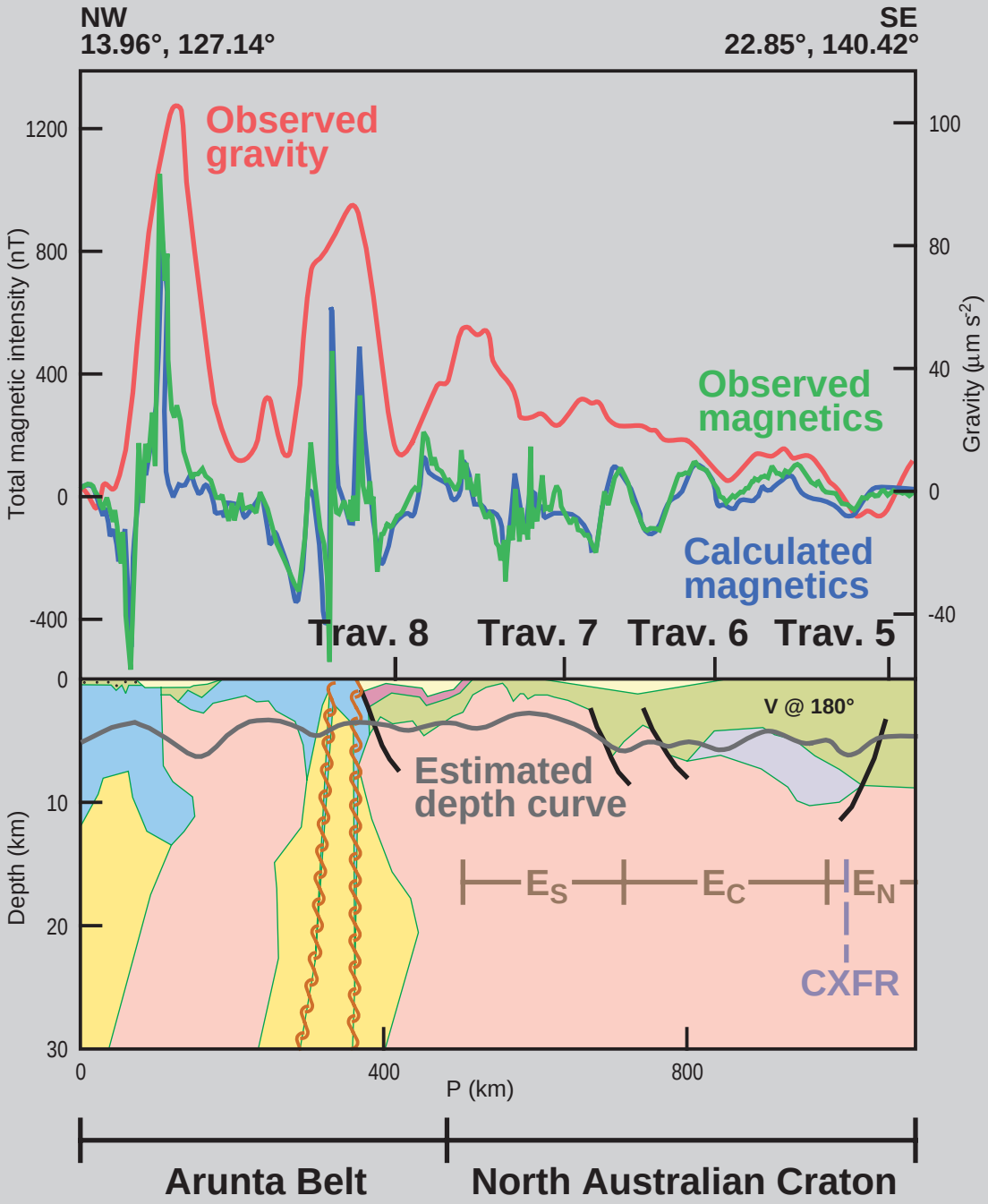

Figure 30 Traverse 3

KB = Kimberley Block, HC-PC = Halls to Pine Creek belt, AB = Arunta Belt, MI = Mt Isa Belt, E_S = Southern Element, E_C= Central Element, E_N = Northern Element of the North Australian Craton (NAC), each divided into western (1), central (2) and eastern (3) domains, by western (WXFR), central (CXFR) and eastern (EXFR) transverse structures or zones.

AGSO
AUSTRALIAN GEOLOGICAL SURVEY ORGANISATION

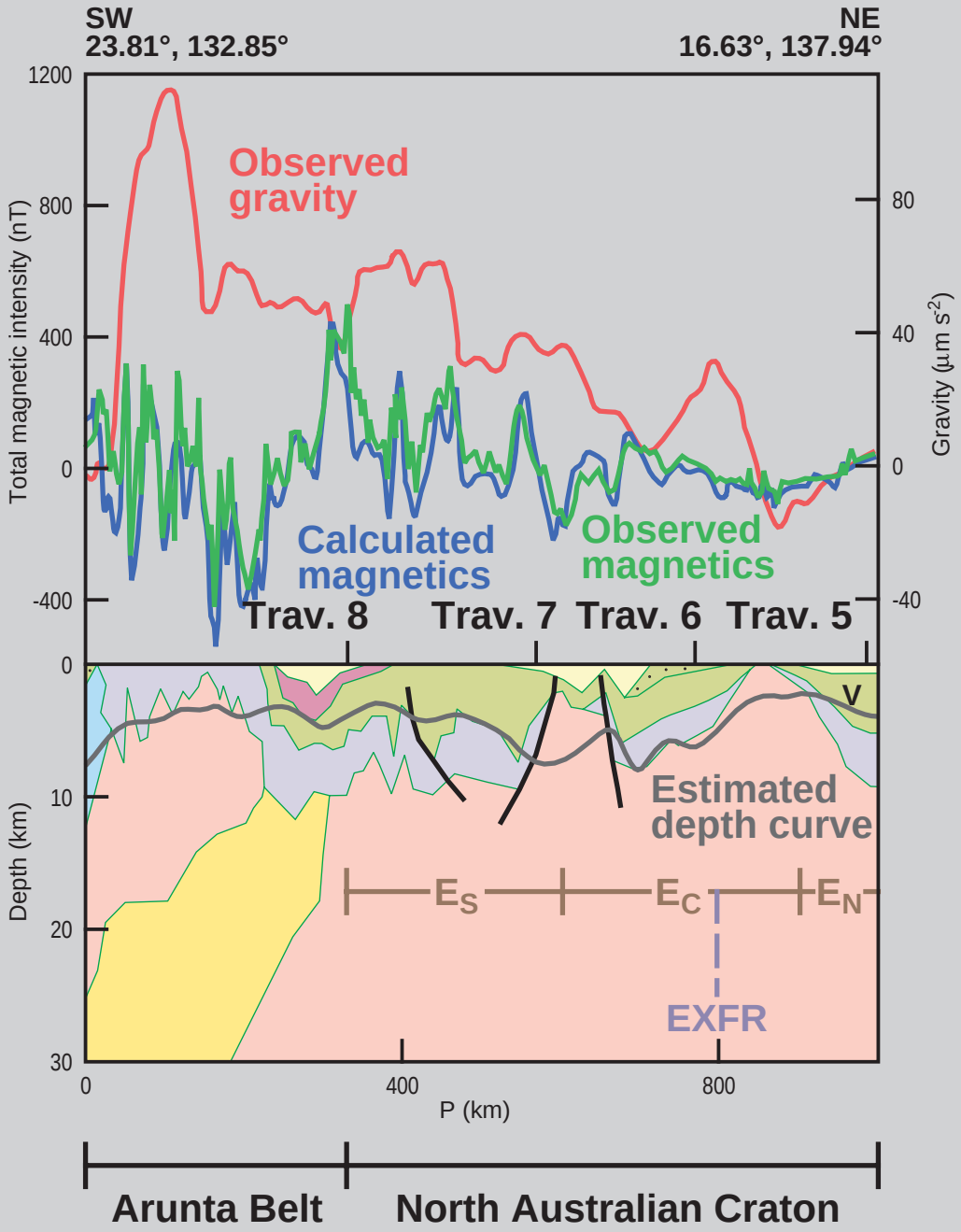

Figure 31 Traverse 4

KB = Kimberley Block, HC-PC = Halls to Pine Creek belt, AB = Arunta Belt, MI = Mt Isa Belt, E_S = Southern Element, E_C= Central Element, E_N = Northern Element of the North Australian Craton (NAC), each divided into western (1), central (2) and eastern (3) domains, by western (WXFR), central (CXFR) and eastern (EXFR) transverse structures or zones.

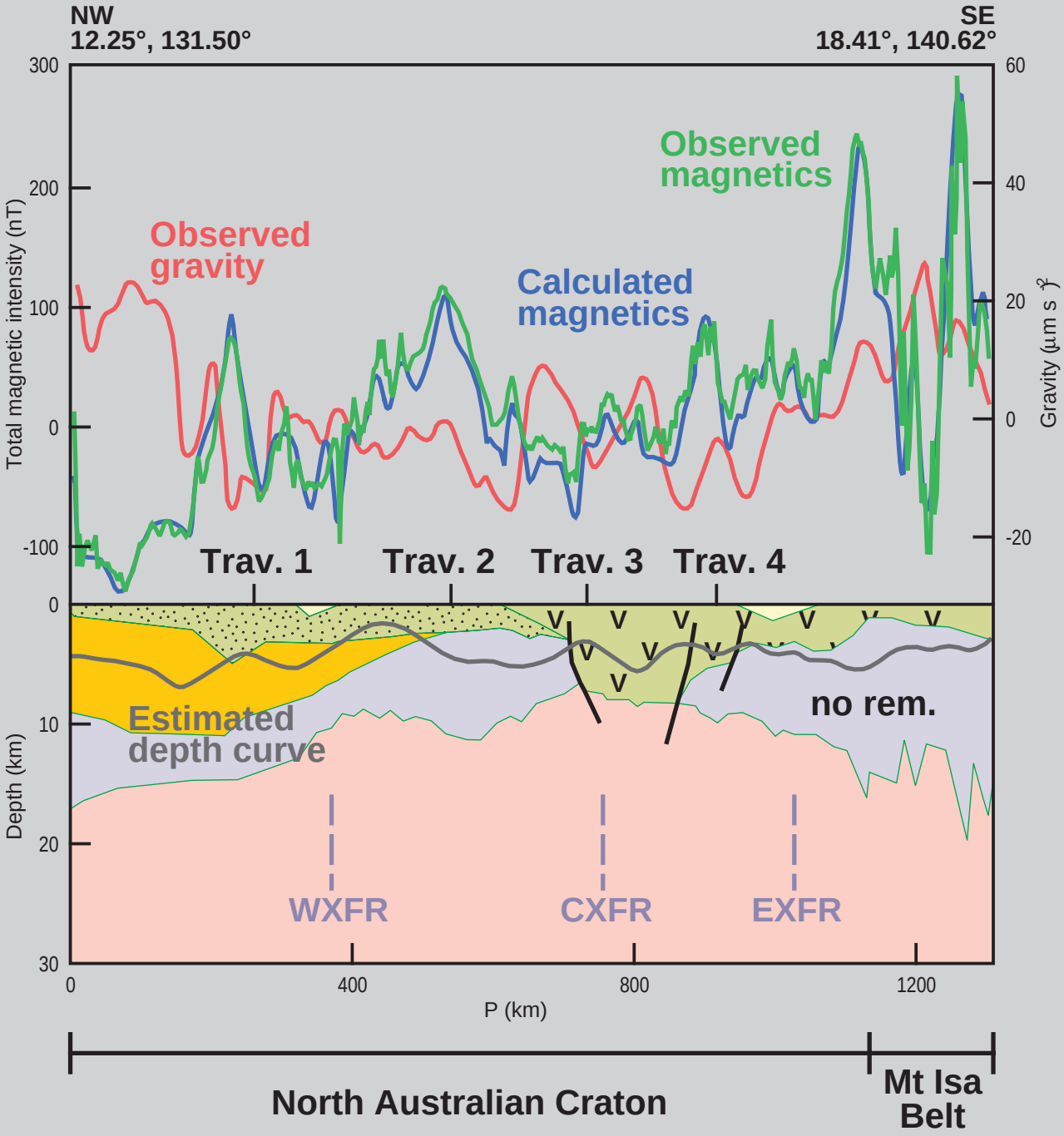

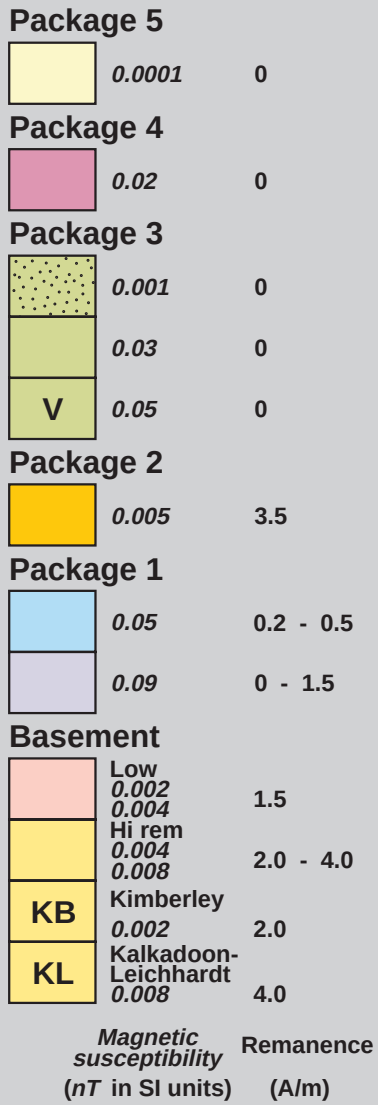

Figure 32 Traverse 5

KB = Kimberley Block, HC-PC = Halls to Pine Creek belt, AB = Arunta Belt, MI = Mt Isa Belt, E_S = Southern Element, E_C= Central Element, E_N= Northern Element of the North Australian Craton (NAC), each divided into western (1), central (2) and eastern (3) domains, by western (WXFR), central (CXFR) and eastern (EXFR) transverse structures or zones.

12/A/532

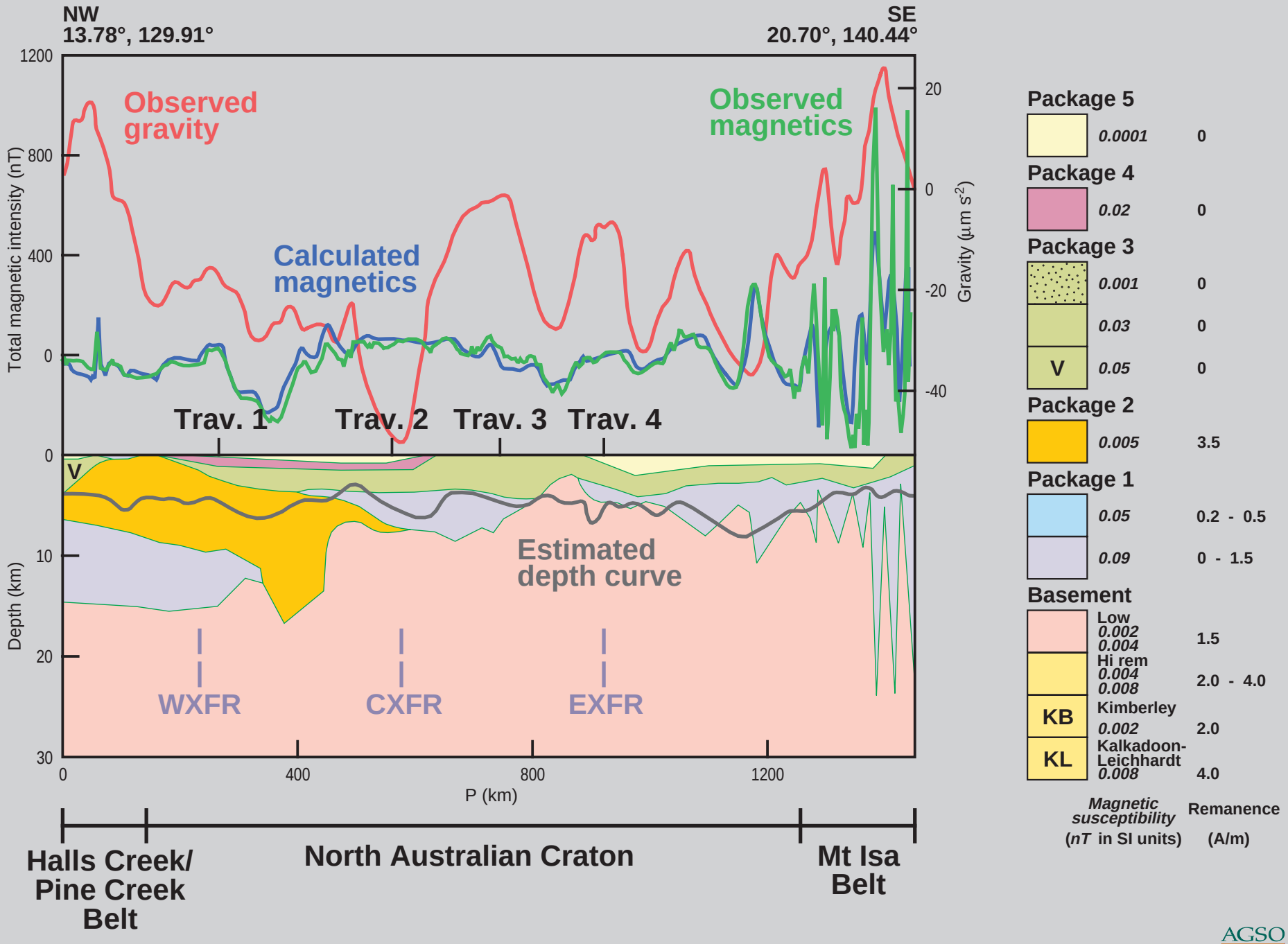

Figure 33 Traverse 6

KB = Kimberley Block, HC-PC = Halls to Pine Creek belt, AB = Arunta Belt, MI = Mt Isa Belt, E_S = Southern Element, E_C= Central Element, E_N = Northern Element of the North Australian Craton (NAC), each divided into western (1), central (2) and eastern (3) domains, by western (WXFR), central (CXFR) and eastern (EXFR) transverse structures or zones.

AGSO
AUSTRALIAN GEOLOGICAL SURVEY ORGANISATION
12/A/533

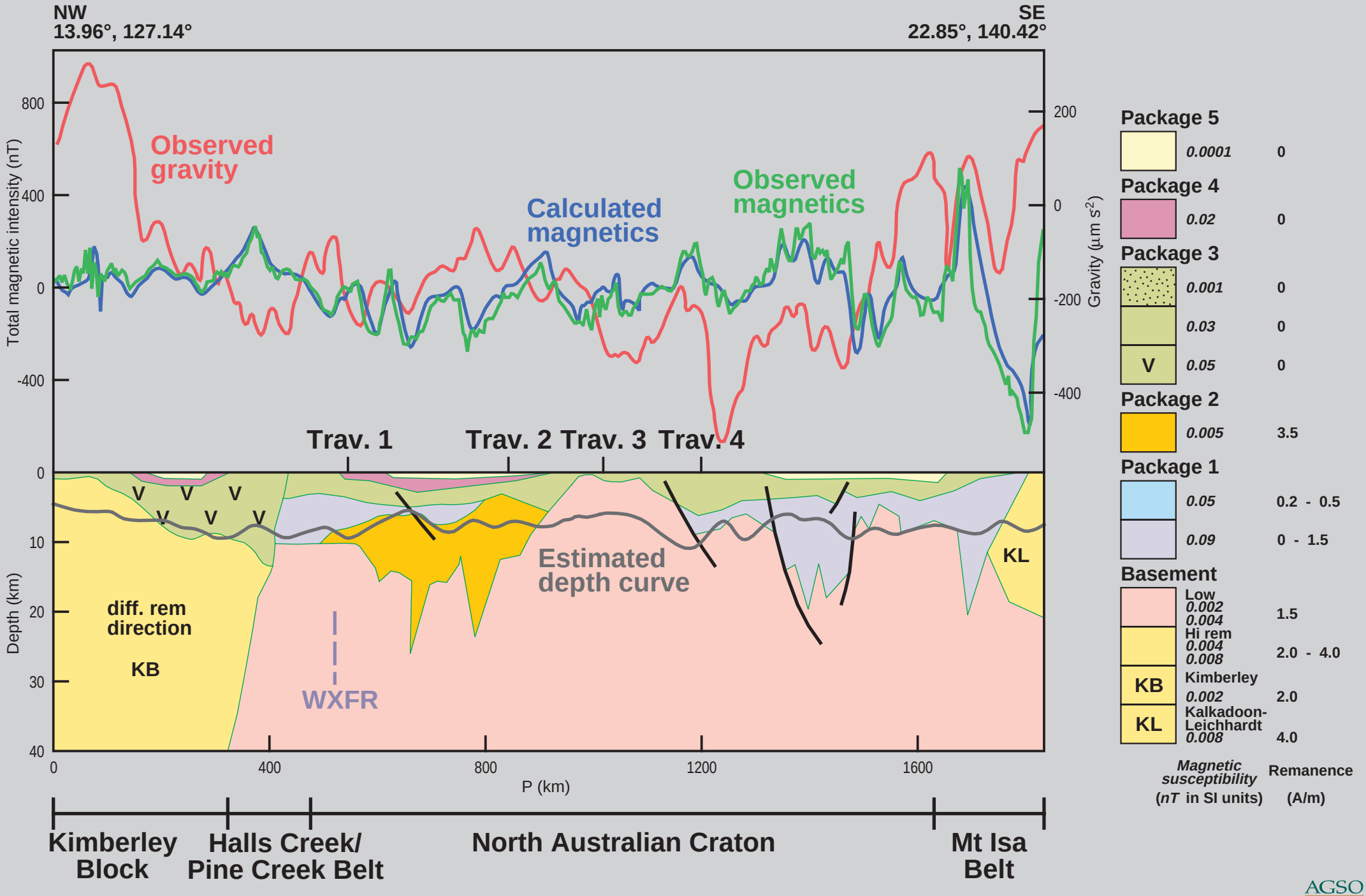

Figure 34 Traverse 7 KB = Kimberley Block, HC-PC = Halls to Pine Creek belt, AB = Arunta Belt, MI = Mt Isa Belt, E_S = Southern Element, E_C= Central Element, E_N = Northern Element of the North Australian Craton (NAC), each divided into western (1), central (2) and eastern (3) domains, by western (WXFR), central (CXFR) and eastern (EXFR) transverse structures or zones.

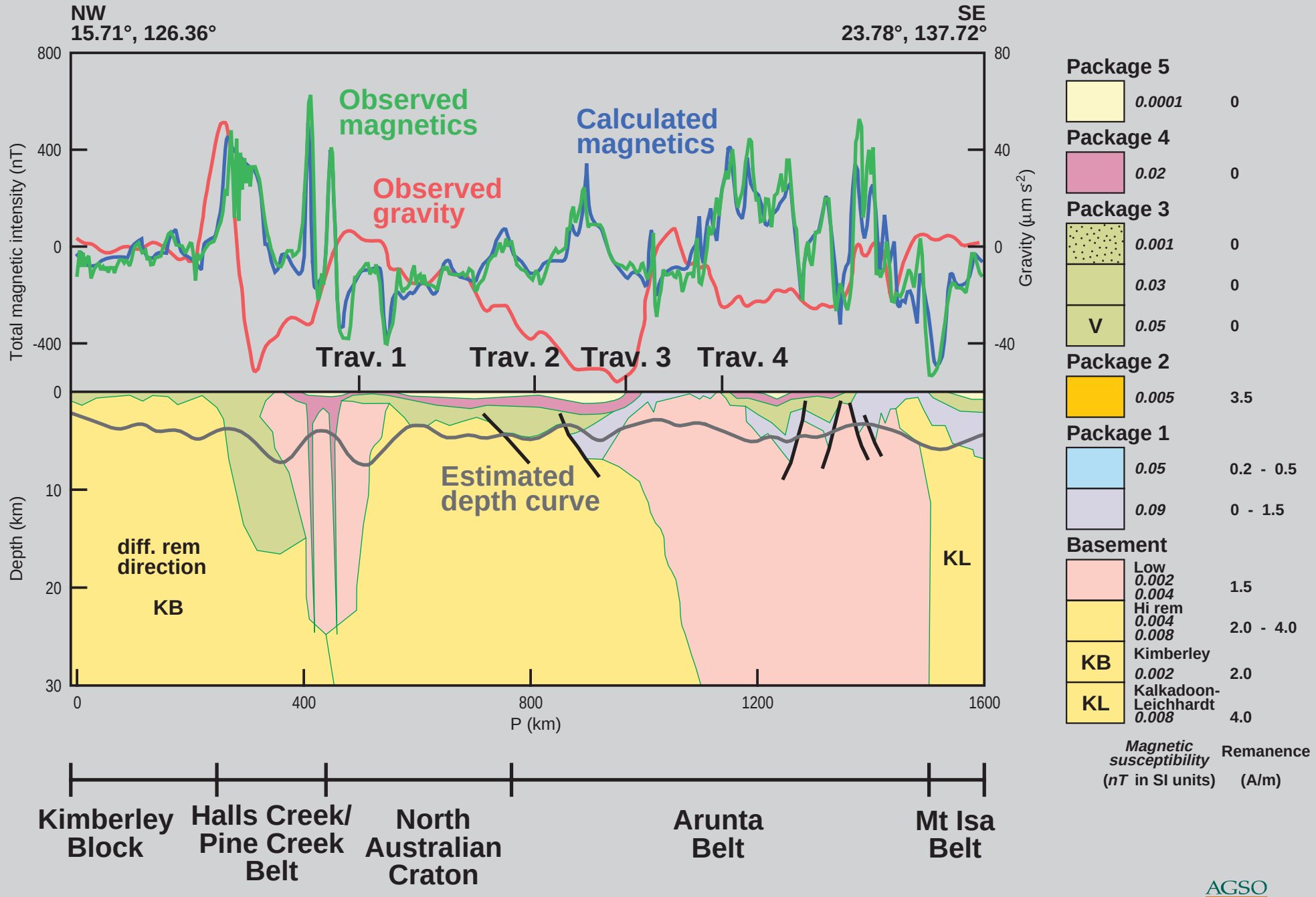

Figure 35 Traverse 8

KB = Kimberley Block, HC-PC = Halls to Pine Creek belt, AB = Arunta Belt, MI = Mt Isa Belt, E_S = Southern Element, E_C= Central Element, E_N = Northern Element of the North Australian Craton (NAC), each divided into western (1), central (2) and eastern (3) domains, by western (WXFR), central (CXFR) and eastern (EXFR) transverse structures or zones.

12/A/535

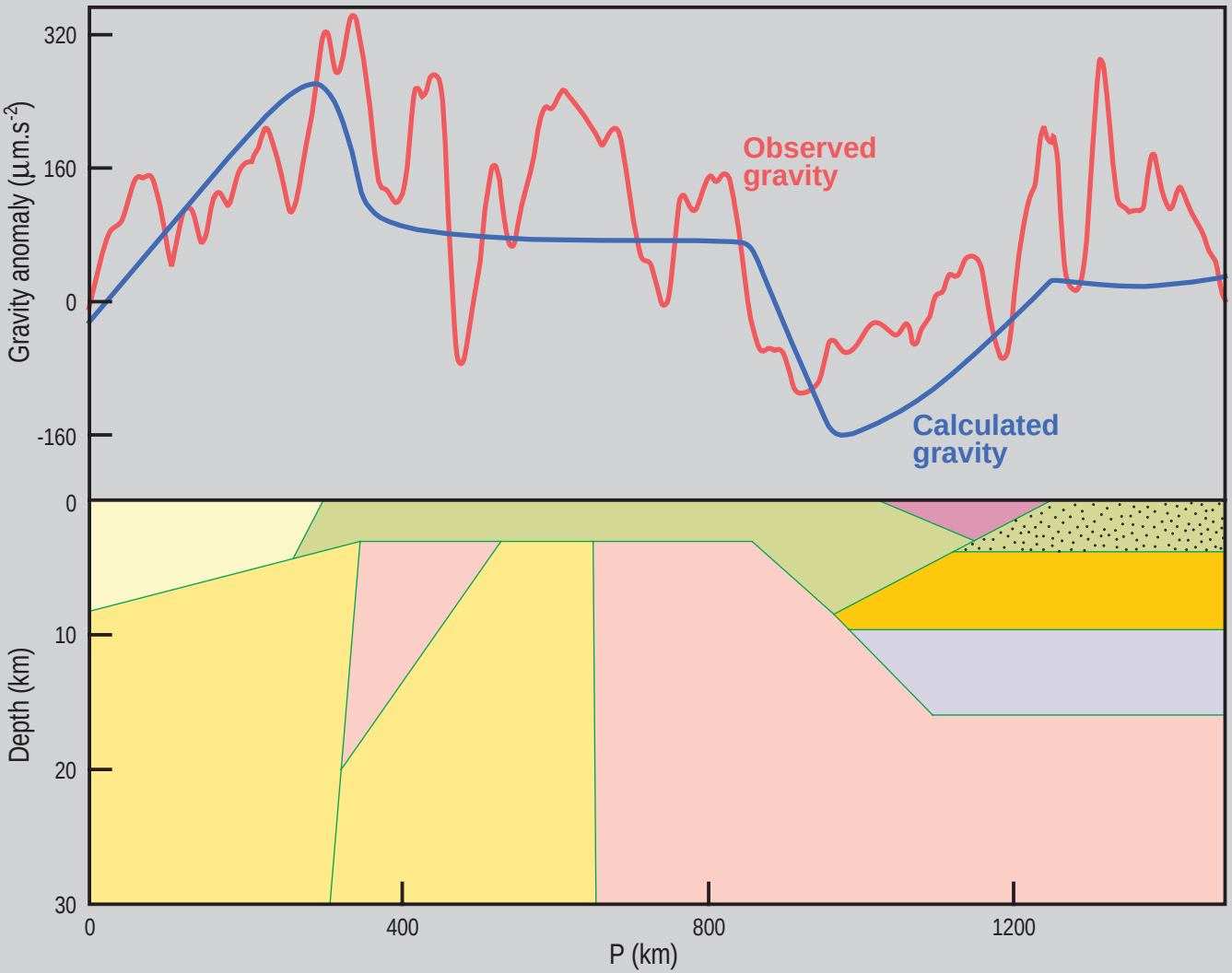

Figure 36 Gravity model of traverse 1. Compare this simple model with the geological model used to calculate the magnetic anomaly match in Figure 28

AGSO
AUSTRALIAN GEOLOGICAL SURVEY ORGANISATION

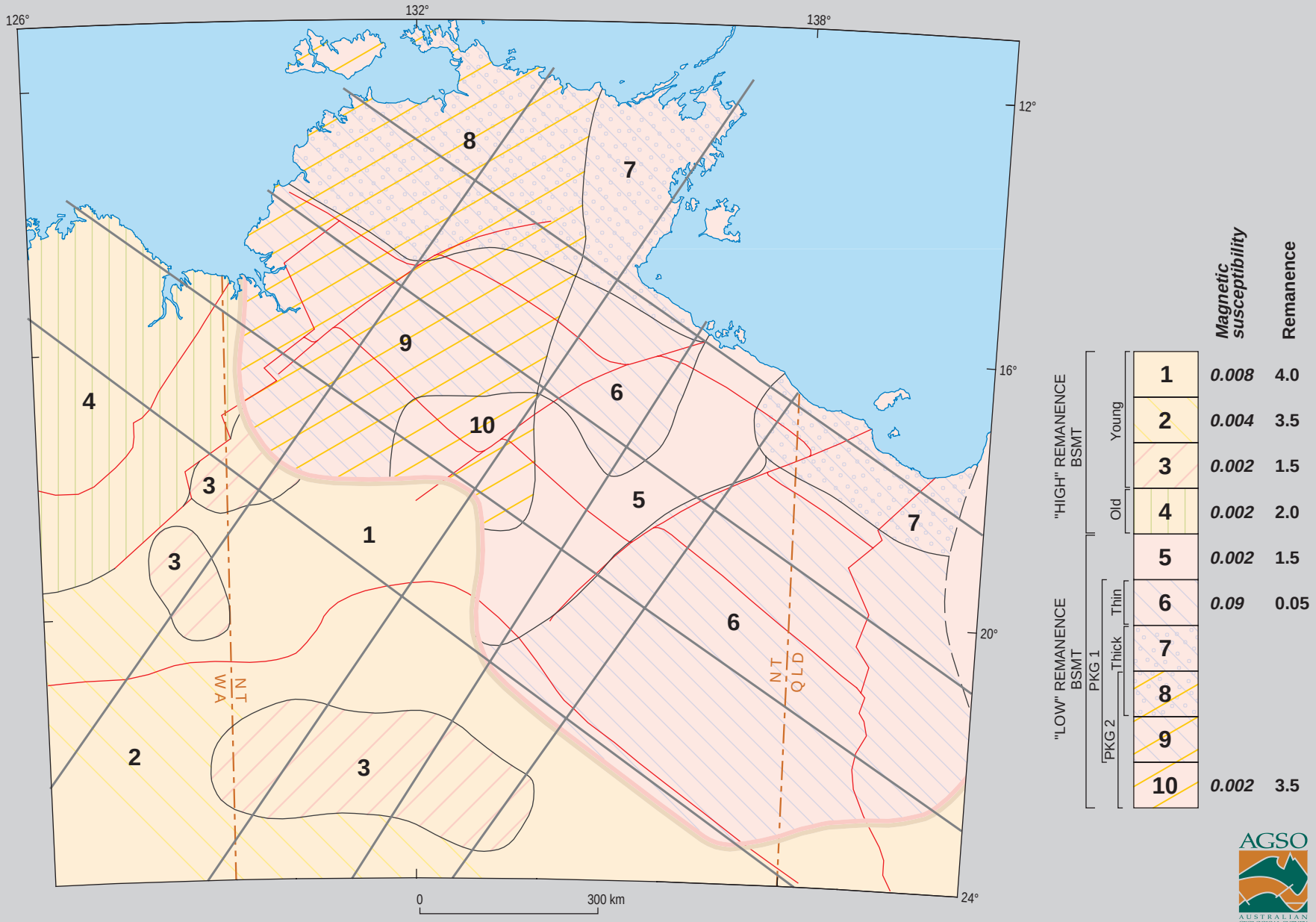

Figure 37 Crustal elements of North Central Australia

AGSO
AUSTRALIAN GEOLOGICAL SURVEY ORGANISATION

12/A/519

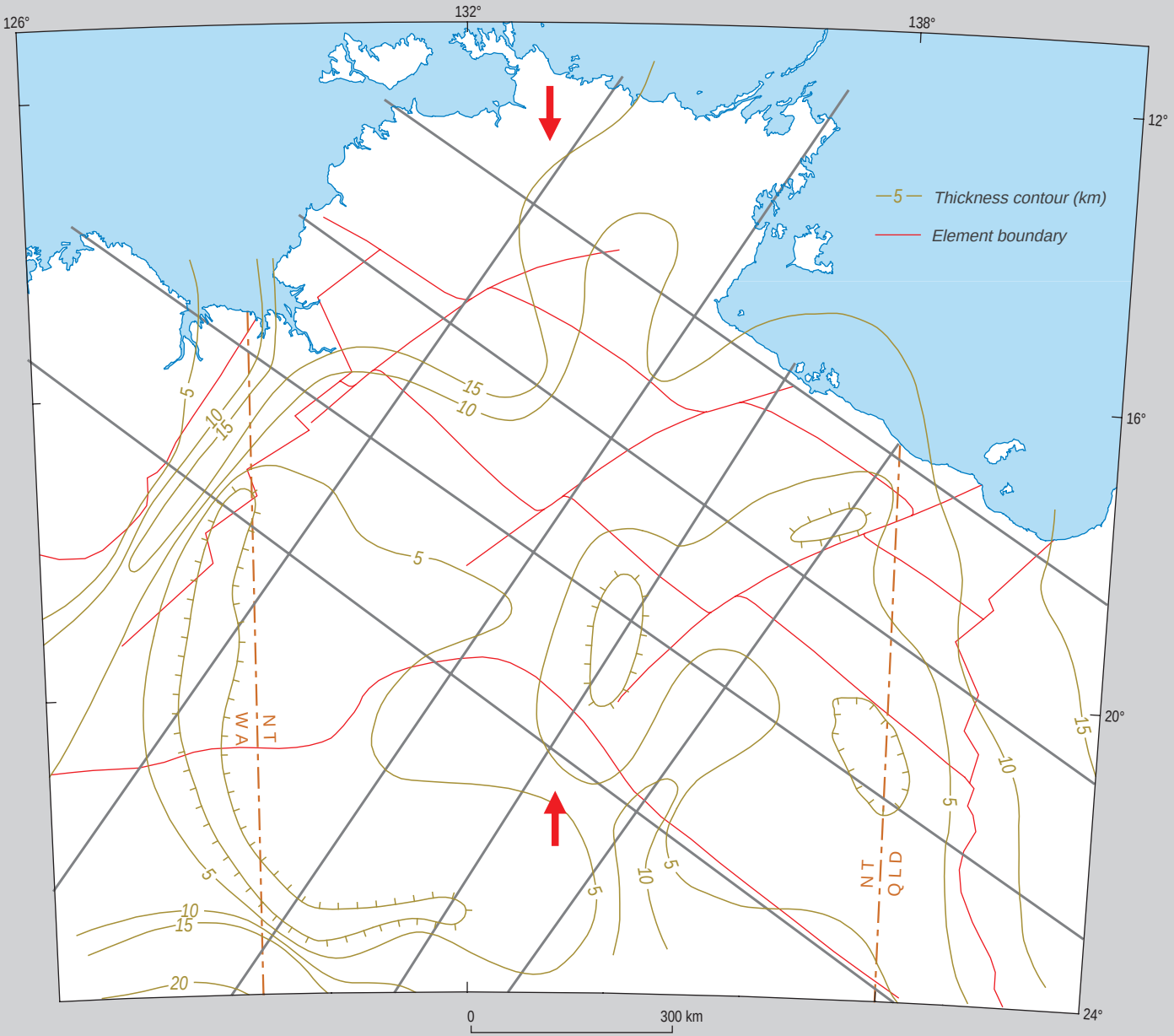

Figure 38 Depth to "Basement" or non-strataform bodies

AGSO
AUSTRALIAN GEOLOGICAL SURVEY ORGANISATION

12/A/520

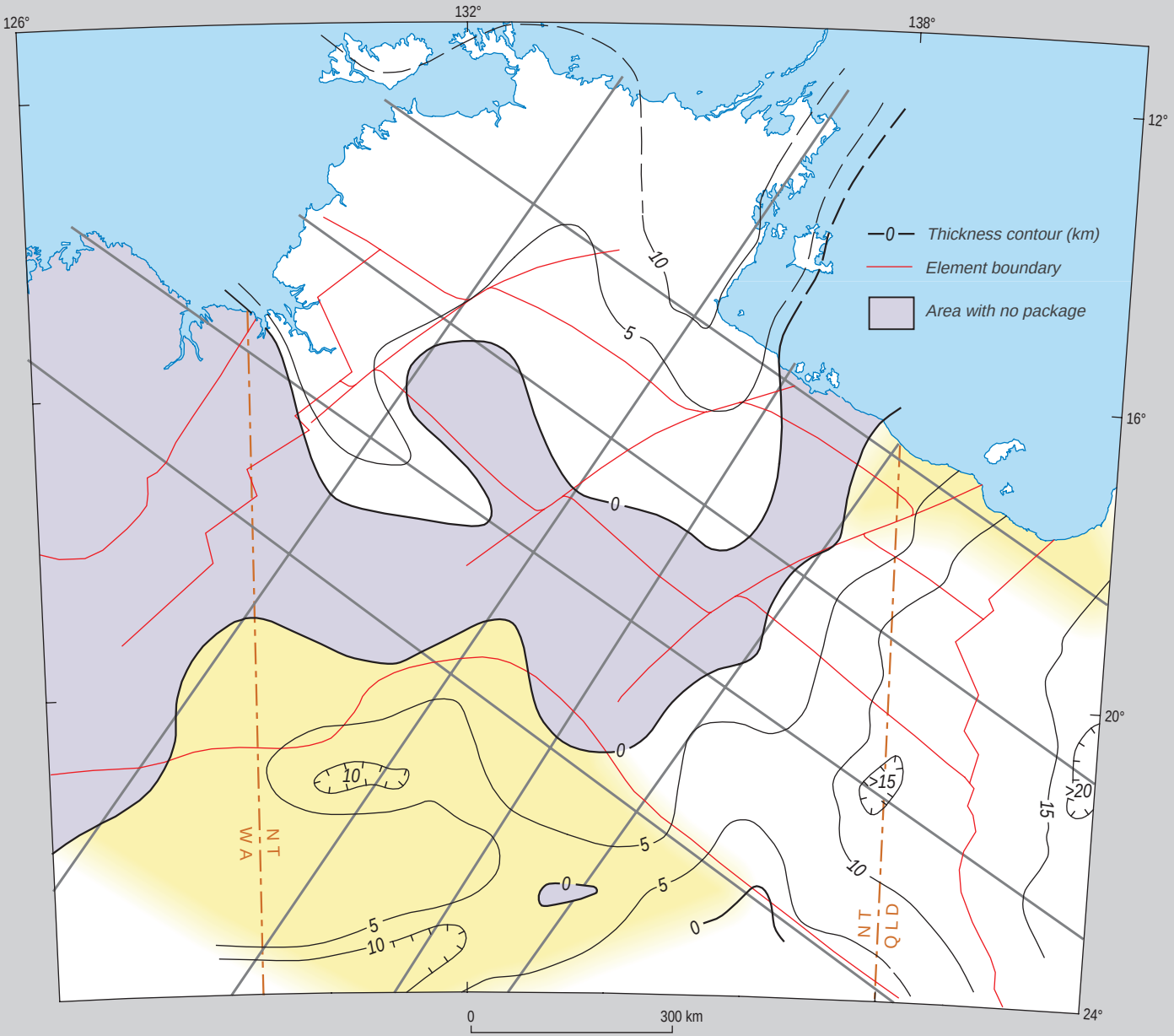

Figure 39 Thickness contours of Package 1

AGSO
AUSTRALIAN GEOLOGICAL SURVEY ORGANISATION

12/A/521

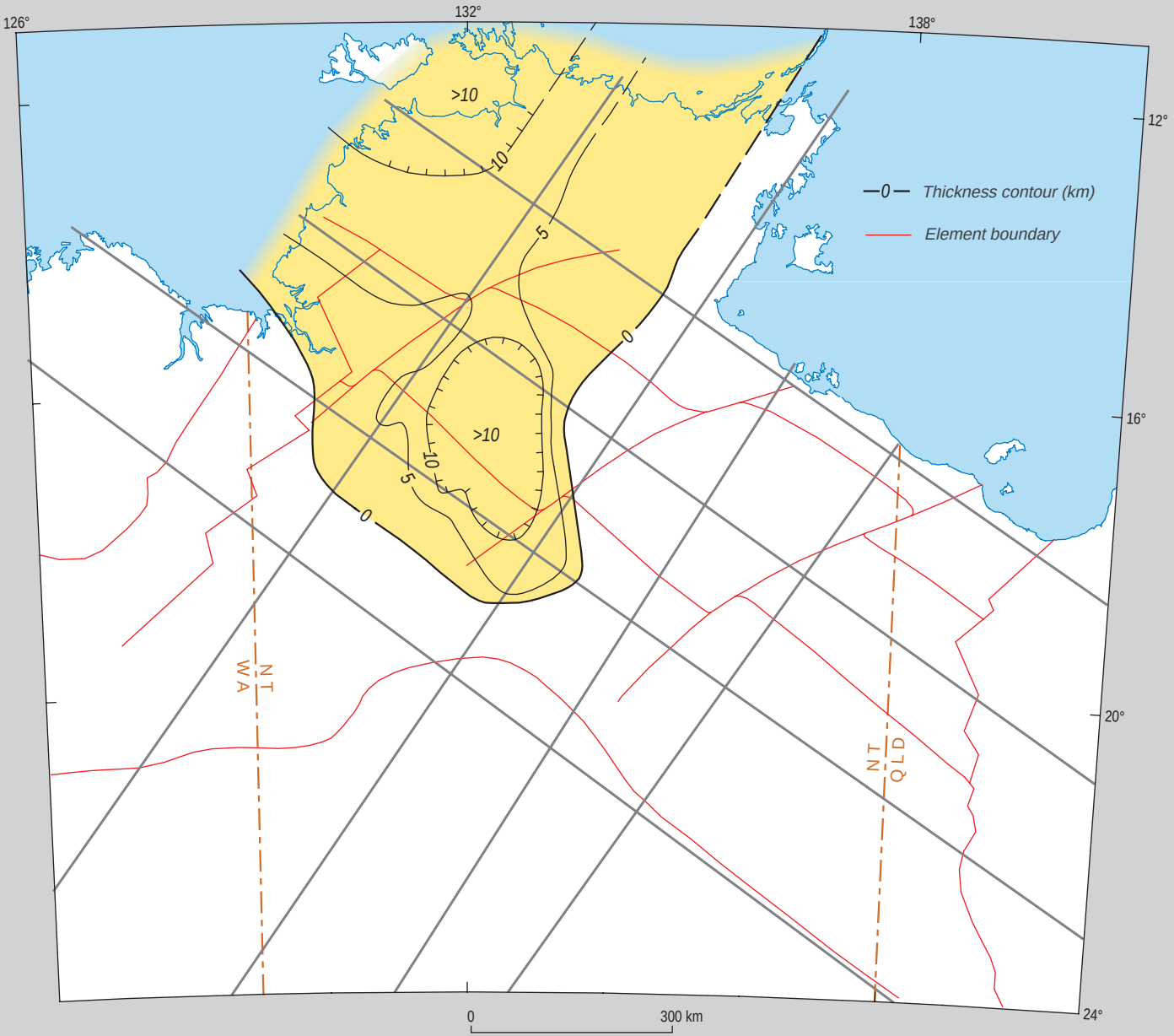

Figure 40 Thickness contours of Package 2

AGSO
AUSTRALIAN GEOLOGICAL SURVEY ORGANISATION

12/A/522

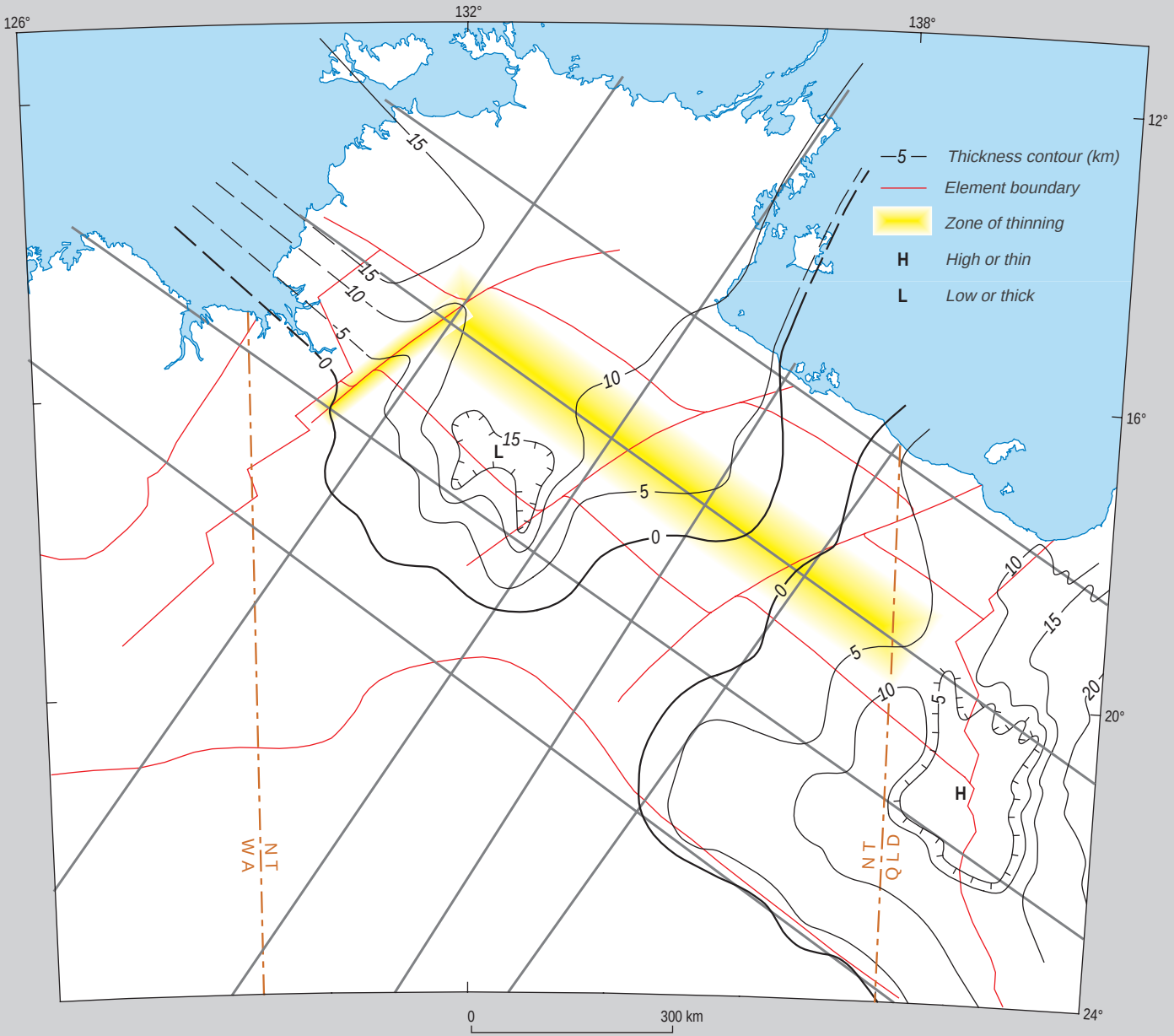

Figure 41 Thickness contours of combined Packages 1 and 2 outside of the Arunta Domain

AGSO
AUSTRALIAN GEOLOGICAL SURVEY ORGANISATION

12/A/523

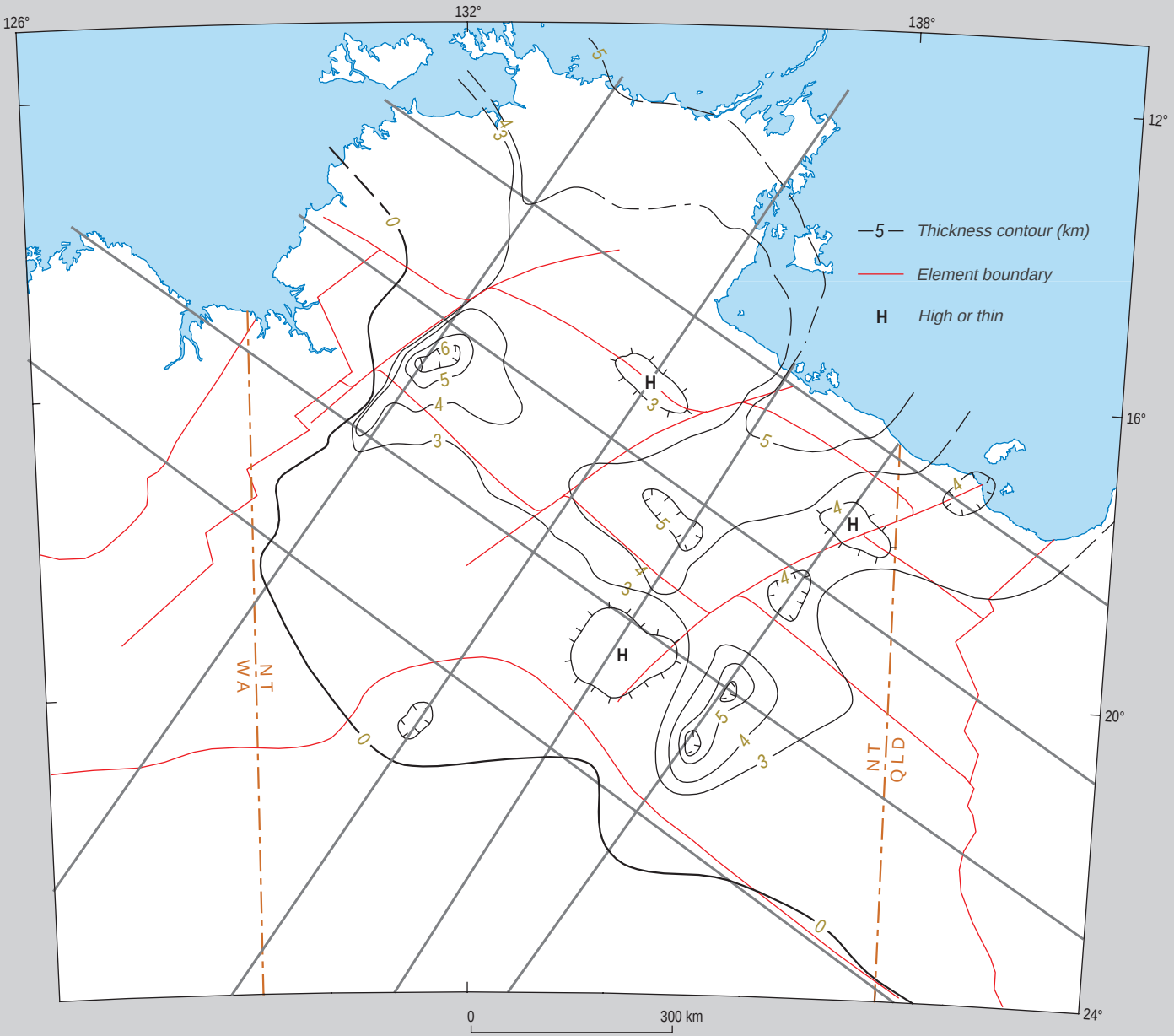

Figure 42 Thickness contours of Package 3

AGSO
AUSTRALIAN GEOLOGICAL SURVEY ORGANISATION

12/A/524

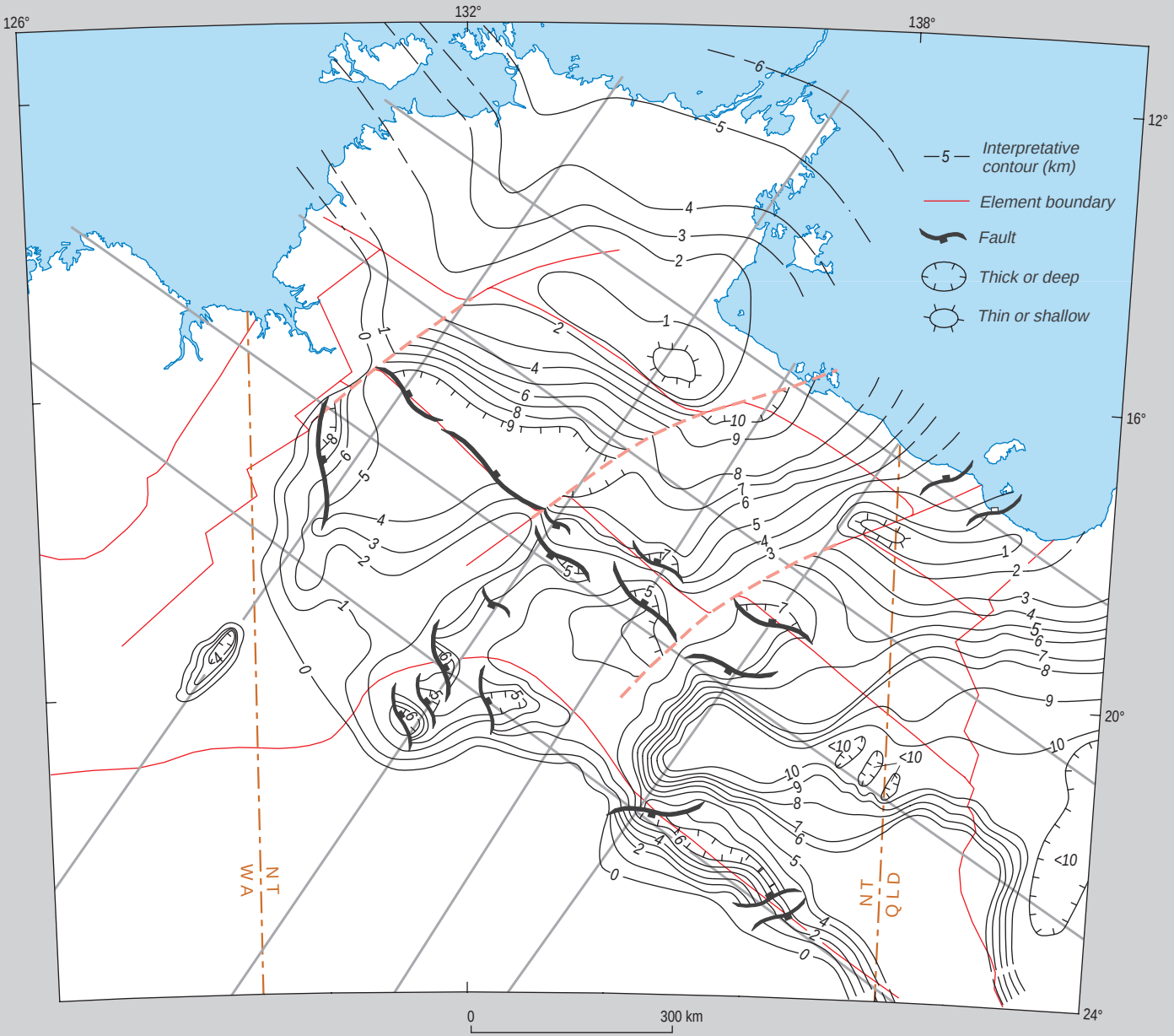

Figure 43 Interpretative thickness and structural style of the Paleoproterozoic basin system proposed to have initiated at ~1750-30 Ma

AGSO
AUSTRALIAN GEOLOGICAL SURVEY ORGANISATION

12/A/525

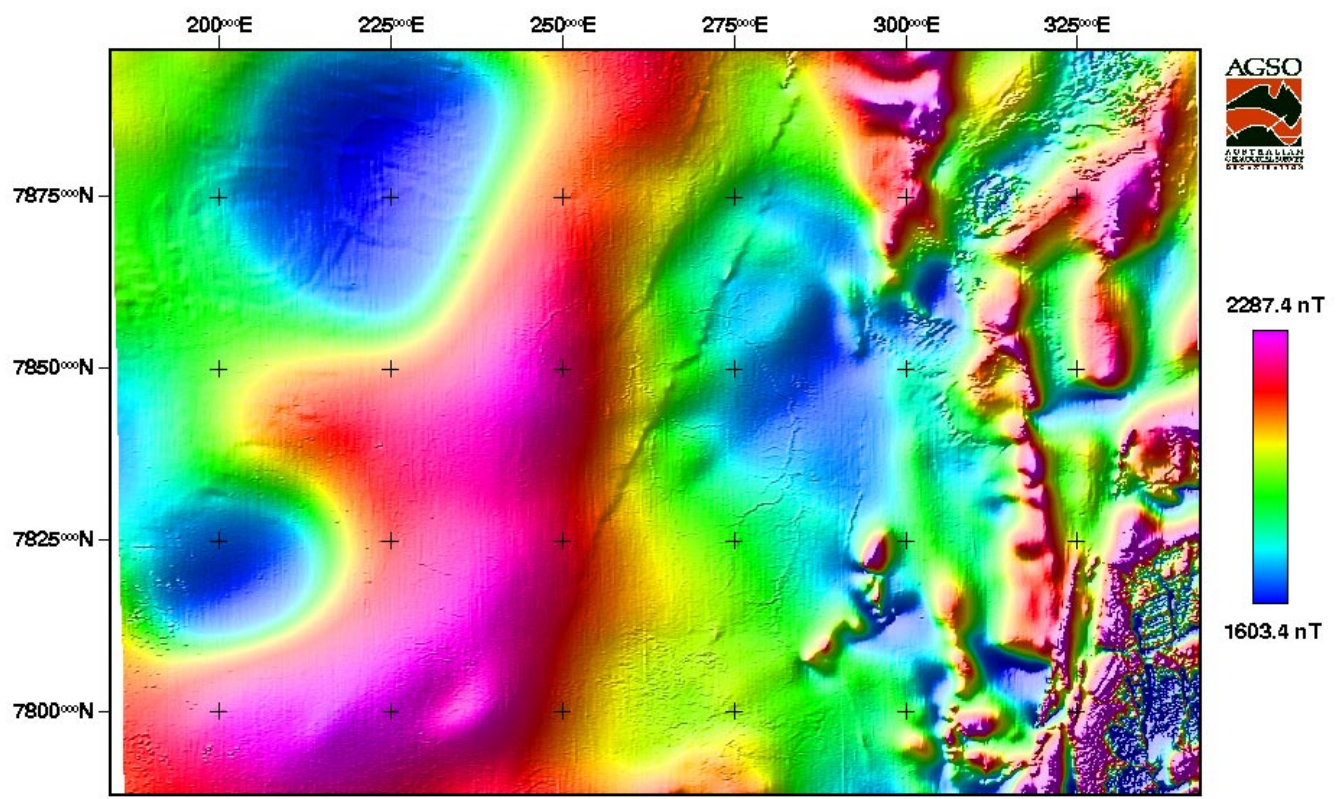

Fig 44 Total Magnetic Intensity (TMI) Camooweal

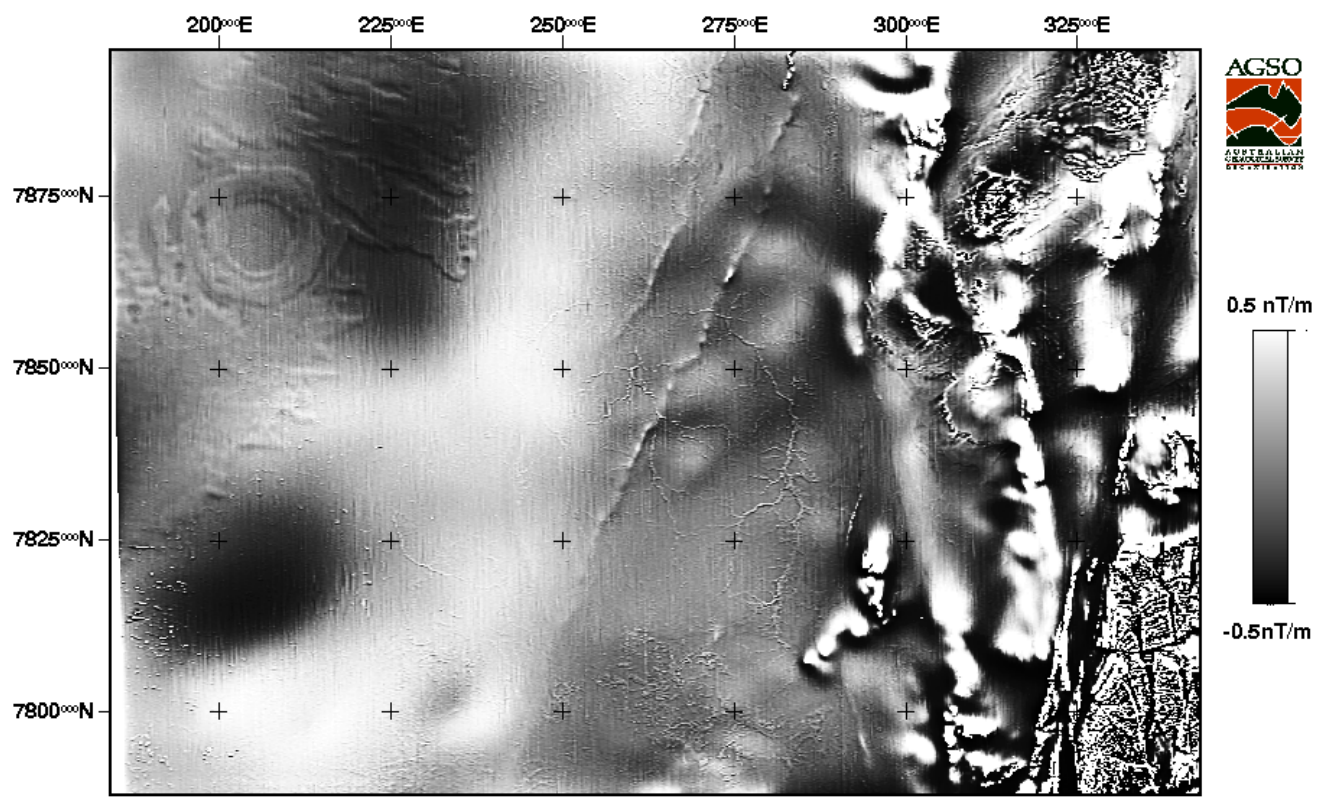

Fig 45 First vertical derivative of TMI Camooweal

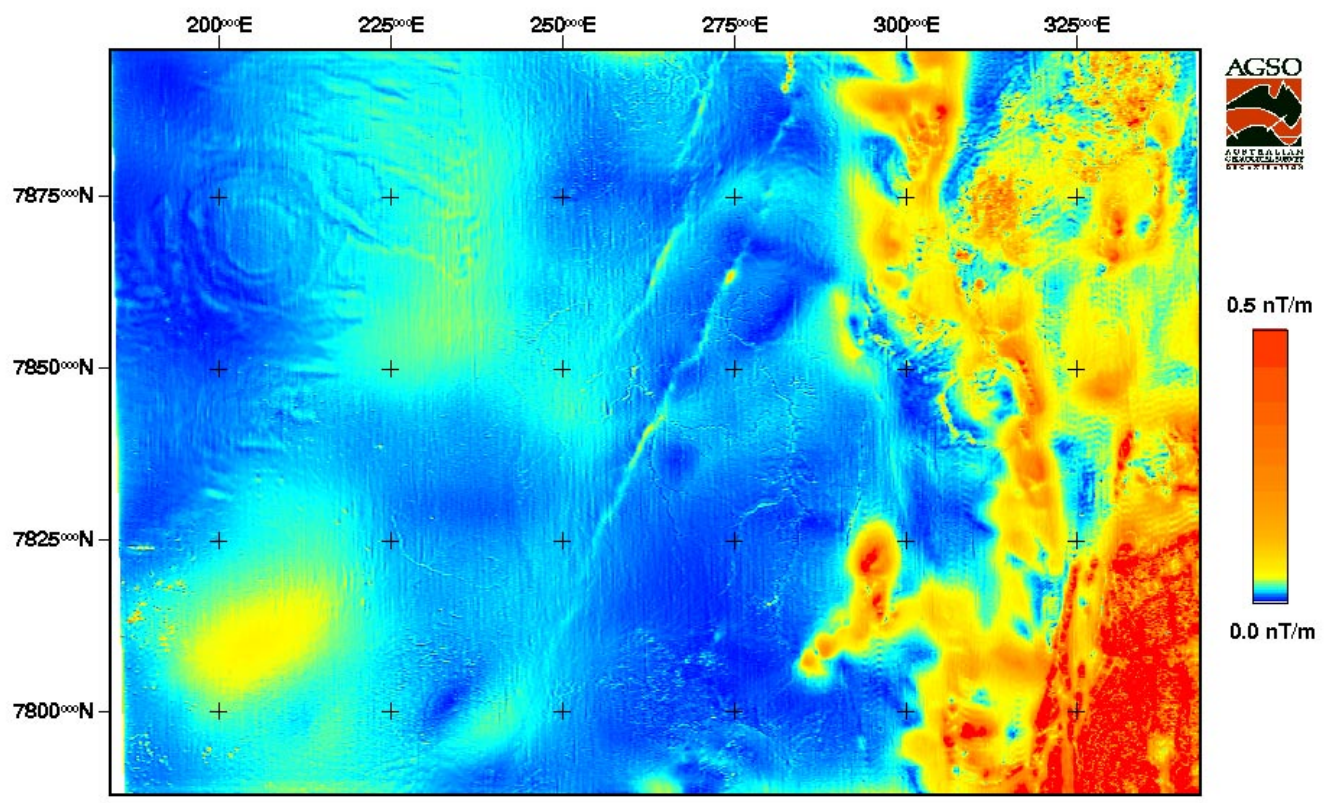

Fig 46 Analytic signal of TMI Camooweal

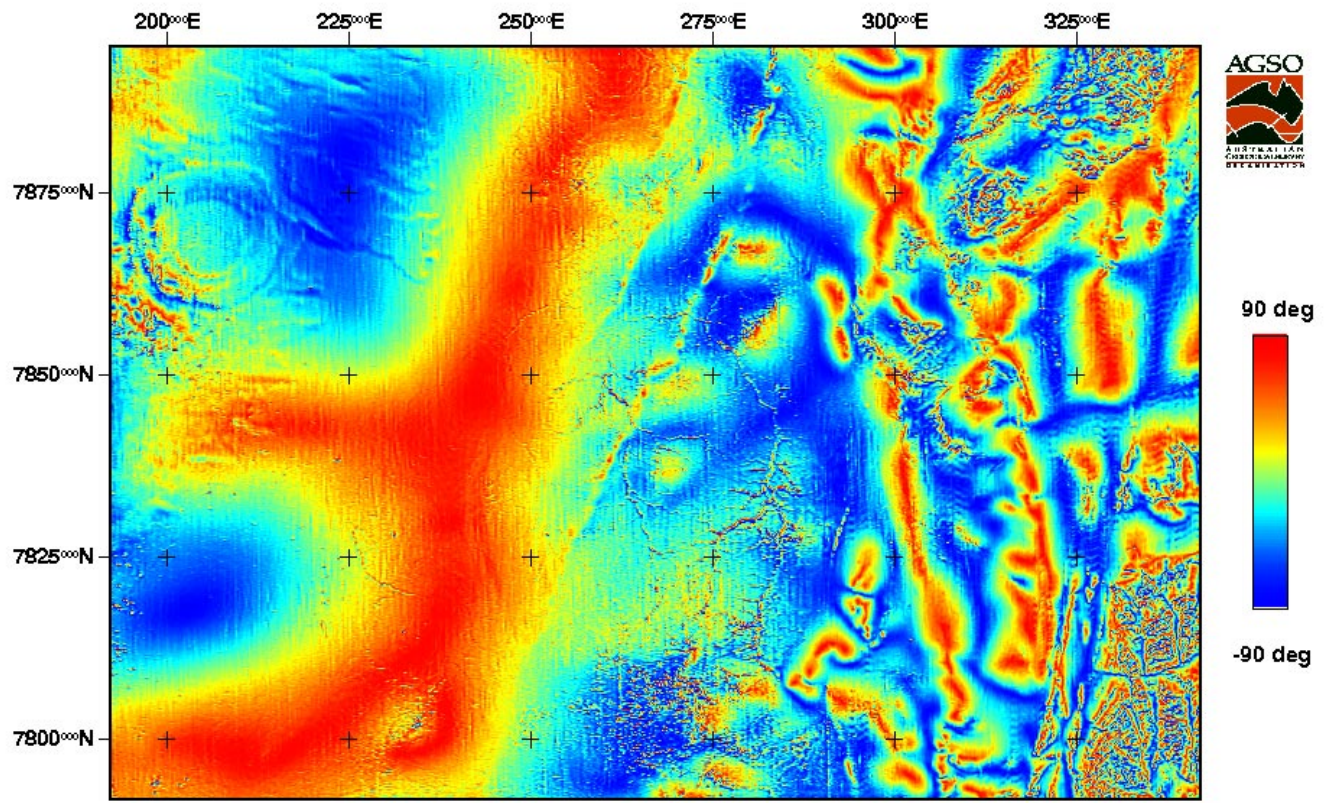

Fig 47 Tilt transformation of TMI Camooweal

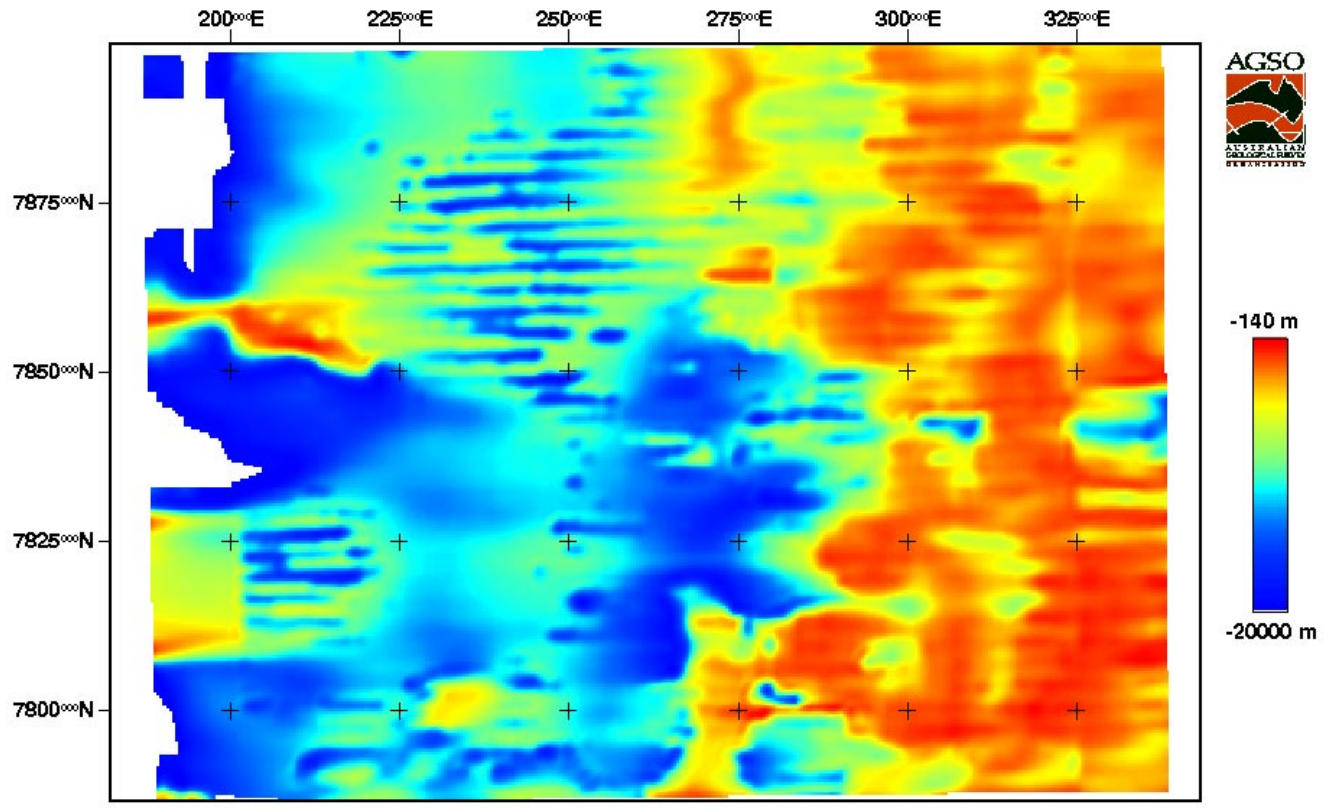

Fig 48 Depths to magnetic sources (low resolution data) Phillips method

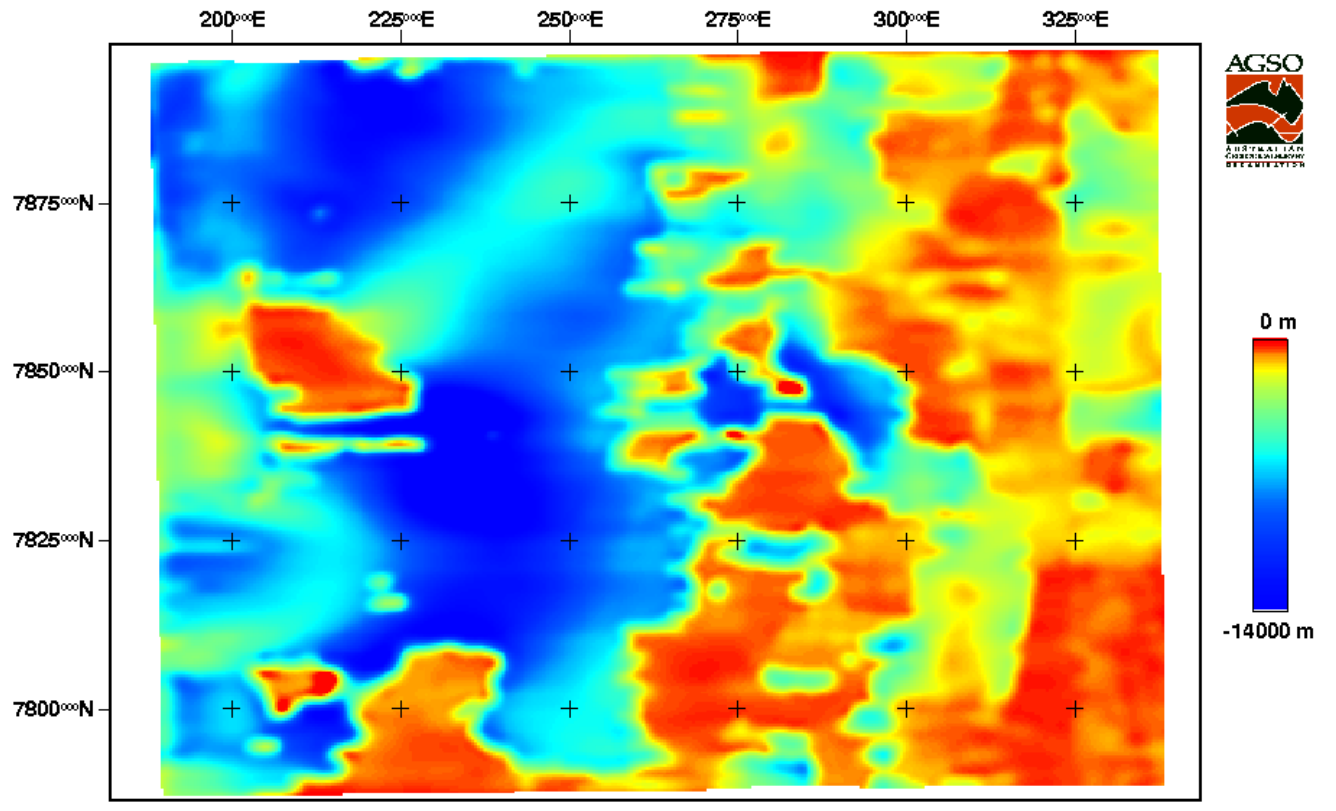

Fig 49 Depths to magnetic sources (high resolution data) Phillips method

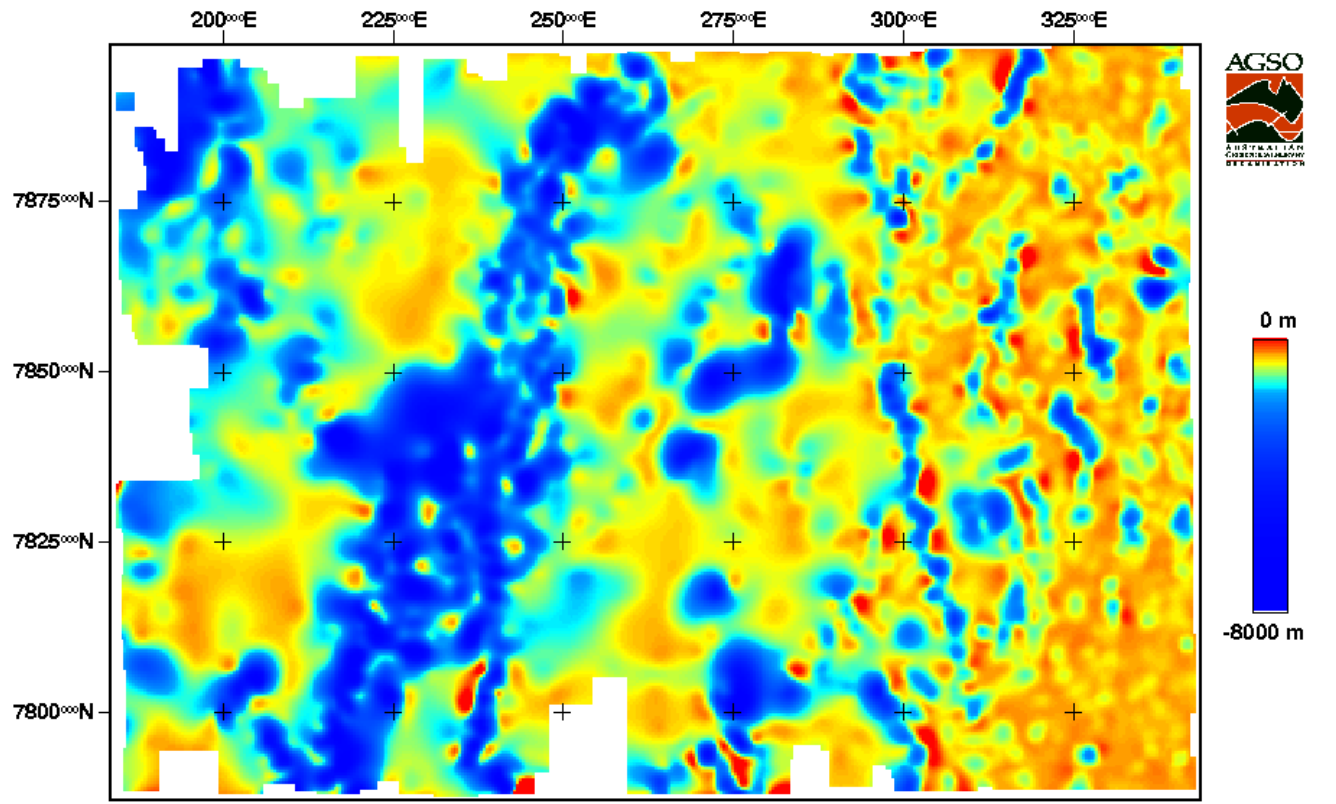

Fig 50 Depths to magnetic sources (high resolution data) Naudy method